

DESIGN TOOL DEVELOPMENT FOR LIQUID PROPELLANT MISSILE SYSTEMS

Except where reference is made to the work of others, the work described in this thesis is my own or was done in collaboration with my advisory committee. This thesis does not include proprietary or classified information.

David Baker Riddle

Certificate of Approval:

John E. Burkhalter
Professor Emeritus
Aerospace Engineering

Roy J. Hartfield, Chair
Associate Professor
Aerospace Engineering

Christopher J. Roy
Assistant Professor
Aerospace Engineering

George T. Flowers
Interim Dean
Graduate School

DESIGN TOOL DEVELOPMENT FOR LIQUID PROPELLANT MISSILE SYSTEMS

David Baker Riddle

A Thesis

Submitted to

the Graduate Faculty of

Auburn University

in Partial Fulfillment of the

Requirements for the

Degree of

Master of Science

Auburn, Alabama

May 10, 2007

DESIGN TOOL DEVELOPMENT FOR LIQUID PROPELLANT MISSILE SYSTEMS

David Baker Riddle

Permission is granted to Auburn University to make copies of this thesis at its discretion, upon the request of individuals or institutions and at their expense. The author reserves all publication rights.

Signature of Author

Date of Graduation

VITA

David Baker Riddle was born on September 25, 1981 in Anniston, Alabama to William and Genie Riddle. His family moved to Madison, Alabama in 1992 where his father began working on Redstone Arsenal as a civil engineer. After graduating from Bob Jones High School in 2000, David followed in the footsteps of both parents and began attending classes at Auburn University. In addition to being a full-time student, he was also an active member of the university's varsity track and cross-country teams. David graduated Summa Cum Laude in December 2004 with a Bachelor of Aerospace Engineering degree and began graduate studies in Aerospace Engineering at Auburn University the following semester.

THESIS ABSTRACT

DESIGN TOOL DEVELOPMENT FOR LIQUID PROPELLANT MISSILE SYSTEMS

David Baker Riddle

Master of Science, May 10, 2007
(B.A.E., Auburn University, 2004)

89 Typed Pages

Directed by Roy J. Hartfield

The use of computer programs driven by genetic algorithms (GA's) has become an increasingly popular method of optimizing engineering designs. This thesis focuses on the modeling and optimization of liquid rocket engine propelled missiles with an emphasis on some recent upgrades to an existing suite of codes. The program is comprised of a series of legacy codes which simulate the performance of liquid rockets and are controlled by a GA. This program is designed so that it can be used to reverse engineer missile designs for which some limited initial data is known. It can also be used to optimize liquid propelled missiles in the more traditional design mode.

Several upgrades were made to the existing code to expand its capabilities and add to the robustness of the program. A new version of the code has been developed in which aerodynamic prediction duties are handled by Missile Datcom instead of the Aerodsn routine used in previous versions. Plots from runs using the two different

aerodynamic codes are presented and their differences discussed. Furthermore, the program now has the ability to handle a varying specific impulse (I_{sp}), and a jet vane control system model has been added. The previous version of the liquid missile GA code assumed that I_{sp} was constant for a given fuel type. The modification described in this thesis gives the GA the ability to choose an equivalence ratio which determines the I_{sp} . In addition to the aerodynamic control system already in place, the ability to simulate a missile controlled by jet vanes has been added to the program. The new control system and accompanying optimization results are examined in detail.

ACKNOWLEDGEMENTS

The author would like to thank Dr. Roy Hartfield and Dr. John Burkhalter for their direction and assistance with this thesis; without their support this project would not have been possible. He would also like to thank the authors of the legacy codes that served as a basis for this research including Dr. John Burkhalter, Dr. Rhonald Jenkins, and Dr. Murray Anderson. Finally, the author wishes to thank his family and friends for all of their encouragement, love, and support.

Style manual or journal used

The American Institute of Aeronautics and Astronautics Journal

Computer software used

IMPROVE 3.1 Genetic Algorithm, General Purpose 6-DOF Simulation, Compaq Visual

Fortran, WinDiff, TecPlot, Microsoft Excel, Microsoft Word

TABLE OF CONTENTS

| | |
|---|-----|
| LIST OF TABLES..... | x |
| LIST OF FIGURES | xi |
| NOMENCLATURE | xii |
| 1. INTRODUCTION | 1 |
| 2. BACKGROUND AND THEORETICAL DEVELOPMENT | 5 |
| 2.1 Genetic Algorithm | 5 |
| 2.2 Aerodynamics | 9 |
| 2.2.1 Aerodsn | 9 |
| 2.2.2 Missile Datcom | 9 |
| 2.3 Mass Properties..... | 12 |
| 2.4 Six Degree-of-Freedom Model | 13 |
| 2.5 Liquid Propulsion System..... | 14 |
| 2.5.1 Background..... | 14 |
| 2.5.2 Variable Specific Impulse..... | 15 |
| 2.6 Guidance System and Autopilot | 18 |
| 2.7 Jet Vane Control System..... | 19 |
| 2.7.1 Motivation..... | 20 |
| 2.7.2 Theory | 21 |
| 2.7.3 Assumptions..... | 24 |
| 2.7.4 Methodology | 24 |
| 2.7.5 Verification | 27 |
| 3. RESULTS | 30 |
| 3.1 Model Validation | 30 |
| 3.2 Unguided Results | 33 |
| 3.3 Aerodynamic Guided Results | 44 |
| 3.4 Vane Control Guided Results | 49 |
| 4. CONCLUSIONS AND RECOMMENDATIONS | 63 |
| REFERENCES | 65 |
| APPENDIX A: GA Input File | 69 |
| APPENDIX B: Global Array Variables | 70 |

LIST OF TABLES

| | |
|---|----|
| Table 1: GA design variables..... | 8 |
| Table 2: Components considered in the mass properties routine | 13 |
| Table 3: Variable specific impulse propellant combinations..... | 16 |
| Table 4: LOX/H2 data table..... | 18 |
| Table 5: Pressure coefficient depending on region (modified from Ref. 32) | 23 |
| Table 6: Missile configuration and performance data (from Ref. 17) | 31 |
| Table 7: List of GA variables for SCUD-B comparison..... | 32 |
| Table 8: Model validation for the SCUD-B..... | 33 |
| Table 9: Case setup | 35 |
| Table 10: Case 1 GA variables | 40 |
| Table 11: Case 2 GA variables | 41 |
| Table 12: Case 3 GA variables | 42 |
| Table 13: Case 4 GA variables | 43 |
| Table 14: GA variables for Aerodsn optimized missile..... | 47 |
| Table 15: GA variables for Datcom optimized missile | 48 |
| Table 16: GA variables for optimized, unguided missile | 52 |
| Table 17: GA variables for optimized, aerodynamically controlled missile | 53 |
| Table 18: GA variables for optimized, vane controlled missile | 54 |
| Table 19: Target data for test cases..... | 58 |

LIST OF FIGURES

| | |
|---|----|
| Figure 1: Aerodsn and Datcom optimized missile trajectories | 12 |
| Figure 2: Earth-centered coordinate system (from Ref. 12) | 14 |
| Figure 3: LOX/H2 specific impulse as a function of equivalence ratio | 18 |
| Figure 4: Polish wz. 8/K-14, Scud-B (from Ref. 26)..... | 20 |
| Figure 5: Regions of influence..... | 22 |
| Figure 6: Differential pressure coefficient on a thin vane at 10° angle of attack | 26 |
| Figure 7: Vane force as a function of vane deflection | 29 |
| Figure 8: SCUD-B diagram (from Ref. 35)..... | 31 |
| Figure 9: Comparison of the simulated missile with the SCUD-B..... | 33 |
| Figure 10: Trajectory plot | 37 |
| Figure 11: Altitude as a function of time | 38 |
| Figure 12: Thrust as a function of time..... | 38 |
| Figure 13: Mach number as a function of time..... | 39 |
| Figure 14: Range as a function of time | 39 |
| Figure 15: Case 1 missile external geometry | 40 |
| Figure 16: Case 2 missile external geometry | 41 |
| Figure 17: Case 3 missile external geometry | 42 |
| Figure 18: Case 4 missile external geometry | 43 |
| Figure 19: Missile external geometry comparison..... | 44 |
| Figure 20: Convergence history..... | 45 |
| Figure 21: Aerodsn optimized, guided missile external geometry | 47 |
| Figure 22: Missile Datcom optimized, guided missile external geometry | 48 |
| Figure 23: Aerodynamically controlled flight trajectories..... | 49 |
| Figure 24: Ballistic missile external geometry | 52 |
| Figure 25: Aerodynamic control missile external geometry..... | 53 |
| Figure 26: Vane control missile external geometry | 54 |
| Figure 27: Trajectory plots for target 1 | 58 |
| Figure 28: Trajectory plots for target 2..... | 59 |
| Figure 29: Trajectory plots for target 3..... | 60 |
| Figure 30: Trajectory plots for target 4..... | 61 |
| Figure 31: Trajectory plots for target 5..... | 62 |

NOMENCLATURE

| | |
|---------------|--|
| CFD | Computational Fluid Dynamics |
| GA | Genetic Algorithm |
| Λ | Sweep Angle |
| α | Angle of Attack |
| $C_{M\delta}$ | Derivative of the Moment Coefficient |
| C_N | Normal Force Coefficient |
| $C_{N\delta}$ | Derivative of the Normal Force Coefficient |
| δ | Vane Deflection Angle |
| f | Fuel to Oxidizer Ratio |
| ϕ | Equivalence Ratio |
| g | Acceleration Due to Gravity |
| h_0 | Total Enthalpy |
| h_e | Exit Enthalpy |
| I_{sp} | Specific Impulse |
| M | Mach Number |
| μ | Mach Angle |
| q | Dynamic Pressure |
| S_{REF} | Reference Area |
| u_e | Exit Velocity |

1. INTRODUCTION

Liquid propelled missiles are complex systems with a broad range of design options. Predicting the performance of a missile for which only a limited amount of information is available is challenging and is not always possible. Genetic algorithms (GA's) have proven to be very effective in optimizing a variety of engineering designs and are now being used to reverse engineer or predict the capabilities of missile systems with only a few known design variables. While it is unlikely that a GA would converge to the exact missile design of interest, GA's are able to efficiently produce multiple close matches to known solutions.¹⁻³

A genetic algorithm is based on the biological concept that a species evolves or adapts over successive generations. Traits that improve fitness or performance are passed from one generation to the next while unfavorable characteristics are gradually eliminated. Over the course of many generations the average fitness of the members in a population will gradually begin to increase and the design will converge toward the objective. Depending on the setup, there can be multiple goals and the GA attempts to find the combination of characteristics that results in performance which matches these goals.⁴

Genetic algorithms can be used to optimize virtually any system with multiple design variables whose performance can be computationally simulated. The use of genetic algorithms has become increasingly popular in the optimization of engineering

designs and has already been used extensively in the aerospace industry to forward optimize designs, where constraints on performance drive the design process. The design of helicopters,⁵ spacecraft controls,⁶ flight trajectories,⁷ gas turbines,⁸ airfoils,⁹ boosted ramjets,¹⁰ interceptor missiles,^{11,12} aircraft,¹³ hybrid rockets,¹⁴ liquid rockets,^{1, 15-17} and solid rockets^{18,19} have all benefited from the application of GA's in this manner.

More recently, genetic algorithms have been shown to be a useful tool in reverse engineering problems, specifically in reverse engineering missile designs. In contrast to design optimization, reverse engineering assumes some of the performance goals or design variables are already known, and the GA attempts to discover a variable set that matches the known goals. With a limited set of initial data, it was determined that a GA is better able to establish the remaining unknown design parameters than a trial-and-error method.¹ In a precursor to the current research, Burkhalter et al.¹ developed a GA-based program that was able to partially reverse engineer ballistic solid rocket missiles. While their program was able to discover much of the external design and some performance characteristics, some of the design variables could not be accurately identified. Using a derivative of this program, Metts⁴ conducted much more extensive research on the performance of the GA in reverse engineering ballistic missile designs. He found that the GA was capable of finding quality reverse engineering matches, but human inspection was still necessary to determine the true best performer from a small group of optimized missile designs. This scenario often occurs because of the fact that multiple designs can achieve identical performance goals.

The research discussed in this thesis directly builds on the work done by Burkhalter et al.² The missile optimization code has been modified to use the GA in

optimizing liquid-fueled missiles. In addition to ballistic missiles, both aerodynamically controlled and vane controlled missile designs are considered. The optimization code is a combination of many individual codes which together are able to simulate the performance of a particular missile design and then determine its fitness in relation to the other candidate designs. A series of legacy codes predict the actual performance of individual liquid missile designs by analyzing a candidate missile design's aerodynamics, mass properties, propulsion characteristics, and guidance and control system. The six degree-of-freedom (6-DOF) model ties everything together, providing the performance data for each missile design. The GA then determines and operates on the best solutions for a given generation of designs depending on the user-defined objective function. Each of the legacy codes and the GA are discussed in detail in the pages that follow.

The goal of this thesis is to upgrade an existing liquid rocket optimization program and obtain results from relevant optimization runs. While the code can be used for preliminary design optimization, the primary motivation that drives this research is to be able to use the program to reverse engineer existing missile designs. If only a limited amount of data about a specific liquid rocket is known, the GA-controlled optimization code is able to produce complete designs with characteristics that match the known parameters. The GA suite of codes also has the ability to optimize a current design and discover possible modifications that might improve the missile's performance.

The upgrades discussed in this thesis add a new level of confidence to the overall optimization results. This process includes the ability to simulate missile types that the program previously was unable to handle. The first upgrade to the suite of codes involved the development of a version of the code that employs an alternate aerodynamic

analysis code known as Missile Datcom.²⁰ The next change made to the code allows for the specific impulse (I_{sp}) to vary as a function of equivalence ratio (ϕ), where it was formerly a constant value dependant only on the selected propellant type. Finally, a jet vane control system is added to the current aerodynamic control system which allows for the optimization of vane controlled missile systems. With the modifications made during the current research, the suite of programs is now able to optimize real-world missile designs that it was formerly incapable of simulating while adding a new level of efficiency and accuracy to its previous abilities.

2. BACKGROUND AND THEORETICAL DEVELOPMENT

The liquid rocket optimization code is comprised of many individual codes that work together to predict the performance of each missile design selected by the GA for analysis. Many of these are referred to as legacy codes because they have remained largely unchanged in the current research effort. Others, including the aerodynamics routine and the liquid propulsion system model, were modified significantly. The main codes of interest will be discussed briefly with special attention paid to the ones which were upgraded. Some background information on the GA will first be provided followed by discussion of the aerodynamics, mass properties, 6-DOF, liquid propulsion system, and guidance system models. Finally, the development of the jet vane control system will be addressed in detail.

2.1 Genetic Algorithm

The GA examined in the current research uses a set of design variables to define a particular missile system. The optimization process begins with the user selecting a range and resolution for each of the design variables. By randomly selecting values for each design variable from within the user-defined boundaries, the GA then generates a population of candidate designs. Each candidate design, otherwise known as a member, in a generation is analyzed by the suite of performance codes. The number of members in a generation and the number of generations that the GA should run are also values set by the user. Next, the GA ranks the members according to the performance of each as

determined by the objective function. The GA employed in this effort uses a tournament selection process which chooses the best performing member from a randomly selected pair. The resulting member is then “mated” with the best performer from a different pair. The mating process combines the two members’ genetic material, which is stored in binary form. A portion of this exchanged genetic material may be mutated depending on the mutation probability factor set in the GA options. The subsequent generation is filled with members that result from the mating process. The process is repeated as each member in the new population is analyzed by the performance codes and its fitness ranked.

Over successive generations, the fitness of the designs will increase as good designs are passed on while poor designs are eliminated. The speed and efficiency of this process is highly dependent on the ranges of the GA variables and the number and types of goals. Allowing wide variations in each of the design variables greatly increases the number of possible solutions that the GA must analyze. However, if several design variables are already known, as is usually the case in reverse engineering problems, a solution can be reached much more quickly.⁴

The objective function has an arguably greater effect on the efficiency of the optimization code. Experience has shown that given one goal, the GA usually finds a solution using a relatively small number of calculations of the objective function. As more goals are added however, optimal solutions can be more difficult to find, as the goals are often competing with one another. For example, the user might wish to maximize range and minimize the system weight of a missile design. Those goals are in direct competition and finding the balance of range and weight based on the goal

description is computationally expensive. In addition, the user must keep the goals evenly proportioned while adjusting a weighting factor to emphasize the more important goal if necessary.

Many of the settings and options that control the behavior of the GA are found in the GA input file (GANNL.DAT). An example GA input file can be found in APPENDIX A. This file is where the bounds and resolution for each of the 27 GA design variables are set and where the number of members in a population and the maximum number of generations are defined. The GA can be configured for multiple goals, and the relative importance of the goals can be adjusted by weighting factors. There are many other parameters that control the performance of the GA located in this file but a few notable ones are a restart switch, an elitist option, the mutation probability factor and a seed for the random number generator. The GA itself is a complicated program that could be the subject of its own thesis, but for the purposes of this research it has been left unaltered from the previous versions.^{2,4,10}

Table 1 lists the 27 GA variables and provides a brief definition for each one. Clearly, all of the possible parameters that affect the design of liquid powered missiles could not be encapsulated in just 27 variables. These variables were selected as being the most critical design options and have the greatest effect on a missile's performance. The remaining design options, which are not variable, are defined in the YYVAR.DAT file which can be found in APPENDIX B. These parameters are read out of the file and stored in a global array which is used by all parts of the program. While there is far too much information stored in this file to discuss in detail, it should be noted that the major categories of information include: constants, material densities, component masses, target

and launch data, external geometry variables, and reverse engineering data. Even with this large data input, the suite of codes employed in this investigation is still arriving at preliminary designs. Detailed design parameters such as turbopump internal parameters, fasteners, detailed plumbing and wiring schematics are not considered in this process.

Table 1: GA design variables

| Number | Variable Name | Description |
|--------|---------------|--|
| 1 | kprop | Propellant type |
| 2 | eqr | Equivalence ratio |
| 3 | po | Maximum chamber pressure (psi) |
| 4 | athroat | Nozzle throat area (in ²) |
| 5 | eps | Nozzle expansion ratio |
| 6 | lf | Fractional nozzle length |
| 7 | tb | Burn time (sec) |
| 8 | paymass | Payload mass (lbs) |
| 9 | dbody | Missile body diameter (ft) |
| 10 | lnose | Nose length (lnose/dbody) |
| 11 | dnose | Nose diameter (dnose/dbody) |
| 12 | crfin1 | Finset 1 root chord (cr/dbody) |
| 13 | trfin1 | Finset 1 taper ratio |
| 14 | angLE1 | Finset 1 leading edge angle (degrees) |
| 15 | b2fin1 | Finset 1 semi-span (b2/dbody) |
| 16 | xcrfin1 | Location of the leading edge of finset 1 (% total length) |
| 17 | crfin2 | Finset 2 root chord (cr/dbody) |
| 18 | trfin2 | Finset 2 taper ratio |
| 19 | angLE2 | Finset 2 leading edge angle (degrees) |
| 20 | b2fin2 | Finset 2 semi-span (b2/dbody) |
| 21 | xtefin2 | Location of the trailing edge of finset 2 (% total length) |
| 22 | tdelay | Autopilot time on delay (sec) |
| 23 | tau | Autopilot time constant (sec) |
| 24 | zeta | Autopilot damping coefficient |
| 25 | wcr | Cross over frequency |
| 26 | pronvg | Pronav gain |
| 27 | theta0 | Initial launch angle (degrees) |

2.2 Aerodynamics

2.2.1 Aerodsn

Aerodsn²¹ is a fast predictor aerodynamic analysis code which has been used successfully in several different versions of the GA missile optimization program. Developed by the U.S. Army Missile Command in the 1980s, it is a very robust code restricted to axis-symmetric cruciform missile shapes. More accurate CFD codes are available, but the high computational cost of this type of analysis makes CFD impractical for use with the GA in the preliminary design mode. Aerodsn is non-linear and assumes that there are no boundary layers and that no separation occurs. Aerodsn uses the vehicle geometry and other parameters necessary for successfully generating an aerodynamic database. The required aerodynamic data is generated for the complete Mach number range and a complete missile orientation sweep in order for the 6-DOF to determine the aerodynamic loads and moments under any flight condition. The missile is assumed to be symmetric so the yawing moments are determined from the pitching moment coefficients and the side forces are determined from the normal force coefficients.

2.2.2 Missile Datcom

While Aerodsn has been used successfully as the aerodynamic prediction code for the GA program, it was determined that the program would benefit from a full-featured and industry standard aerodynamic code. Consequently, an alternate version of the optimization suite has been developed which uses Missile Datcom. Missile Datcom²⁰ is also a fast predictor missile aerodynamic analysis tool with a wide range of capabilities. Even though Aerodsn borrowed some of its source code from Missile Datcom, the two programs function differently. Missile Datcom receives the missile geometry input and

writes output in formats that differ greatly from that of Aerodsn. As a result, the process of integrating Missile Datcom required a considerable amount of modification to the optimization program as a whole.

Since the GA optimization process selects numerous missile designs which each must be simulated to analyze their performance, the aerodynamic code must be run repeatedly to generate the aerodynamic coefficients for each member. This fact creates a problem with Missile Datcom as it will not run multiple cases one after another without being completely closed between cases. Missile Datcom maintainers have acknowledged the issue, but currently do not have a solution. The initial plan for implementing Missile Datcom was to insert it into the liquid missile GA code as a subroutine. The Missile Datcom subroutine would be called instead of Aerodsn each time a new missile geometry is produced, and the coefficients could be transferred into the regular program as needed. But because the optimization program is not exited between runs, Missile Datcom does not work properly in this configuration.

In order to use Missile Datcom with the GA, a method of running the code which allows Missile Datcom to be exited after each run was devised. Instead of running Missile Datcom as a subroutine, it is compiled as a standalone executable file and called directly from the performance prediction program. This allows Missile Datcom to completely close after each time it is called while the liquid optimization program continues running. A new subroutine is added to the optimization program to transfer the missile geometry parameters into a form that Missile Datcom accepts and another subroutine is added to retrieve the coefficients from the output file and enter them into

the GA code. The only modification that must be made to the actual Missile Datcom source is to redirect the paths for the input and output files.

Although this method is functional, it is not a perfect solution for running the GA with Missile Datcom. Whenever Missile Datcom is called, a command window is opened for a brief moment and then immediately closed. Because of the number of missile designs analyzed by the GA, it is normal to have a new window opening every second. While this only causes a slight decrease in the performance of the program as a whole, it is very inconvenient for the computer user as it steals focus from other applications running on the machine and renders that computer almost unusable for any other purpose while the GA is running. The development environment supplied for this research, Compaq Visual Fortran, appears to have no compiler option that allows this window to be suppressed. A possible solution that has been suggested is to call Missile Datcom with a piece of C++ code that can hide the window. This option has not been pursued within the scope of the current research effort.

The aforementioned issues have made it impractical to implement Missile Datcom in the final version of the liquid missile GA program, but it can be used to corroborate results obtained from the Aerodsn version. An extensive study was made comparing the two aerodynamic codes and Figure 1 shows a plot comparing the trajectories of missiles optimized using Missile Datcom and Aerodsn. The GA goal was set to maximize range, and the cases had Mach number limits of 7.1 and 8.5 respectively. The trajectory plot illustrates how similar the predictions of two aerodynamic codes were to each other. The close agreement in the maximum range, as well as flight path, suggests Aerodsn and

Missile Datcom are providing comparable results for the aerodynamic coefficients. A complete set of results and analysis can be found in a later section of this thesis.

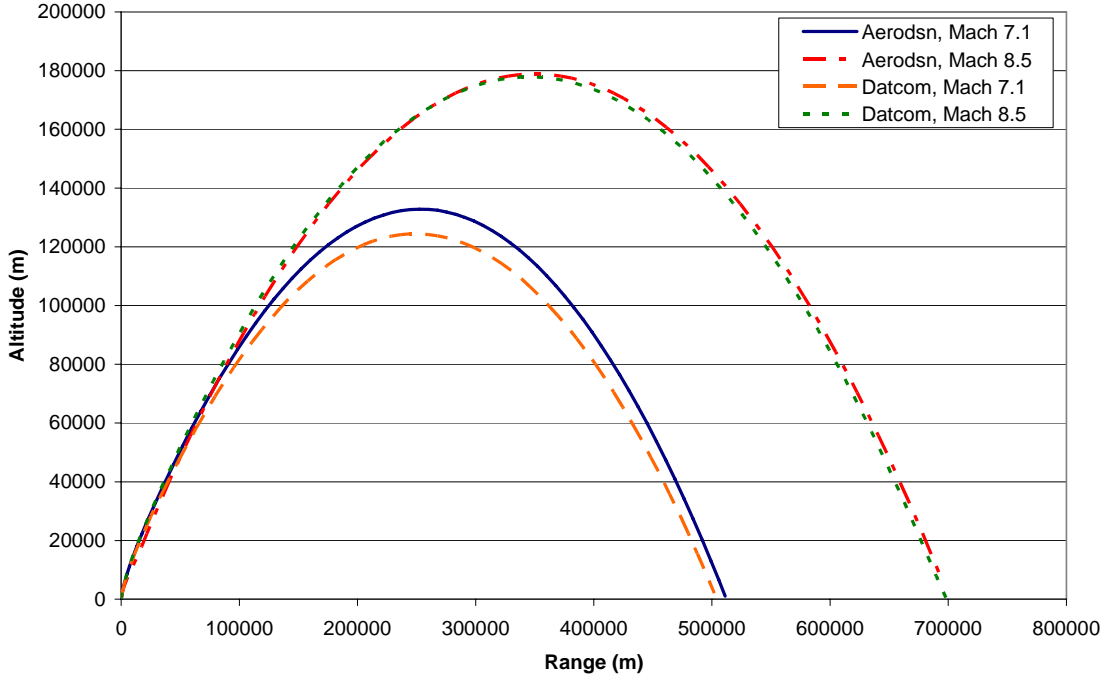


Figure 1: Aerodsn and Datcom optimized missile trajectories

2.3 Mass Properties

The mass properties routine is a comprehensive analysis of the missile system component masses and moments of inertia about all three axes. Cross product moments of inertia are assumed to be zero since missile symmetry is assumed. The moment of inertia for each of the missile components is calculated. Once the center of gravity (CG) of the missile is determined, the moments are transferred to the CG and subsequently stored for future use. In this same routine, the mass and moment of inertia of the fuel and oxidizer are also determined as a function of time. This information, with the time dependent thrust data, is written to a file (TMASS.DAT) which is later used by the 6-DOF model. The components that are considered in the analysis are shown in Table 2.

Also listed in the table are six generic “boxes” which have been built into the code. These boxes allow the user to place custom payloads or other equipment inside the missile. The boxes can also be positioned at any location within the missile with the exception of *box1* which is always located at the nose.

Table 2: Components considered in the mass properties routine

| Part No. | Component |
|----------|-------------------------------------|
| 1 | Box1 |
| 2 | Avionics or electronics |
| 3 | Compressed gas for pressurization |
| 4 | Compressed gas tank |
| 5 | Fuel |
| 6 | Fuel tank |
| 7 | Oxidizer |
| 8 | Oxidizer tank |
| 9 | Engine assembly |
| 10 | Nozzle |
| 11 | Nosecone fairing |
| 12 | Cylindrical (main) fairing & wiring |
| 13 | Aft fins |
| 14 | Gimbals |
| 15 | Warhead |
| 16 | Forward fins |
| 17 | Servos |
| 18 | Box2 |
| 19 | Box3 |
| 20 | Box4 |
| 21 | Box5 |
| 22 | Box6 |

2.4 Six Degree-of-Freedom Model

The 6-DOF routine is based on the equations of motion found in Etkin.²² It is assumed that the missile is rigid, that all masses are stationary, and that all cross products of inertia are negligible. The 6-DOF uses an earth-centered coordinate system, similar to the one shown in Figure 2. The equations of motion accept aerodynamic data from

Aerodsn or Missile Datcom, mass and moments of inertia from the mass properties routine, thrust data from the liquid rocket module, and other required information is passed through the an array. The 6-DOF uses a 7-8th order Runge-Kutta numerical integration routine to simulate the flight of the missile. The time step is a variable and is dependent on the magnitude of the largest derivative in the equations of motion.¹² The flight of the missile is recorded, and necessary information is stored in an array and passed back to the GA routine for further analysis.

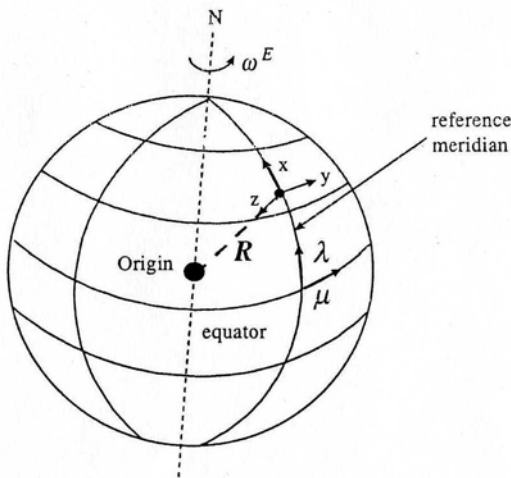


Figure 2: Earth-centered coordinate system (from Ref. 12)

2.5 Liquid Propulsion System

2.5.1 Background

The liquid rocket model is based on a generic set of required parameters that define the operation of a single stage liquid rocket engine. The oxidizer and fuel are stored in cylindrical tanks with hemispherical end caps which are sized based on the specific missile design. Standard equations are used to predict the thrust for a variety of fuel and oxidizer combinations at different operating combustion pressures and throat

areas. Variation of the thrust due to altitude change is also accounted for in the equations. The pressure and temperature in the combustion chamber are assumed to be constant, and it is also assumed that the thrust instantly drops to zero at burnout. The nozzle is designed to connect to the combustion chamber and can be configured to extend aft of the base of the missile or to have the nozzle exit flush with the base of the missile. The system assumes that turbopumps are required to compress the fuel and oxidizer prior to injection into the combustion chamber and the fuel and oxidizer tanks are under relatively low pressure, around 100 psia. All necessary plumbing and wiring are included as uniformly distributed mass.¹⁹

The propellant is a design variable which can be chosen from a list of 29 included fuel and oxidizer combinations. Propellant properties such as stoichiometric mixture ratio, combustor total temperature, molecular weight, characteristic exhaust velocity, sea level specific impulse, and the ratio of specific heats are included in the list with their corresponding fuel type. Propellants with sufficient data have been approximated with a curve fit to determine specific impulse as a function of equivalence ratio.

2.5.2 Variable Specific Impulse

A method for determining the specific impulse (I_{sp}) as a function of the equivalence ratio (ϕ) has been implemented in the optimization code. This allows the I_{sp} to be calculated based on the equivalence ratio that the GA chooses. It should be noted however, that some of the propellants available in the program are rare, and the necessary thermochemical data for these propellants was not readily available. As a result, these propellant combinations are still included but have a constant specific impulse. The fuels that currently have variable I_{sp} capability are listed in Table 3.

Table 3: Variable specific impulse propellant combinations

| Number | Propellant Name | I_{sp} (s) at $\phi=1$ |
|--------|--|--------------------------|
| 1 | IRFNA/UDMH | 274 |
| 2 | IRFNA/Hydrazine | 287 |
| 4 | IRFNA/RP-1 | 257 |
| 5 | IRFNA/JP-4 | 254 |
| 6 | IRFNA/MMH | 268 |
| 11 | N ₂ O ₄ /UDMH | 284 |
| 13 | N ₂ O ₄ /Kerosene | 283 |
| 14 | N ₂ O ₄ /Hydrazine | 291 |
| 15 | N ₂ O ₄ /MMH | 301 |
| 23 | LOX/Hydrazine | 314 |
| 25 | LOX/UDMH | 309 |
| 26 | LOX/LH ₂ | 367 |

The process of characterizing the thermodynamic conditions in a combustion chamber is highly complex. The large amounts of individual chemical species that appear make solving the chemical equations by hand impractical. Computer codes are routinely used to determine these values instead. STANJAN²³ is one such code and was used in calculating the I_{sp} as a function of equivalence ratio for the propellants in the optimization program. STANJAN solves for the thermodynamic conditions using linear programming to minimize the Gibbs free energy.

The specific impulse values for the propellants with sufficient data are approximated by a 5th-order curve fit that can be used to obtain the I_{sp} given an equivalence ratio. The equivalence ratio is defined as

$$\phi \equiv \frac{f}{f_{stoich}} \quad (1)$$

where f is the fuel to oxidizer ratio by mass.²⁴ The I_{sp} curve is valid for equivalence ratios between 0.25 and 4.0 for most of the propellant combinations. STANJAN was used to determine the I_{sp} at approximately eight equivalence ratios for each fuel and oxidizer

combination. Given the initial enthalpy of the propellant, STANJAN calculates the total temperature in the combustion chamber assuming 1000 psi (68 atm) total pressure. Assuming entropy is constant, STANJAN then calculates the exit enthalpy of the flow when the nozzle exit pressure is 14.7 psi (1 atm). The exit velocity is calculated by hand and then divided by the acceleration due to gravity to obtain the specific impulse as shown in Equation 2.

$$I_{sp} = \frac{\sqrt{2(h_0 - h_e)}}{g} = \frac{u_e}{g} \quad (2)$$

The resulting value is a reference I_{sp} and the actual performance is adjusted based on the flow characteristics and the selected chamber pressure. The mixture ratio is also adjusted based on the chosen equivalence ratio so that the mass of the oxidizer and fuel, as well as the size their respective tanks, is calculated correctly.

Figure 6 is a plot of the I_{sp} as a function of equivalence ratio for one of the available propellant combinations, LOX/LH₂. A trend line is fitted to the curve and the corresponding 5th-order equation is also shown on the plot. The data used to plot the I_{sp} curve is listed in Table 4. Similar plots were made for each propellant combination and the equation of the trend line corresponding to each propellant type was inserted into the liquid fuels subroutine. The curve fits were compared to published data²⁵ to validate the results. Except for propellant combinations containing hydrogen, the maximum specific impulse occurs very near the stoichiometric fuel to oxidizer ratio. The I_{sp} is higher for the fuel rich LOX/H₂ mixture because the molecular weight of the fuel (H₂) is much lower than the molecular weight for the oxidizer (O₂).

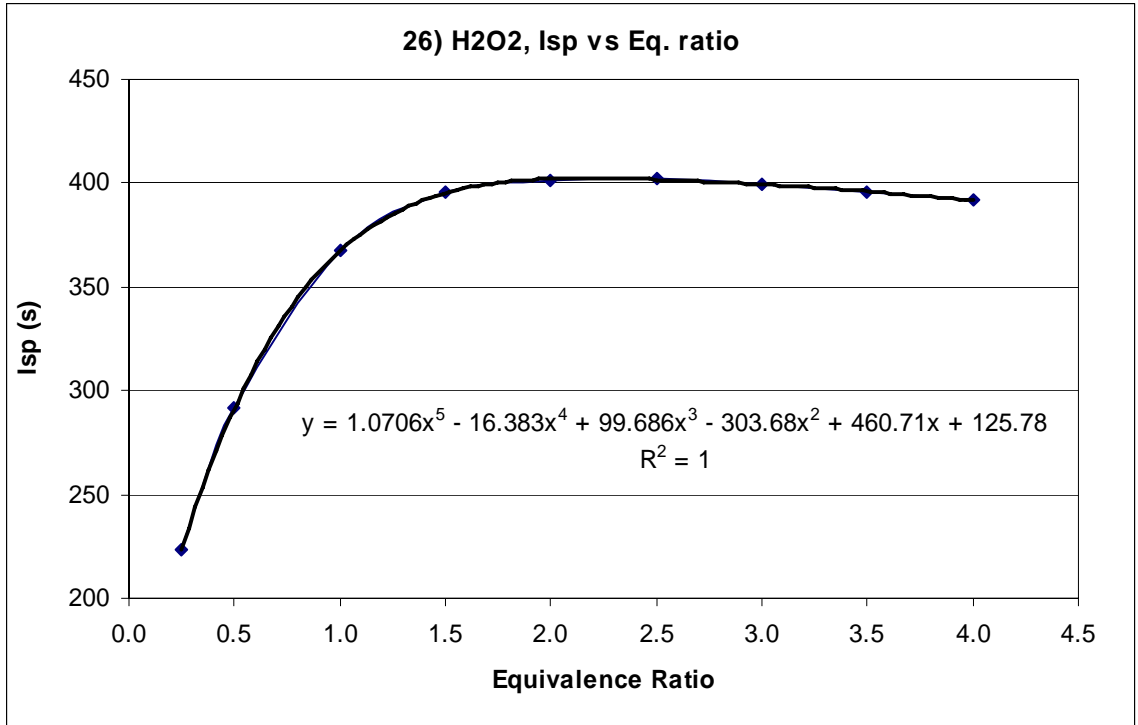


Figure 3: LOX/H2 specific impulse as a function of equivalence ratio

Table 4: LOX/H2 data table

| Equiv. ratio | Reactants | h_o (J/kg) | h_e (J/kg) | u_e (m/s) | I_{sp} (s) |
|--------------|-----------|--------------|--------------|-------------|--------------|
| 0.25 | 1/2H2+O2 | -1.29E+05 | -2.53E+06 | 2192.81 | 223.5 |
| 0.5 | H2+O2 | -1.66E+05 | -4.26E+06 | 2860.25 | 291.6 |
| 1.0 | 2H2+O2 | -2.33E+05 | -6.72E+06 | 3602.22 | 367.2 |
| 1.5 | 3H2+O2 | -2.94E+05 | -7.82E+06 | 3879.01 | 395.4 |
| 2.0 | 4H2+O2 | -3.48E+05 | -8.11E+06 | 3940.94 | 401.7 |
| 2.5 | 5H2+O2 | -3.97E+05 | -8.17E+06 | 3942.56 | 401.9 |
| 3.0 | 6H2+O2 | -4.42E+05 | -8.12E+06 | 3918.78 | 399.5 |
| 3.5 | 7H2+O2 | -4.83E+05 | -8.03E+06 | 3884.06 | 395.9 |
| 4.0 | 8H2+O2 | -5.20E+05 | -7.91E+06 | 3844.12 | 391.9 |

2.6 Guidance System and Autopilot

The guidance system is based on the proportional navigation guidance law. The system attempts to rotate the missile at a rate proportional to the rate at which the line-of-site to the target is moving. It is a two-axis feedback control system that uses the pitch

and yaw acceleration rates, but does not factor in the roll rate. The autopilot generates the elevator and rudder commands based on the acceleration rates determined in the guidance routine. The GA variables used by the guidance system and autopilot are the time delay, autopilot time constant, damping coefficient, crossover frequency, and the pronav gain. These variables are numbers 22 through 26 listed in Table 1.

2.7 Jet Vane Control System

Missiles with jet vane control systems use small, movable fins, usually composed of graphite, placed just downstream of the nozzle to vector the thrust and control the missile. The vanes take advantage of the high dynamic pressure of the supersonic nozzle exit flow to produce forces and moments that are large enough to guide the missile. Just after takeoff, while flying at low speeds, vanes provide an effective method of control, especially before speeds are attained where aerodynamic control surfaces become effective. The disadvantage of vanes is that they become less and less effective as flight Mach number increases, and after burnout they are completely useless because they require thrust to produce the controlling forces and moments. Adjusted by actuators which are built into the missile body, the attitude of jet vanes is controlled in much the same way as with aerodynamic fins. Figure 4 shows a missile with a jet vane control system. The vanes are positioned just aft of the nozzle and are mounted inside the tail fins.



Figure 4: Polish wz. 8/K-14, Scud-B (from Ref. 26)

2.7.1 Motivation

While jet vanes are not common in modern missile designs, many older missiles still being used and upgraded today rely on vanes as their only form of control. Since a major motivation driving the development of the optimization program is to be able to use the GA to reverse engineer a wide range of missiles, including some that employ jet vanes, a vane control model was determined to be a necessary upgrade. The model should predict the aerodynamic forces and moments on the vanes which are immersed in the supersonic exhaust flow. This modification gives the suite of codes the ability to predict the performance of a large number of missiles, including SCUD-class missiles, with a much higher degree of accuracy than before.

2.7.2 Theory

During the late 1940's, John Evvard^{27,28} and several other engineers²⁹⁻³¹ solved the irrotational flow equations for a source distribution over a flat plate in supersonic flow. Evvard's theory divides the planar fin into regions which are affected by similar types of disturbances. These regions are defined by the intersection of the Mach cones produced by leading edge discontinuities and the surface of the fin. The primary disturbance types that affect each region are infinite wing, triangular fin, and wing tip. These disturbance types divide the wing into four regions of flow. A fifth region can also be present in the case of swept wings when the Mach cone produced by the root chord leading edge is reflected by the fin tip. The potential flow solution that corresponds to the type of disturbance experienced in a particular region can be used to determine the pressure difference between the upper and lower surfaces of the fin at angle of attack. A generic fin is shown in Figure 5 and illustrates the different regions and the Mach lines that divide them. The Mach lines on the surface of a flat plate are inclined at a Mach angle, μ , which is defined as:

$$\mu = \sin^{-1}\left(\frac{1}{M}\right) \quad (3)$$

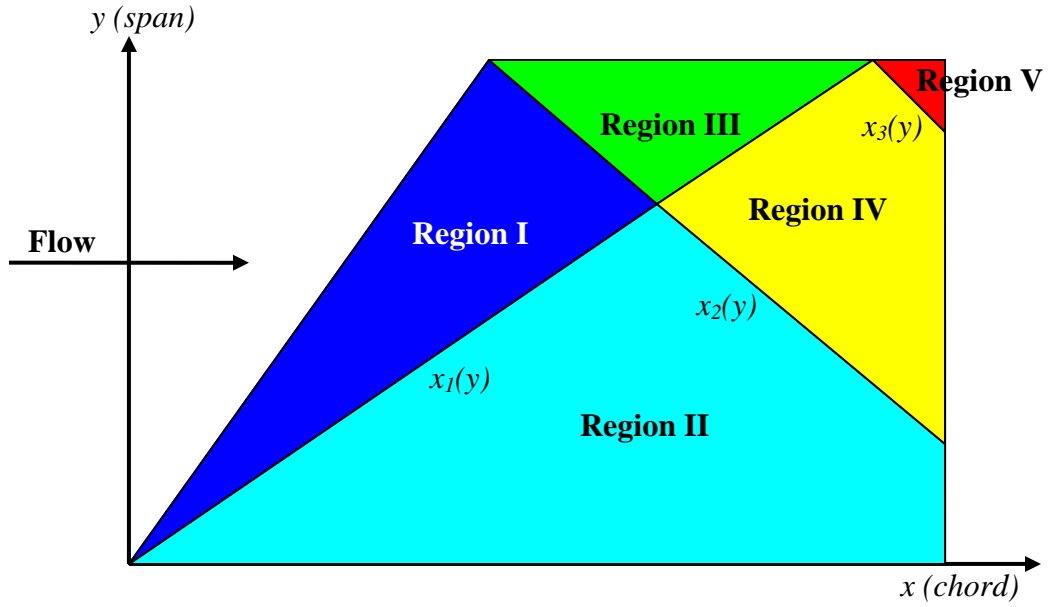


Figure 5: Regions of influence

The regions can be identified by their location in the chord-wise direction as follows:

Region 1: $x < x_1(y)$ and $x < x_2(y)$

Region 2: $x > x_1(y)$ but $x < x_2(y)$

Region 3: $x > x_2(y)$ but $x < x_1(y)$

Region 4: $x > x_1(y)$ and $x > x_2(y)$ but $x < x_3(y)$

Region 5: $x > x_3(y)$

In order to use the zoning laws above $x_1(y)$, $x_2(y)$, and $x_3(y)$ must be determined as a function of the span-wise location, y .

$$x_1(y) = \beta y \quad (4)$$

$$x_2(y) = \tan \Lambda + \beta(1.0 - y) \quad (5)$$

$$x_3(y) = \beta + \beta(1 - y) \quad (6)$$

$$\beta = \sqrt{M^2 - 1.0} = \frac{1}{\tan \mu} \quad (7)$$

Finally, the equations for the pressure differential between the upper and lower surfaces of a planar fin at some angle of attack, α , are derived in References 27 and 28 given in Table 5. For the case of a jet vane, the angle of attack is equal to the deflection angle.

Table 5: Pressure coefficient depending on region (modified from Ref. 32)

| Region | Region Conditional | Differential Pressure Coefficient |
|--------|--|--|
| I | $x < x_1(y)$ and $x < x_2(y)$ | $dC_{p,I} = \frac{4\alpha}{\sqrt{\beta^2 - \tan^2 \Lambda}}$ |
| II | $x > x_1(y)$ but $x < x_2(y)$ | $dC_{p,II} = \frac{4a}{\pi\sqrt{\beta^2 - \tan^2 \Lambda}} \left[\cos^{-1} \frac{\tan \Lambda + \beta T}{T \tan \Lambda + \beta} + \cos^{-1} \frac{\tan \Lambda - \beta T}{T \tan \Lambda - \beta} \right]$ |
| III | $x > x_2(y)$ but $x < x_1(y)$ | $dC_{p,III} = dC_{p,I} - \frac{4\alpha}{\pi\sqrt{\beta^2 - \tan^2 \Lambda}} \left[\cos^{-1} \frac{[x_{tip} + y_{tip}(2\beta + \tan \Lambda)]}{x_{tip} - y_{tip} \tan \Lambda} \right]$ |
| IV | $x > x_1(y)$ and $x > x_2(y)$ but $x < x_3(y)$ | $dC_{p,IV} = dC_{p,II} - \frac{4\alpha}{\pi\sqrt{\beta^2 - \tan^2 \Lambda}} \left[\cos^{-1} \frac{[x_{tip} + y_{tip}(2\beta + \tan \Lambda)]}{x_{tip} - y_{tip} \tan \Lambda} \right]$ |
| V | $x > x_3(y)$ | $dC_{p,V} = \frac{4\alpha}{\pi\sqrt{\beta^2 - \tan^2 \Lambda}} \left[\cos^{-1} \frac{x_{tip} - y_{tip}(\tan \Lambda - 2\beta) + 2 \tan \Lambda}{x_{tip} + (y_{tip} + 2)\tan \Lambda} \right]$ |
| where | | $T = \beta \frac{y}{x}, \quad x_{tip} = x - \tan \Lambda, \quad \text{and} \quad y_{tip} = 1.0 - y$ |

Evvard's theory provides a closed form solution that is exact for small angles of attack. It assumes no shocks and no loss in total pressure. While these assumptions do not hold in reality, other solutions such as supersonic potential methods or CFD analysis would be impractical for use in the optimization program. One-dimensional linearized supersonic aerodynamic theory could also be used to predict the forces and moments on the vanes but it is a less accurate solution than Evvard's theory. Evvard's solution is a better method because it accounts for the disturbance types found in two dimensions,

such as the wing tip effect, that are neglected in a one dimensional analysis. An efficient and accurate method for this application, Evvard's theory is extended here to estimate the forces and moments produced by the vanes depending on their deflection angle in the exhaust flow.

2.7.3 Assumptions

To simplify the jet vane analysis several assumptions were made. First, it is assumed that the vanes are placed immediately downstream of the nozzle exit and the flow of exhaust gases around the vanes is parallel. Parallel flow can be assumed because the nozzle design generated by the performance codes turns the flow to within ten degrees of the axial direction. In addition, the nozzle is designed to be over-expanded at low altitudes and under-expanded at high altitudes, further affecting the direction of the flow as it exits the nozzle. This assumption greatly simplifies the calculations because it allows pressure gradients across the vanes to be neglected. It is further assumed that the average flow velocity experienced by the vanes is equal to the Mach number at the nozzle exit plane. The vanes are considered to be flat plates and testing has shown that low aspect ratio surfaces in high Mach number flows behave accordingly.³³ Real gas effects, vane interactions, losses, and vane erosion have all been neglected. Finally, since only vane deflections up to 15 degrees are considered, it can be safely assumed that the variation of the normal force on the vanes is a linear function of deflection angle. Experimental testing³³ of vane control systems has shown this to be the case.

2.7.4 Methodology

An additional model has been added to the GA optimization code to handle the calculations necessary to simulate a vane control system. After the applicable constants

are transferred in, the program iterates to determine the Mach number at the nozzle exit based on the nozzle expansion ratio and the specific heat ratio for the chosen propellant. The vane itself is currently set as a trapezoid shape with its dimensions normalized by the nozzle exit plane diameter. The root chord is set at 0.9, the tip chord at 0.3, the semi-span at 0.7 and the leading edge sweep angle is 45 degrees. This configuration is similar to the shape of the vanes observed on several common jet vane controlled missiles. In future revisions, the vane dimensions could be included as GA variables to further optimize the control system. A 10 degree deflection angle is assumed in order to determine the pressure coefficient as a linear function of angle of attack.

In order to determine the load distribution on the vane, the flat plate that approximates the vane is divided into rectangular elements. These are currently fixed at 50 elements in the span-wise direction and 40 elements in the chord-wise direction. The code then marches through the elements and calculates the differential pressure coefficient for each element according to the region it lies within. The normal force coefficient and moment coefficient about the leading edge of the vane are calculated from the differential pressure coefficient and summed for the entire plate. Figure 6 shows the elements and differential pressure distribution on a generic thin vane control surface at 10 degrees angle of attack as configured in the actual optimization program. Because the vane is in a high Mach number flow which produces low Mach angles, this particular example only contains three of the five possible regions which are defined by Esvard's theory.

Thrust degradation is an issue with jet vane control systems that does not affect missiles with only aerodynamic control. An estimation of the thrust loss has been made

to account for the thrust degradation that occurs in reality. The two primary contributors to thrust degradation are induced vane drag and viscous drag. The induced vane drag is estimated by calculating the component of the vane normal force that is oriented perpendicular to the axial flow. The viscous drag is estimated by assuming a skin friction drag coefficient of 0.005. This value is a preliminary estimate and is much higher than the 0.003 typically assumed for flat plates. The induced and viscous drag components are summed for all four vanes and then subtracted from the thrust in the 6-DOF simulation. This is currently a very rough estimation for the thrust degradation and the losses could be significantly higher in reality.

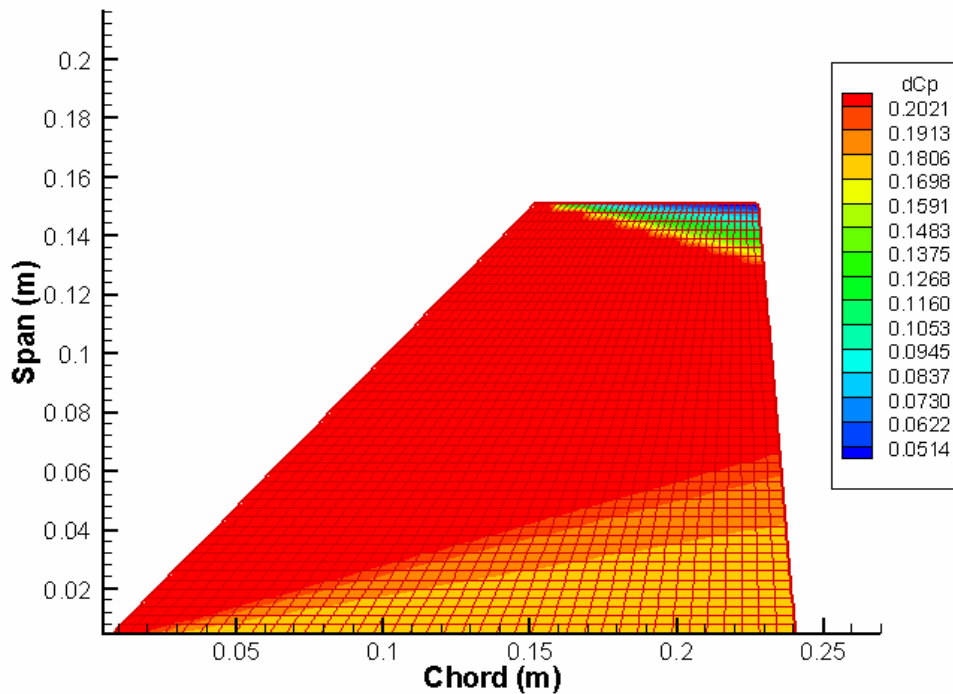


Figure 6: Differential pressure coefficient on a thin vane at 10° angle of attack

The normal force and moment coefficients that are returned from the vane control model are valid for one vane at 10 degrees deflection. These values are first converted

into actual forces and moments and multiplied by two to account for the two sets of vanes, where one set acts as the elevator and the other as a rudder. The forces and moments must be nondimensionalized by dividing by the missile reference area and freestream dynamic pressure. Since freestream dynamic pressure is calculated during the simulation, this step must be completed within the guidance and 6-DOF routines. The moment coefficient must also be transferred from the vane leading edge to the missile center of gravity. Dividing by the deflection angle provides the coefficients $C_{N\delta}$ and $C_{M\delta}$ which are the normal force coefficient and moment coefficient per radian of vane deflection, respectively. The coefficients are now compatible with the aerodynamically generated $C_{N\delta}$ and $C_{M\delta}$ used in the fin control case. The vane control coefficients are substituted for the aerodynamic values in the guidance and 6-DOF routines when vane control is activated. The aerodynamic control coefficients are used when the vane control system becomes inactive after burnout.

2.7.5 Verification

The vane control model is verified by comparing the normal force on the vanes calculated by the program to an approximation obtained from one-dimensional linearized supersonic aerodynamic theory. In static ground tests, this approximation has been shown to be an accurate method of predicting the forces and moments produced by the vanes.³³ Linearized theory provides a relation for the lift coefficient on a thin airfoil at small angle of attack, regardless of shape.³⁴

$$C_L = \frac{4\alpha}{\sqrt{M^2 - 1}} \quad (8)$$

The lift coefficient is defined as:

$$C_L = C_N \cos \alpha - C_A \sin \alpha \quad (9)$$

Since linearized theory only holds for small angles of attack, the normal force coefficient is approximately equal to the lift coefficient. The angle of attack of a vane is equal to its deflection angle, δ , so the resulting equation for normal force coefficient is:

$$C_N \approx \frac{4\delta}{\sqrt{M^2 - 1}} \quad (10)$$

The normal force acting on a vane when assumed to be a linear function of deflection angle is defined as:

$$N = C_{N_\delta} \delta q S_{REF} \quad (11)$$

where the derivative of the normal force coefficient is simply

$$\frac{dC_N}{d\delta} \equiv C_{N_\delta} = \frac{C_N}{\delta} \quad (12)$$

Since the vane deflection is limited to 15 degrees within the code, the linearized theory approximations are expected to be valid.

The normal force values predicted by Evvard's theory as applied in this effort correlate well to the values derived from linearized supersonic theory. The percent difference between the two methods of calculation was generally observed to be less than 5 percent. For example, the vane shown in Figure 6 deflected 10 degrees in a Mach 3.6 exhaust flow was predicted by Evvard's theory to produce a normal force of 5336 N. Assuming the same vane geometry and setup, the relation derived from linear supersonic theory approximates the normal force to be 5502 N. A comparison plot of Evvard's theory calculations and values derived from linear supersonic aerodynamic theory is shown in Figure 7. Linear supersonic theory over-predicts the normal force as expected

because it is only a one-dimensional analysis method and it neglects the effects of the Mach cones that Eward's theory takes into account. The close agreement between the results from Eward's solution and one-dimensional linearized supersonic aerodynamics provides verification that the program is functioning correctly. Differences that do exist can be attributed to the greater degree of accuracy that Eward's method affords being a two-dimensional analysis. There is no experimental data available, however, to allow the code to be validated.

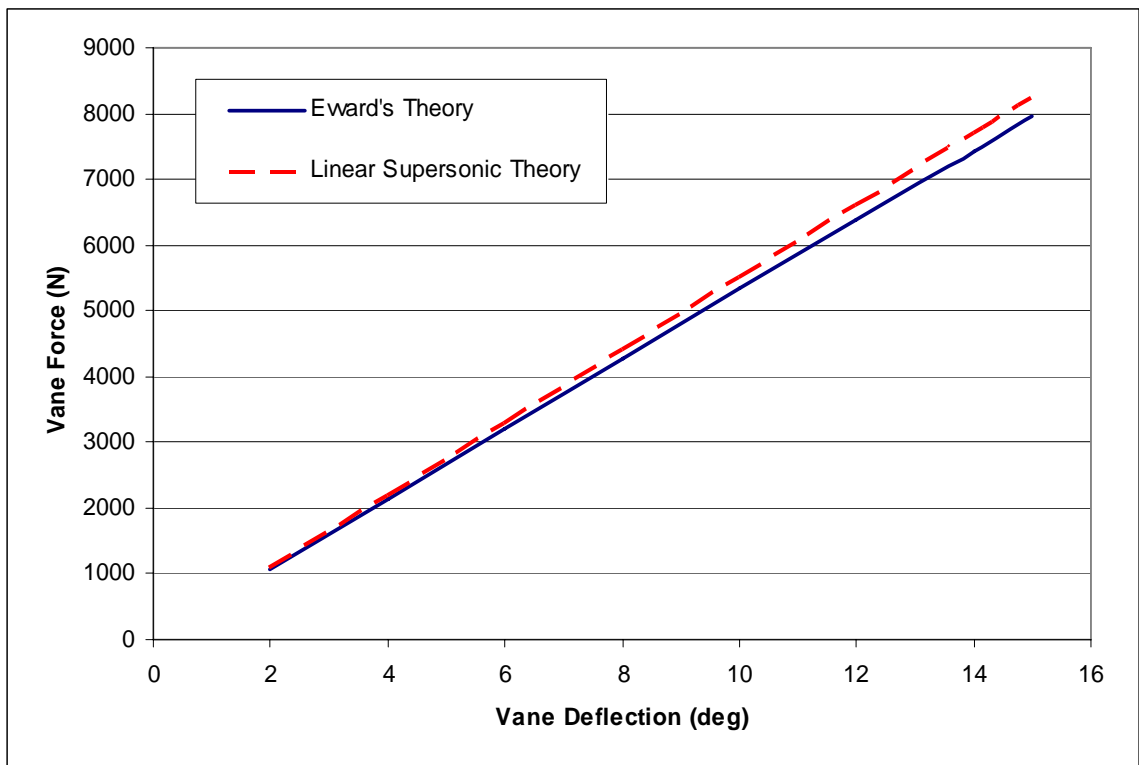


Figure 7: Vane force as a function of vane deflection

3. RESULTS

The liquid missile system model has been validated against a known missile configuration and the results are provided. Performance data for a generic short range ballistic missile similar to the SCUD-B are given. Results from a simulated flight of the same missile design are compared to the known performance data. Results from unguided missile optimization runs with either Aerodsn or Missile Datcom producing the aerodynamic coefficients will also be presented. The next section of results examines Aerodsn and Missile Datcom produced missiles with aerodynamic control systems. Simulating aerodynamically controlled designs highlights the differences between the aerodynamic codes and offers a much more complete comparison than the unguided cases. Finally, optimized missile designs featuring aerodynamic control, vane control, and no control are compared through a series of different cases. All of the results presented here employ the variable I_{sp} upgrade that was discussed previously.

3.1 Model Validation

The liquid missile performance model is validated by flying a single run case with a configuration very similar to the SCUD-B. A diagram of the SCUD-B is shown in Figure 8 and the corresponding missile data¹⁷ is given in Table 6.

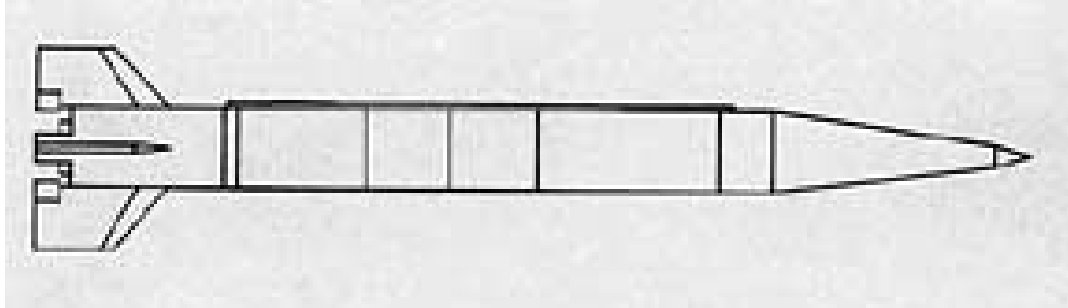


Figure 8: SCUD-B diagram (from Ref. 35)

Table 6: Missile configuration and performance data (from Ref. 17)

| Parameter | Value | |
|------------------------|-------------------|-----------|
| Missile Length | 10.93 m | 35.86 ft |
| Missile Diameter | 0.88 m | 2.887 ft |
| Launch Weight | 5.83 metric tons | 12850 lbs |
| Warhead Weight | 1000 kg | 2200 lbs |
| Range | 300 km | 186 mi |
| Thrust | 13.35 metric tons | 29436 lbs |
| Isp | 238 sec | 238 sec |
| Burn time | 62 sec | 62 sec |
| Chamber pressure | 6.71 MPa | 973.7 psi |
| Nozzle expansion ratio | 10.32 | 10.32 |

This set of data was input into the performance model along with additional data such as the fin geometry, and the resulting design was flown by the 6-DOF simulation. A list of the GA variables that were used for this design is given in Table 7. The I_{sp} and other fuel parameters were set manually in the liquid fuels subroutine, and both Aerodsn and Missile Datcom were used as aerodynamic predictors for this case. One difference of note is the SCUD-B has a conical nose section while the simulated missile design has a blunted ogive nose. This fact, however, should have little impact on the performance of the simulated missile when compared to the SCUD-B.

Table 7: List of GA variables for SCUD-B comparison

| Value | GA variable name |
|-----------|---------------------------------------|
| 4.000000 | propellant type |
| 1.120000 | equivalence ratio |
| 973.70000 | chamber pressure (psi) |
| 19.253000 | nozzle throat area (in ²) |
| 10.320000 | nozzle expansion ratio |
| 0.6000000 | fractional nozzle length |
| 62.000000 | burn time (sec) |
| 2200.0000 | payload mass (lbs) |
| 2.8887000 | missile body diameter (ft) |
| 3.3290000 | nose length/dbody |
| 0.1114300 | nose dia/dbody |
| 1.6138000 | fin2 root chord fraction = cr/dbody |
| 0.6197000 | fin2 taper ratio |
| 38.600000 | fin2 le angle (degrees) |
| 0.7693000 | fin2 semi-span fraction = b2/dbody |
| 1.0000000 | x loc of fin2 (% totlen) |
| 60000.000 | autopilot time on delay - tdelay |
| 0.5078700 | autopilot time constant - tau |
| 0.5800000 | autopilot damping coef - zeta |
| 63.571430 | cross over frequency - cohz |
| 2.7143000 | pronav gain -pronvg |
| 85.000000 | initial launch angle (degrees) |

The results of the model validation are given in Table 8 and a rendering of the resulting missile compared to the SCUD diagram is shown in Figure 9. All other design parameters not listed in Table 8 were either direct inputs into the model, or no data was available for comparison. The results show close agreement between the known missile's performance and the performance of the model which used Aerodsn. Missile Datcom predicts the range to be about 25 km farther than the actual SCUD. For both models, the major design parameters are only a few percent off from the actual values. This result provides a high level of confidence that the missile performance model utilizing Aerodsn produces accurate results.

Table 8: Model validation for the SCUD-B

| Parameter | Known | Model (Aerodsn) | Model (Datcom) |
|----------------|--------------|-----------------|----------------|
| Missile Length | 10.93 m | 11.40 m | 11.40 m |
| Range | 299.4 km | 304.1 km | 324.7 km |
| Launch Weight | 5828 kg | 5769 kg | 5769 kg |
| Thrust | 13.35 m tons | 13.18 m tons | 13.18 m tons |

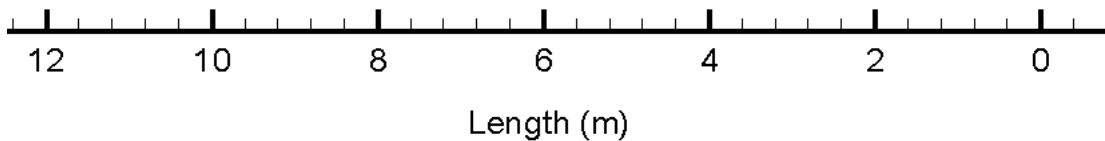
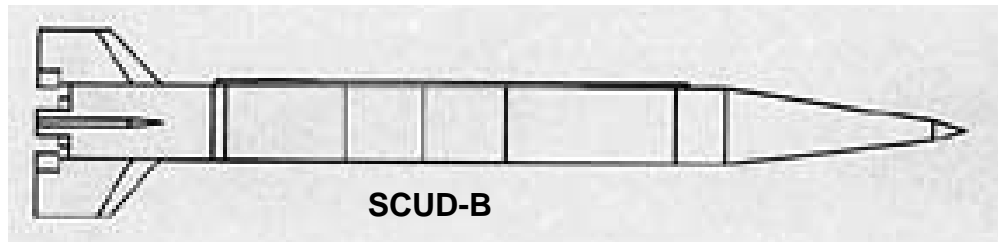


Figure 9: Comparison of the simulated missile with the SCUD-B

3.2 Unguided Results

The following results are from a series of unguided missile optimization runs. The primary objective of this set of missile optimizations is to obtain missile designs using both aerodynamic prediction routines so the results can be compared. The optimization codes are identical aside from changes made to accommodate their respective aerodynamic prediction codes. The goal of each optimization run was to determine the viability of a single-stage, liquid propelled ballistic missile with specific constraints delivering a payload to a range of 700 km. The primary constraints included a

maximum thrust limit of 28 metric tons, IRFNA/RP-1 propellant, and a payload of 2000 kg. The specific goals and constraints used for these optimization runs are not important to this thesis other than to provide a common baseline.

In order to determine the feasibility of such a missile, the GA was configured to run a single goal case to match a range of 700 km. Alternatively, the GA could have been set up to maximize range, but either strategy would determine whether a missile with these requirements could achieve the range goal. Matching the thrust and payload could have been additional GA goals, but doing so would have complicated the runs. The optimization program works more efficiently when only a single goal is employed, so limiting the number of goals to only those that are high priorities is advantageous. To account for these limitations though, a thrust ceiling was fixed in the program and the payload, being one of the 27 GA variables, was limited to be 2000 kg in all cases.

The complete GA input file, where the GA settings and design variable bounds are defined, is provided in Appendix A. The input file in Appendix A was used for all four of the runs conducted for this particular study. Table 9 shows the major differences between each run. The aerodynamics column identifies which code was used for the aerodynamic prediction for a particular case and the Mach limit column lists the maximum allowable Mach number for each case. All of the cases were run to 100 generations with 300 members in each generation. The convergence history of each case was recorded and all of the cases were found to be sufficiently converged with this configuration.

Table 9: Case setup

| Case | Aerodynamics | Mach Limit |
|------|--------------|------------|
| 1 | Aerodsn | 7.1 |
| 2 | Aerodsn | 8.5 |
| 3 | Datcom | 7.1 |
| 4 | Datcom | 8.5 |

A note should be made about the Mach limit, which has not been mentioned until now and is listed in the table above. Aerodsn uses supersonic theory to predict the aerodynamics and the accuracy of this method becomes marginal in the hypersonic range. However, an extrapolation of the theory in this range is adequate for preliminary designs such as the ones in question. To account for this fact, in the original Aerodsn code, an upper bound on the Mach number was fixed at 7.1. As the plots show, the optimized missile designs were not able to achieve the goal range with this configuration. Close examination revealed that the Mach number bound was a limiting factor in the missile performance. Revisions made to the Aerodsn code prior to this study provided an increased level of confidence in the aerodynamic predictions at high Mach numbers. The Mach number limit was raised accordingly until the GA was able to find a design capable of reaching the target. The new Mach number upper bound of 8.5 was used in conjunction with the previous two Mach 7.1 optimization runs to further support the comparisons of Aerodsn and Missile Datcom.

Performance plots generated from these optimization runs are provided in Figures 10 through 14. Figure 10 plots the trajectory of each of the four resulting missile designs. The Aerodsn, Mach 7.1 case flies slightly higher and farther than did the comparable Missile Datcom design, but the two Mach 8.5 missiles have almost identical trajectories. The altitude as a function of time for the cases is shown in Figure 11 and shows again

how the Aerodsn, Mach 7.1 design flies higher and slower than the Missile Datcom missile. Figure 12 plots the thrust as a function of time for each missile. The Mach 8.5 missiles start with about the same thrust, but the Aerodsn missile burns out with a greater final thrust. The lower Mach number cases have quite different thrust curves. The Datcom thrust is much higher initially, but its curve is very flat, and the Aerodsn missile eventually achieves the maximum thrust value. The Mach number as a function of time is plotted in Figure 13 for all cases and the curves show good agreement. The brief dips present in the curves are a result of temperature fluctuations within the atmosphere that affect the speed of sound and thus the Mach number. Lastly, Figure 14 shows that the range as a function of time is very similar for comparable cases.

Results from the four ballistic missile optimization runs demonstrate preliminary design level agreement between the aerodynamic codes. The maximum achievable ranges for cases with comparable Mach number limits are very similar regardless of the aerodynamic code used. In addition, the trajectory, thrust, and Mach number as a function of time are all very similar for comparable runs. The provided missile renderings demonstrate that typical missile designs were achieved with only small differences between the designs, mostly occurring in the size and placement of the fin sets. This can be seen in Figures 15 through 18 which show the external configuration of each of the resulting missile designs along with important performance data. Figure 19 provides an illustration of all four missile designs side-by-side for easy comparison of their external geometries.

While the performance plots indicate close agreement between the two different aerodynamic prediction routines at comparable Mach number limits, these results alone

cannot validate the aerodynamic prediction codes or even confirm that their predictions are similar to one another's. The reason for this is that much of the flight time for these ballistic cases occurs at very high altitudes. Because the missiles have no aerodynamic control, the primary aerodynamic force is drag, and above 10,000 m the drag force is very small. As shown in Figure 10, these missile designs spend a considerable amount of time at altitudes where the aerodynamics has little effect. For cruise missiles powered by air breathing propulsion, the comparison and conclusion could be significantly different.

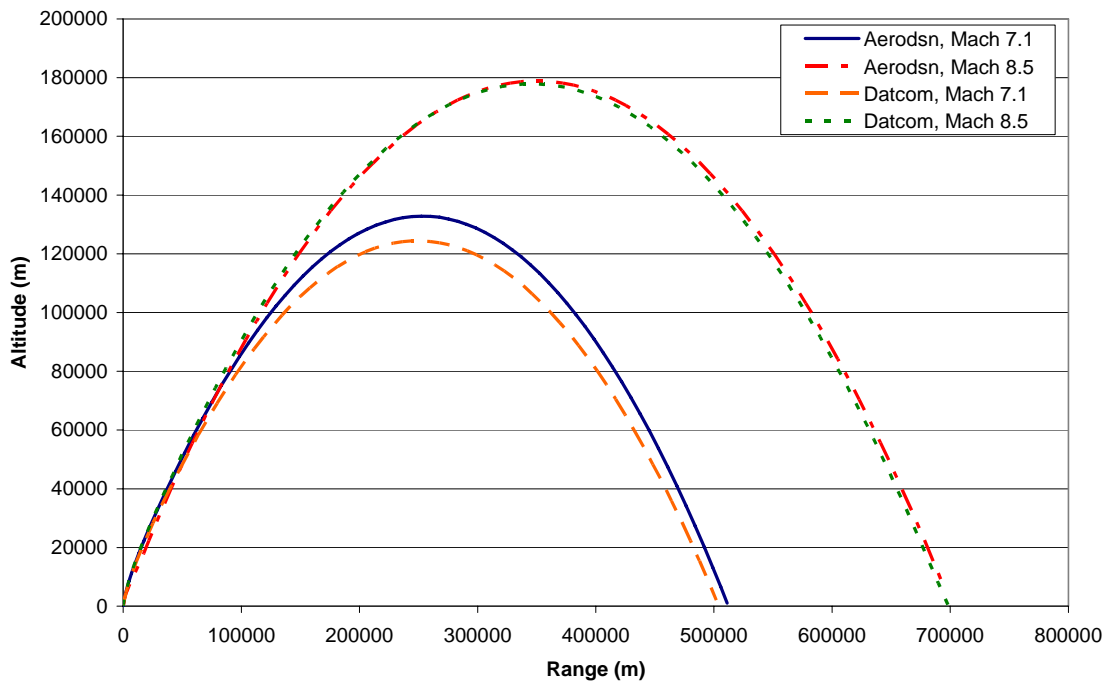


Figure 10: Trajectory plot

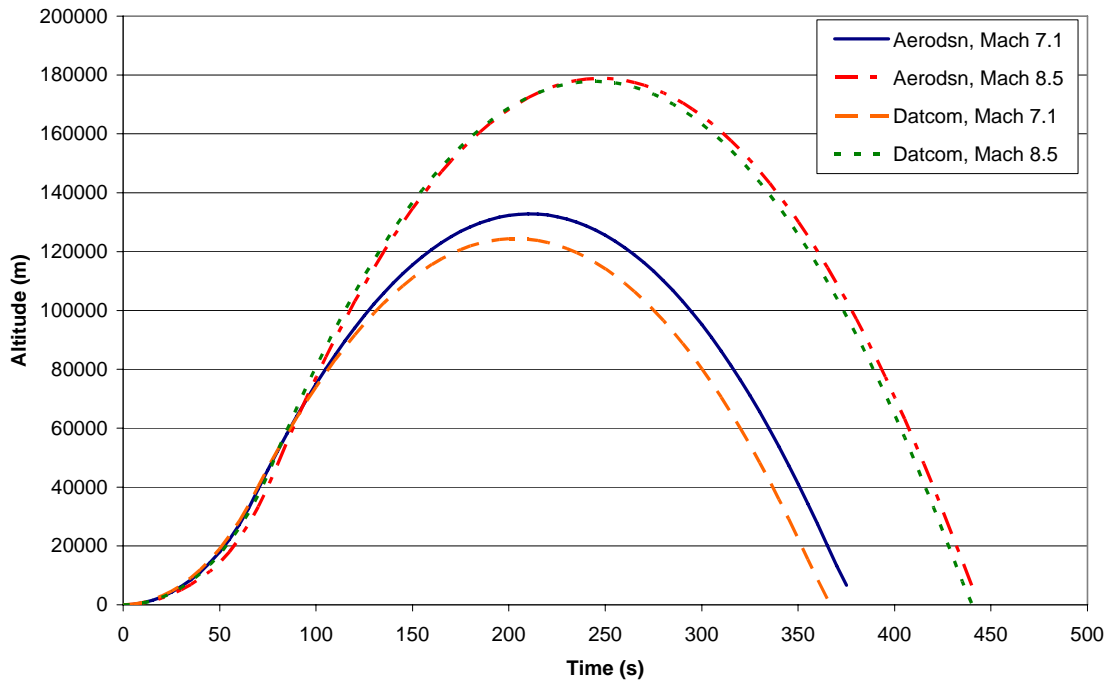


Figure 11: Altitude as a function of time

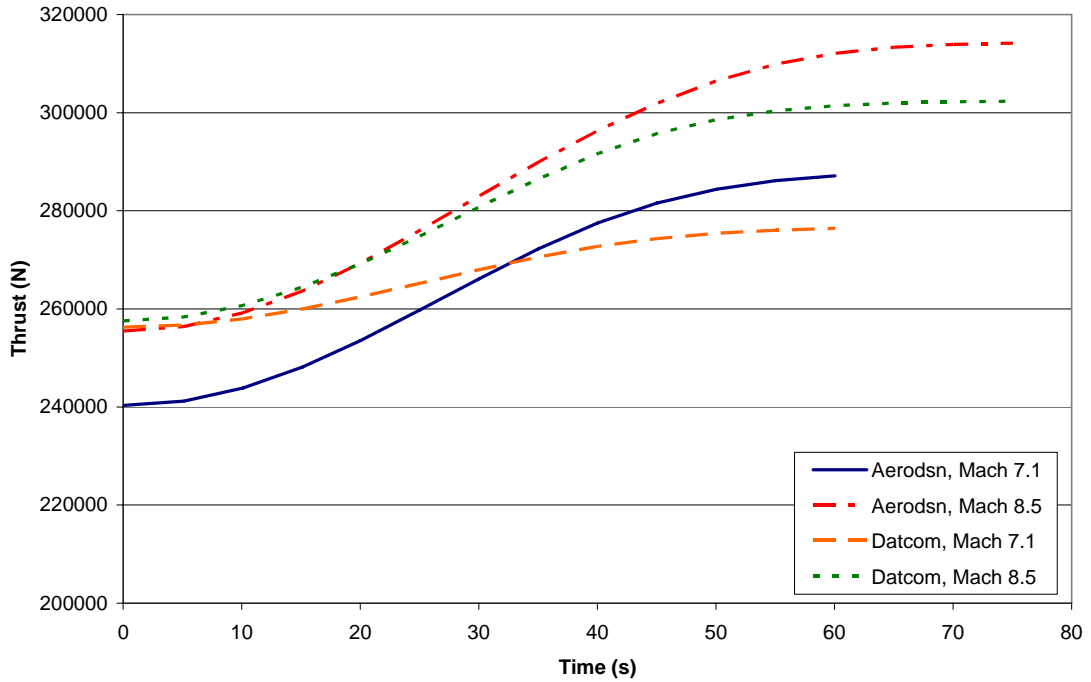


Figure 12: Thrust as a function of time

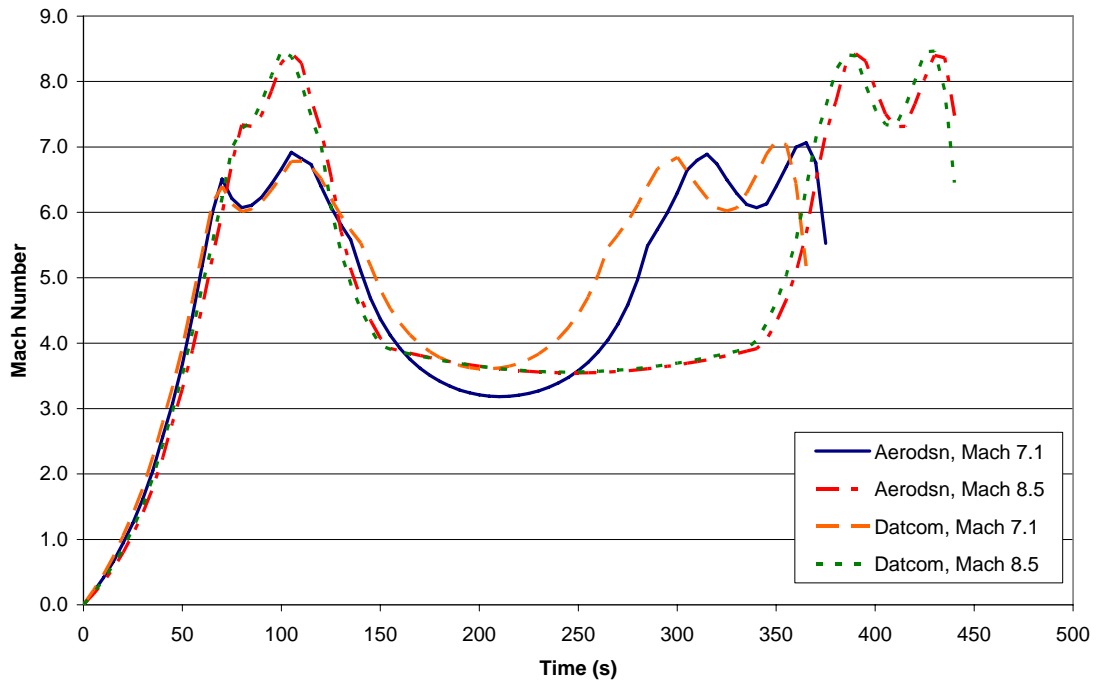


Figure 13: Mach number as a function of time

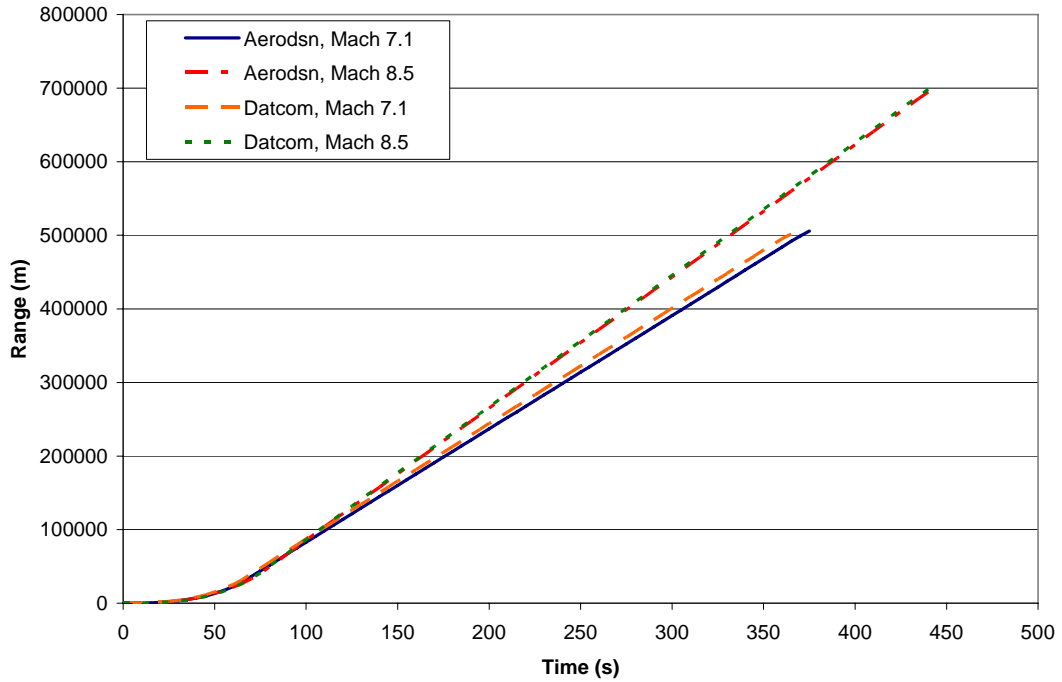


Figure 14: Range as a function of time

Aero Code: Aerodsn
 Range: 512.1 km
 Initial Mass: 10783 kg
 Flight Time: 381.33 s

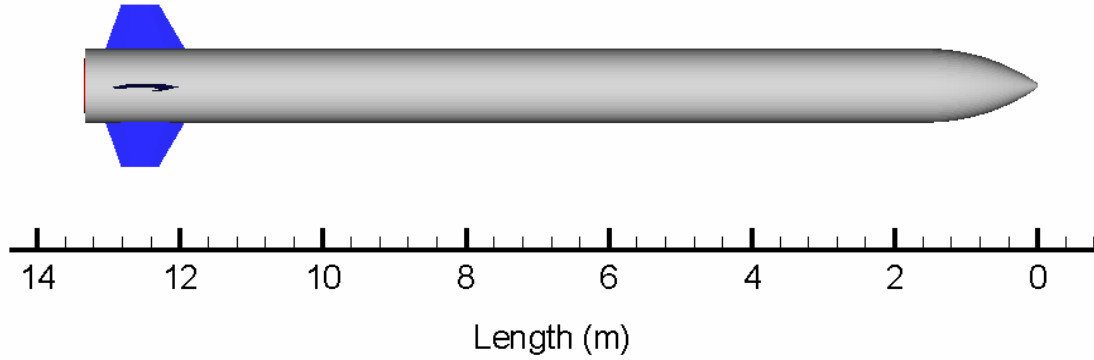


Figure 15: Case 1 missile external geometry

Table 10: Case 1 GA variables

| Value | GA variable name |
|-----------|---------------------------------------|
| 4.0000000 | propellant type |
| 0.6526419 | equivalence ratio |
| 1210.3718 | chamber pressure (psi) |
| 24.418379 | nozzle throat area (in ²) |
| 14.360078 | nozzle expansion ratio |
| 0.8200000 | fractional nozzle length |
| 70.845139 | burn time (sec) |
| 4400.0000 | payload mass (lbs) |
| 3.4761906 | missile body diameter (ft) |
| 2.4126983 | nose length/dbody |
| 0.1535484 | nose dia/dbody |
| 2.8709679 | fin2 root chord fraction = cr/dbody |
| 0.2951613 | fin2 taper ratio |
| 20.047245 | fin2 le angle (degrees) |
| 0.8870968 | fin2 semi-span fraction = b2/dbody |
| 1.0000000 | x loc of fin2 (% totlen) |
| 7.9804306 | autopilot time on delay - tdelay |
| 0.7944882 | autopilot time constant - tau |
| 0.7816536 | autopilot damping coef - zeta |
| 57.857143 | cross over frequency - cohz |
| 6.6190476 | pronav gain -pronvg |
| 72.888885 | initial launch angle (degrees) |

Aero Code: Aerodsn
 Range: 700.9 km
 Initial Mass: 12602 kg
 Flight Time: 444.1 s

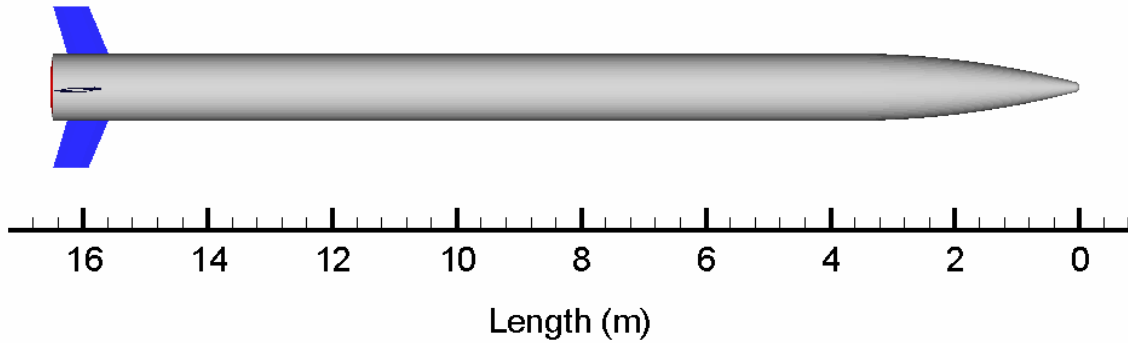


Figure 16: Case 2 missile external geometry

Table 11: Case 2 GA variables

| Value | GA variable name |
|-----------|---------------------------------------|
| 4.0000000 | propellant type |
| 1.2954991 | equivalence ratio |
| 940.31311 | chamber pressure (psi) |
| 38.152493 | nozzle throat area (in ²) |
| 23.606653 | nozzle expansion ratio |
| 0.6600000 | fractional nozzle length |
| 78.935028 | burn time (sec) |
| 4400.0000 | payload mass (lbs) |
| 3.5396826 | missile body diameter (ft) |
| 3.4047618 | nose length/dbody |
| 0.1535484 | nose dia/dbody |
| 0.6129032 | fin2 root chord fraction = cr/dbody |
| 0.8596774 | fin2 taper ratio |
| 22.834646 | fin2 le angle (degrees) |
| 0.6935484 | fin2 semi-span fraction = b2/dbody |
| 0.9857143 | x loc of fin2 (% totlen) |
| 3000.0000 | autopilot time on delay - tdelay |
| 0.5244095 | autopilot time constant - tau |
| 0.5578740 | autopilot damping coef - zeta |
| 63.571430 | cross over frequency - cohz |
| 4.3333335 | pronav gain -pronvg |
| 85.317459 | initial launch angle (degrees) |

Aero Code: Missile Datcom
 Range: 503.8 km
 Initial Mass: 10711.7 kg
 Flight Time: 366.9 s

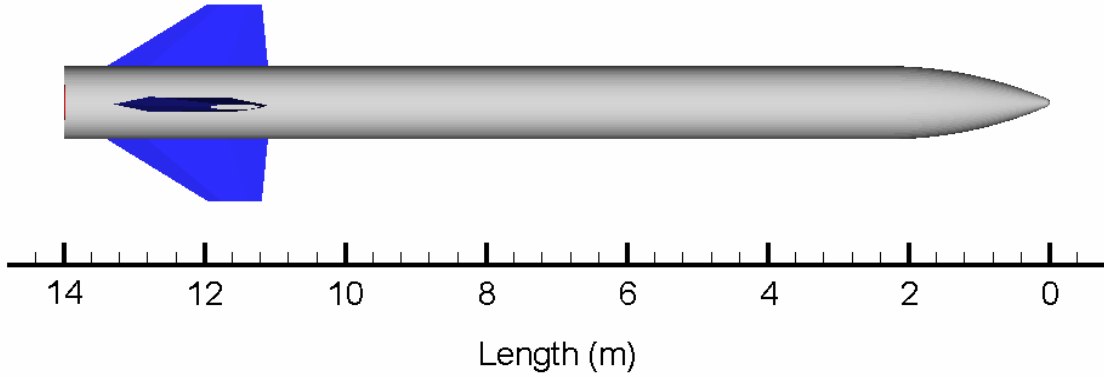


Figure 17: Case 3 missile external geometry

Table 12: Case 3 GA variables

| Value | GA variable name |
|------------|---------------------------------------|
| 4.0999999 | propellant type |
| 1.1751468 | equivalence ratio |
| 1019.56950 | chamber pressure (psi) |
| 32.385143 | nozzle throat area (in ²) |
| 9.657535 | nozzle expansion ratio |
| 0.9000000 | fractional nozzle length |
| 67.547630 | burn time (sec) |
| 4400.0000 | payload mass (lbs) |
| 3.4126985 | missile body diameter (ft) |
| 2.2142856 | nose length/dbody |
| 0.1187097 | nose dia/dbody |
| 2.1935484 | fin2 root chord fraction = cr/dbody |
| 0.3403226 | fin2 taper ratio |
| 5.6456695 | fin2 le angle (degrees) |
| 0.8387097 | fin2 semi-span fraction = b2/dbody |
| 0.9571428 | x loc of fin2 (% totlen) |
| 2998.0000 | autopilot time on delay - tdelay |
| 0.7614173 | autopilot time constant - tau |
| 0.9629921 | autopilot damping coef - zeta |
| 72.142860 | cross over frequency - cohz |
| 1.4761904 | pronav gain -pronvg |
| 84.857140 | initial launch angle (degrees) |

Aero Code: Missile Datcom
 Range: 698.1 km
 Initial Mass: 12084 kg
 Flight Time: 440.2 s

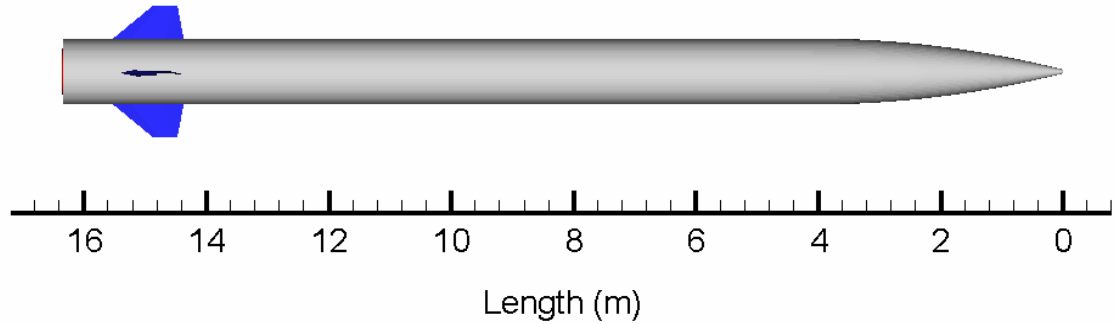


Figure 18: Case 4 missile external geometry

Table 13: Case 4 GA variables

| Value | GA variable name |
|-----------|---------------------------------------|
| 4.0000000 | propellant type |
| 1.0048923 | equivalence ratio |
| 946.18396 | chamber pressure (psi) |
| 36.686218 | nozzle throat area (in ²) |
| 18.692759 | nozzle expansion ratio |
| 0.8200000 | fractional nozzle length |
| 77.176353 | burn time (sec) |
| 4400.0000 | payload mass (lbs) |
| 3.5396826 | missile body diameter (ft) |
| 3.8015873 | nose length/dbody |
| 0.0722581 | nose dia/dbody |
| 1.0645162 | fin2 root chord fraction = cr/dbody |
| 0.3403226 | fin2 taper ratio |
| 10.755905 | fin2 le angle (degrees) |
| 0.5000000 | fin2 semi-span fraction = b2/dbody |
| 0.9500000 | x loc of fin2 (% totlen) |
| 2998.0000 | autopilot time on delay - tdelay |
| 0.2157480 | autopilot time constant - tau |
| 0.6388977 | autopilot damping coef - zeta |
| 72.142860 | cross over frequency - cohz |
| 1.4761904 | pronav gain -pronvg |
| 85.777779 | initial launch angle (degrees) |

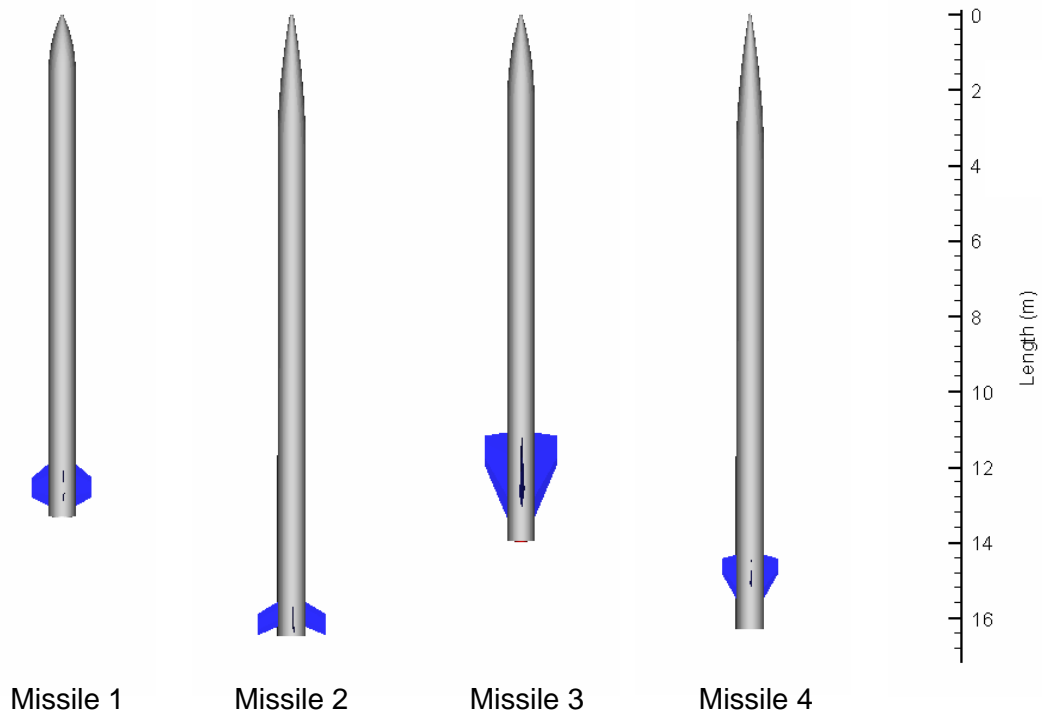


Figure 19: Missile external geometry comparison

3.3 Aerodynamic Guided Results

While Aerodsn shows good agreement with Missile Datcom for unguided missile designs, comparing optimized designs of guided missiles is a much better test. The aerodynamic analysis plays a much more critical role when the aerodynamic surfaces are actively being used to direct the missile to a target. The following results compare guided missile designs that were optimized using the two aerodynamic codes. The goals were set to minimize the miss distance to a target and minimize system mass, both common goals in real-world missile development. For the optimization, the target was set at 122 km (400,000 ft) in the x-direction (down range), 7.62 km (25,000 ft) in the y-direction, and moving with a velocity of -15.24 m/s (-50 ft/sec) on the y-direction. Each case had 100 members per generation and was run for 100 generations. The necessary

number of members per generation is dependent on the number of bits required to define the design space.⁴ A plot of the convergence history for these cases is given in Figure 20 and shows there is little increase in fitness for either design during the last 50 generations. The stair-stepping convergence common to GA optimizations can also be clearly seen in this figure.

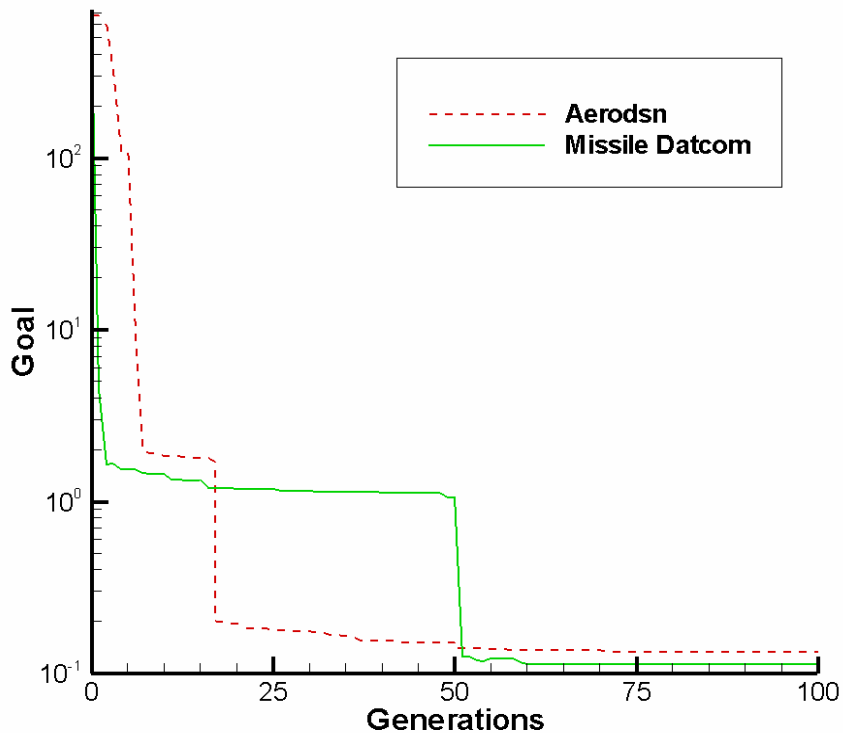


Figure 20: Convergence history

Figures 21 and 22 show the two resulting missile designs with the corresponding aerodynamics code, miss distance, take-off weight and flight time listed. Both missiles were able to hit the target but there are some differences in the designs. The Missile Datcom optimized missile is slightly longer, but much slimmer and lighter than the Aerodsn missile. Most notably, the diameter of the Aerodsn missile is over a foot larger than the Missile Datcom design as can be seen in Tables 14 and 15 which provide a full

list of the GA variables for each design. Both missiles have the fins placed as far aft as possible, and the flight times only differ by 16 seconds. The trajectories of these flights are plotted in Figure 23. The Aerodsn missile takes a much higher altitude approach than does the Missile Datcom designed missile.

The optimized missile configurations were also flown with the aerodynamic code not used for their optimization, and these trajectories are also shown in Figure 23. When the Missile Datcom optimized missile was flown using Aerodsn, the program predicted that the missile would land over 24 km from the target; it did not have the range to reach the goal. Missile Datcom, however, predicts that the Aerodsn optimized missile will hit the target. These results suggest that Aerodsn may be over predicting the drag on a missile. On the other hand, Missile Datcom might be overly optimistic and could be under predicting the drag. It is impossible to tell from this analysis which aerodynamic predictor is more accurate, but it is a safe assumption that the Aerodsn optimized missile is a more conservative design since both aerodynamic codes will fly it to the target. But, if minimizing weight is a major goal, Missile Datcom clearly predicts that this flight can be made with a much lighter missile. Regardless, the GA produced designs are similar to current real-world missile configurations and both codes agree that the target can be reached with aerodynamic control.

Aero Code: Aerodsn
 Miss Distance: 0.01 m
 Initial Mass: 6066 kg
 Flight Time: 250.6 s

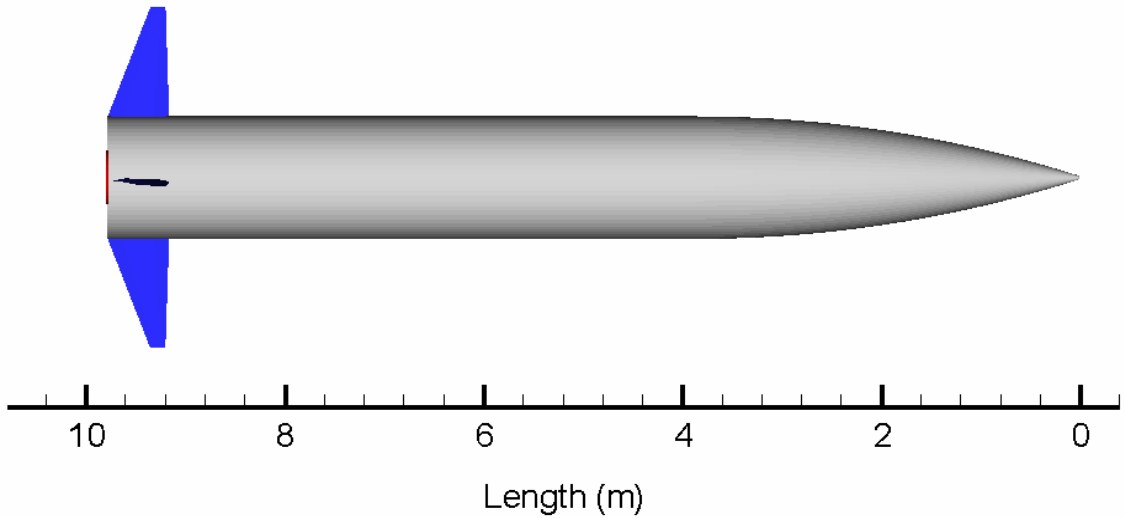


Figure 21: Aerodsn optimized, guided missile external geometry

Table 14: GA variables for Aerodsn optimized missile

| Value | GA variable name |
|------------|---------------------------------------|
| 4.09999990 | propellant type |
| 1.18982390 | equivalence ratio |
| 734.833680 | chamber pressure (psi) |
| 35.4643210 | nozzle throat area (in ²) |
| 10.0273970 | nozzle expansion ratio |
| 0.75999999 | fractional nozzle length |
| 34.6604800 | burn time (sec) |
| 4400.00000 | payload mass (lbs) |
| 4.04761890 | missile body diameter (ft) |
| 3.12698410 | nose length/dbody |
| 0.03741936 | nose dia/dbody |
| 0.50000000 | fin2 root chord fraction = cr/dbody |
| 0.25000000 | fin2 taper ratio |
| 1.92913390 | fin2 le angle (degrees) |
| 0.88709676 | fin2 semi-span fraction = b2/dbody |
| 1.00000000 | x loc of fin2 (% totlen) |
| 12.1232880 | autopilot time on delay - tdelay |
| 0.52992123 | autopilot time constant - tau |
| 0.99000001 | autopilot damping coef - zeta |
| 60.7142870 | cross over frequency - cohz |
| 2.71428560 | pronav gain -pronvg |
| 68.7460330 | initial launch angle (degrees) |

Aero Code: Missile Datcom
 Miss Distance: 0.20 m
 Initial Mass: 4799 kg
 Flight Time: 234.1 s

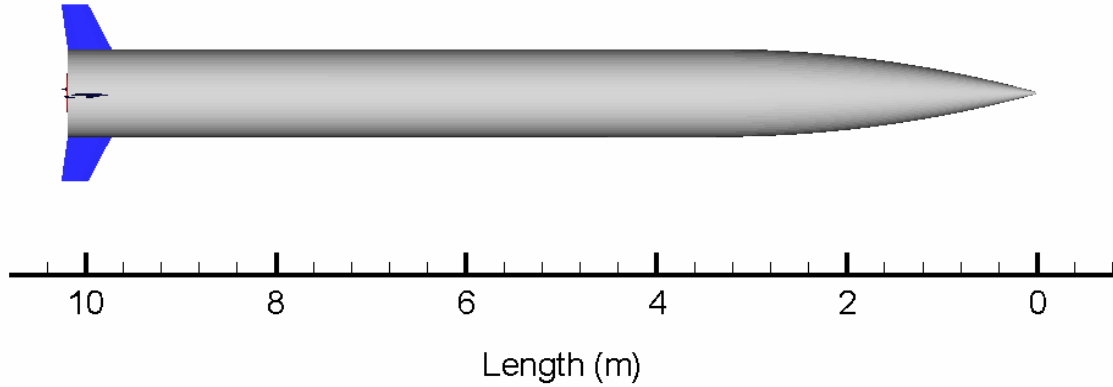


Figure 22: Missile Datcom optimized, guided missile external geometry

Table 15: GA variables for Datcom optimized missile

| Value | GA variable name |
|-----------|---------------------------------------|
| 4.000000 | propellant type |
| 1.2778865 | equivalence ratio |
| 752.44617 | chamber pressure (psi) |
| 23.636364 | nozzle throat area (in ²) |
| 8.2837572 | nozzle expansion ratio |
| 0.780000 | fractional nozzle length |
| 32.857841 | burn time (sec) |
| 4400.0000 | payload mass (lbs) |
| 3.0317461 | missile body diameter (ft) |
| 3.6428571 | nose length/dbody |
| 0.0316129 | nose dia/dbody |
| 0.500000 | fin2 root chord fraction = cr/dbody |
| 0.6112903 | fin2 taper ratio |
| 27.944881 | fin2 le angle (degrees) |
| 0.500000 | fin2 semi-span fraction = b2/dbody |
| 1.000000 | x loc of fin2 (% totlen) |
| 24.608610 | autopilot time on delay - tdelay |
| 0.7393701 | autopilot time constant - tau |
| 0.9437008 | autopilot damping coef - zeta |
| 63.571430 | cross over frequency - cohz |
| 4.5238094 | pronav gain -pronvg |
| 74.730156 | initial launch angle (degrees) |

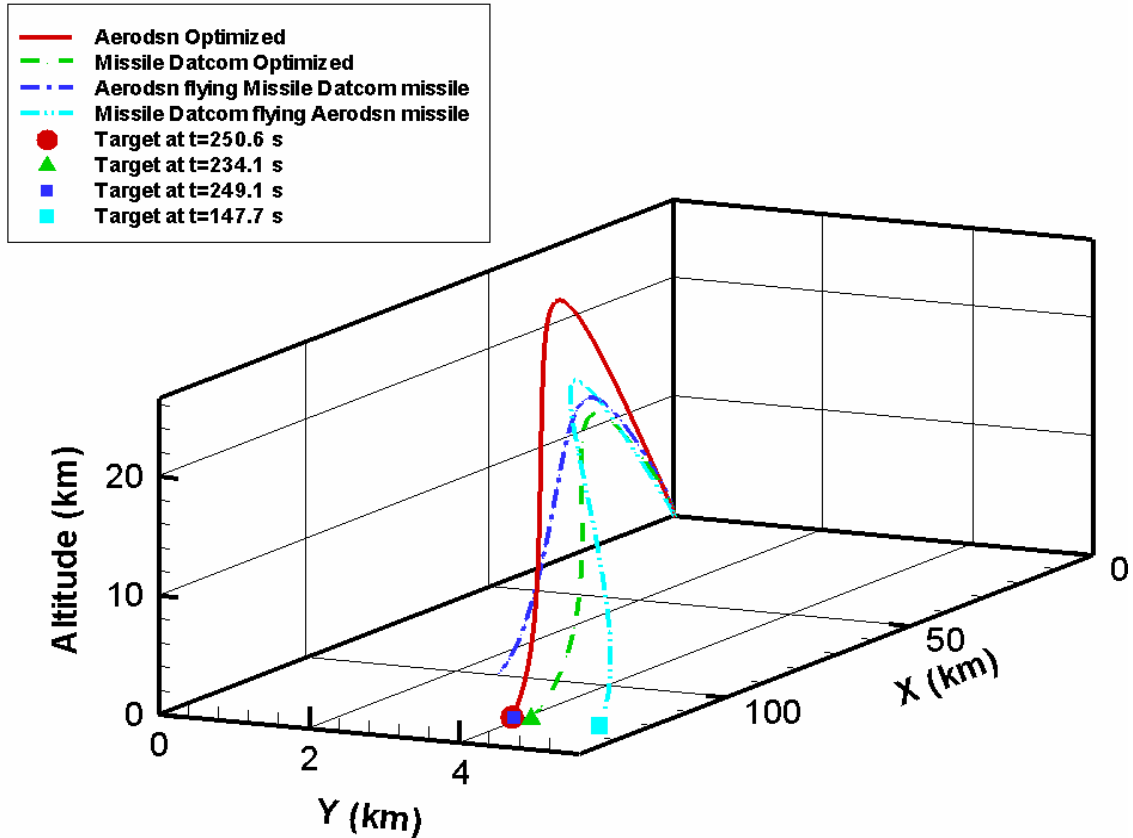


Figure 23: Aerodynamically controlled flight trajectories

3.4 Vane Control Guided Results

The jet vane control system model has been integrated into the liquid performance model. Results from GA runs to optimize a variety of missiles are presented here. Three types of missiles were considered so performance comparisons could be made. These include a missile with no active control system, an aerodynamically controlled missile, and a missile with a vane control system. For each of these optimization runs, the target was placed at $x=122$ km (400,000 ft), $y=7.62$ km (25,000 ft), and at $z=0$ km. The target was kept stationary and each missile had a payload of 2000 kg. The goals were set to minimize the miss distance and minimize the take-off weight. The aerodynamic

prediction for all cases was handled by Aerodsn. The results are presented below, starting with the missile design that results from the optimization run for each case. After an optimized missile design of each control type was obtained, the target's position was moved to several different locations and each optimized design was flown again, attempting to hit the new targets. Clearly, the unguided missile design is not affected by a change in the position of the target, but it is still shown in each plot for reference.

The first optimized design, shown in Figure 24, is the missile with no control. It is about 12 m long with nearly rectangular fins set a noticeable distance from the aft end of the missile. The missile has a mass of 10300 kg and has a flight time of about 150 seconds. A complete set of design parameters for this missile is provided in Table 16. As expected, this missile only comes within 7.5 km of the target because it lacks a control system. The main purpose of this design is to serve as a baseline to which the other cases can be compared. The trajectory of the missile, plotted in the Figures 27 through 31, is unchanged regardless of the location of the target.

The external geometry of the missile with aerodynamic control is shown in Figure 25 along with other important details pertaining to its flight. The missile design appears very reasonable at about 11 meters long with small swept fins placed as far aft as possible. It is also quite thin with a long sharp nose. This design is predicted to hit the target with a great deal of accuracy, coming closer than the other two designs. It is much smaller and lighter than either the unguided or vane control missile, but its flight time is also much longer. As can be seen from the list of GA variables in Table 17, this particular design has a burn time of only about 32 seconds. However, it is able to use its

aerodynamic control to glide the rest of the way into the target. This fact explains its low take-off weight but relatively long flight time.

Figure 26 provides the results from the vane control missile optimization run. Compared to the missile with aerodynamic control, this design is much larger, weighing almost 3000 kg more even though their respective optimization runs had the same goal of minimizing the initial weight. This result is not unexpected though because this type of control system can only provide control when the missile is thrusting. As a result, the GA selects long burn times in order to provide control for as long as possible. This substantially increases the weight of the missile because of the additional propellant that must be carried. The aerodynamically controlled missile is not required to carry as much propellant to reach the target, but it does fly significantly slower because thrust is only provided for a short period of time. Flight time could be added as a third goal and this would most likely bring the weight of the aerodynamically controlled missile closer to that of the vane controlled design.

Aero Code: Aerodsn
 Miss Distance: 7.46 km
 Initial Mass: 10301 kg
 Flight Time: 148.05 s

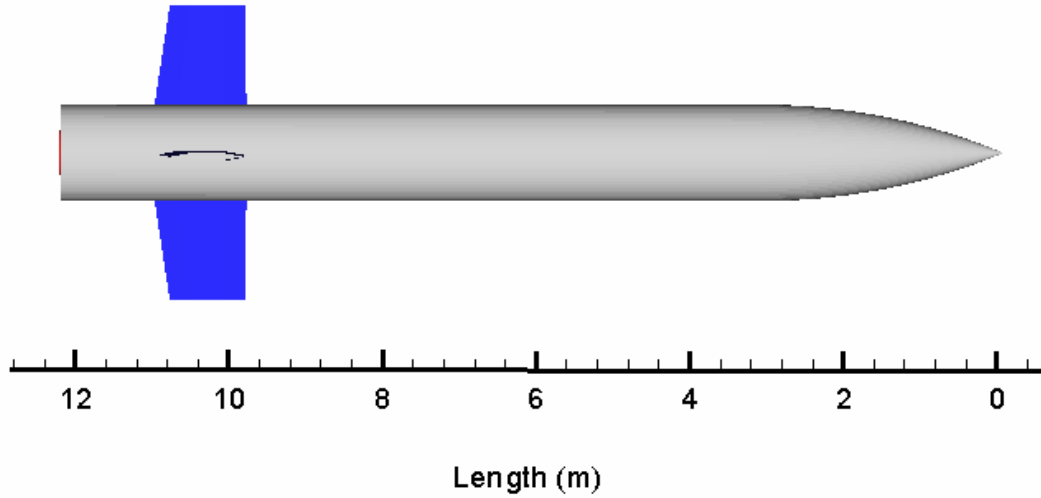


Figure 24: Ballistic missile external geometry

Table 16: GA variables for optimized, unguided missile

| Value | GA variable name |
|-----------|---------------------------------------|
| 4.0999999 | propellant type |
| 1.9236791 | equivalence ratio |
| 1139.9218 | chamber pressure (psi) |
| 45.043991 | nozzle throat area (in ²) |
| 9.6046963 | nozzle expansion ratio |
| 0.8000000 | fractional nozzle length |
| 39.892525 | burn time (sec) |
| 4400.0000 | payload mass (lbs) |
| 4.1111112 | missile body diameter (ft) |
| 2.4920635 | nose length/dbody |
| 0.0210000 | nose dia/dbody |
| 0.9516130 | fin2 root chord fraction = cr/dbody |
| 0.8145161 | fin2 taper ratio |
| 1.0000000 | fin2 le angle (degrees) |
| 1.0322580 | fin2 semi-span fraction = b2/dbody |
| 0.9000000 | x loc of fin2 (% totlen) |
| 499.00000 | autopilot time on delay – tdelay |
| 0.6015748 | autopilot time constant – tau |
| 0.5038583 | autopilot damping coef – zeta |
| 69.285713 | cross over frequency – cohz |
| 1.2857143 | pronav gain –pronvg |
| 67.825394 | initial launch angle (degrees) |

Aero Code: Aerodsn
 Miss Distance: 0.1 m
 Initial Mass: 6565 kg
 Flight Time: 436.7 s

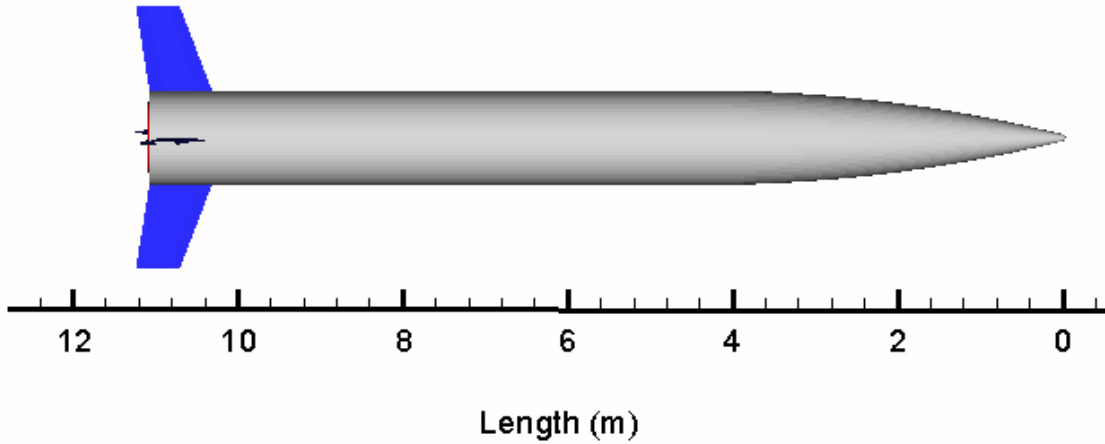


Figure 25: Aerodynamic control missile external geometry

Table 17: GA variables for optimized, aerodynamically controlled missile

| Value | GA variable name |
|-----------|---------------------------------------|
| 4.0999999 | propellant type |
| 1.9442271 | equivalence ratio |
| 740.70447 | chamber pressure (psi) |
| 43.333336 | nozzle throat area (in ²) |
| 24.399218 | nozzle expansion ratio |
| 0.7400000 | fractional nozzle length |
| 31.758671 | burn time (sec) |
| 4400.0000 | payload mass (lbs) |
| 4.0476189 | missile body diameter (ft) |
| 3.5634921 | nose length/dbody |
| 0.0722581 | nose dia/dbody |
| 0.6129032 | fin2 root chord fraction = cr/dbody |
| 0.7016129 | fin2 taper ratio |
| 19.582678 | fin2 le angle (degrees) |
| 0.8870968 | fin2 semi-span fraction = b2/dbody |
| 1.0000000 | x loc of fin2 (% totlen) |
| 12.350294 | autopilot time on delay – tdelay |
| 0.1440945 | autopilot time constant – tau |
| 0.9900000 | autopilot damping coef – zeta |
| 60.714287 | cross over frequency – cohz |
| 6.3333335 | pronav gain –pronvg |
| 68.285713 | initial launch angle (degrees) |

Aero Code: Aerodsn
 Miss Distance: 18.8 m
 Initial Mass: 9442 kg
 Flight Time: 164.8 s

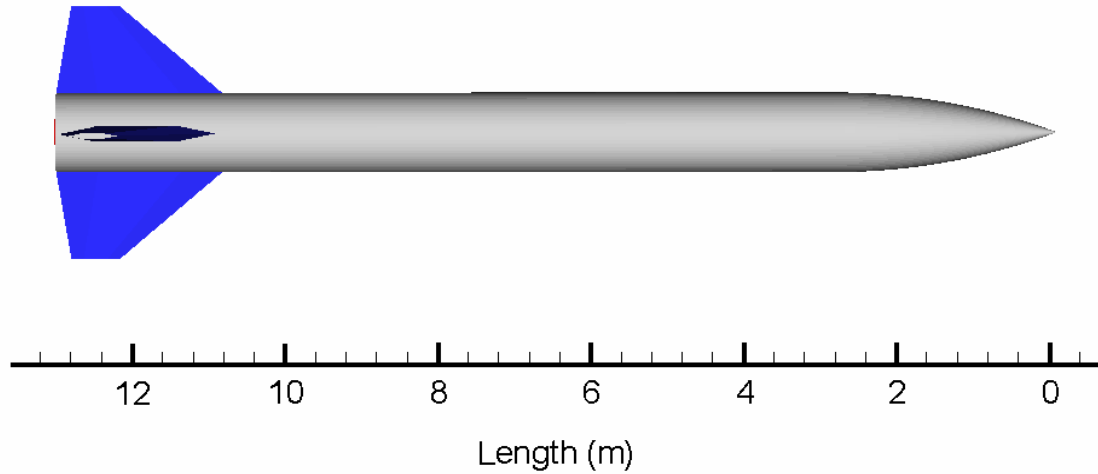


Figure 26: Vane control missile external geometry

Table 18: GA variables for optimized, vane controlled missile

| Value | GA variable name |
|-----------|---------------------------------------|
| 4.0999999 | propellant type |
| 0.7348337 | equivalence ratio |
| 1075.3424 | chamber pressure (psi) |
| 26.666668 | nozzle throat area (in ²) |
| 15.311154 | nozzle expansion ratio |
| 0.7800000 | fractional nozzle length |
| 64.601860 | burn time (sec) |
| 4400.0000 | payload mass (lbs) |
| 3.4126985 | missile body diameter (ft) |
| 2.7698412 | nose length/dbody |
| 0.0258065 | nose dia/dbody |
| 2.0806453 | fin2 root chord fraction = cr/dbody |
| 0.2951613 | fin2 taper ratio |
| 49.779530 | fin2 le angle (degrees) |
| 1.0806452 | fin2 semi-span fraction = b2/dbody |
| 1.0000000 | x loc of fin2 (% totlen) |
| 15.982388 | autopilot time on delay - tdelay |
| 0.4803150 | autopilot time constant - tau |
| 0.6890551 | autopilot damping coef - zeta |
| 69.285713 | cross over frequency - cohz |
| 2.6190476 | pronav gain -pronvg |
| 77.031746 | initial launch angle (degrees) |

The optimized missile designs for an unguided case, an aerodynamically controlled case, and a vane controlled case have been established. The resulting missiles have been flown to various target locations which are listed in Table 19 to demonstrate the effect of the control systems. Figure 27 plots the trajectory of each optimized missile flying to the baseline target location. The vane controlled and aerodynamically controlled missiles both impact the ground very near the target locations despite having significantly different flight paths. The vane control missile turns toward the target early in its flight and flies straight for the majority of its time in the air. The aerodynamically controlled missile, however, takes a lower altitude approach and continually corrects its flight path, curving back to the target during the last few seconds of flight. It is no surprise that these designs hit the target because they were optimized to do so.

Moving the target to different locations emphasizes the effect of each control system on the missile flights. Figures 27 through 31 present trajectory plots for the three different missiles aimed at the target locations listed in Table 19. The second target location has the target placed at -7.62 km (-25000 ft) in the y-direction while keeping the distance downrange the same. This change should have little effect on the accuracy of the missiles because only the direction of the flight changes. As Figure 28 illustrates though, the vane controlled missile impacts over 300 m from the target while the aerodynamic control case is right on target once again. This vane controlled design actually flies too far in the negative y-direction. It is apparent that the vane control case has the physical capability of reaching the target at this location, but the proportional navigation control system does not direct it to the correct location when the target is on the opposite side of the x-axis.

The third target location forces the designs to fly significantly farther away from the launch point. Neither design is able to fly very close to the target location in this case although the aerodynamically controlled missile lands considerably closer once again as shown in Figure 29. This result is obviously a side effect of minimizing the take-off weight of the missile designs; both designs lack the thrust needed to reach a target this far from the launch point. It appears that the fin controlled missile would hit the target if it had an adequate propulsion system, but the vane controlled design is unable to fly in the direction of the target.

The fourth target location result, shown in Figure 30, demonstrates what happens when the target is moved closer to the launch point. The aerodynamically controlled missile now has no problem hitting the target. But the vane controlled missile is only able to come within 13 km of hitting the target. This missile is able to successfully shorten its flight, but the control system is not able to make the adjustments needed to force the missile to land at 3.05 km in the y-direction.

The fifth and final target position tested takes advantage of the GA's capability to simulate a missile performance with moving targets. The target was set to move at 15.24 m/s (50 ft/sec) in the y-direction, starting from the baseline target position. The placement of the two target dots in Figure 31 accounts for the differences in position of the target at the time of each missile's impact. The aerodynamically controlled missile is still able to hit the target even though it is moving. The vane controlled missile performs quite well, only landing about 360 m from the target. This result is surprising because vane control theoretically should not respond well to a moving target since control is lost

after burnout. It is clear that this particular missile is highly optimized for hitting a target near the baseline location, and does not perform well when moved elsewhere.

Although the results indicate that aerodynamic control seems to be a clear winner when it comes to minimizing weight and miss distance, it does have a drawback. Aerodynamic control systems do not provide adequate force to control the missile at low Mach numbers. Just after launch, fins on a missile have little effect because the freestream dynamic pressure is very low. This time period early in the flight is where a jet vane control system is highly effective. High dynamic pressure in the nozzle, relative to the freestream dynamic pressure, produces large forces and moments on the vanes which steer the missile. For this reason, vanes are historically used for stabilization and pitch control in missiles shortly after take-off. As previously discussed, vanes are considerably less effective as the flight speed increases and of course have no effect once burnout occurs. So while vane control systems are poor choices when attempting to hit a moving target, they can serve an important purpose which has not been investigated in this research.

It should also be acknowledged that many vane control missiles, such as those similar to the SCUD, would rarely be aimed in a direction other than directly toward the intended target. The target position for this research was deliberately placed to test the control system models. Furthermore, SCUD class missiles have a pre-programmed flight path that is not well-modeled by the proportional navigation system used in this research. To accurately simulate this type of missile, more information about the specific guidance algorithm used by the SCUD would have to be known.

Table 19: Target data for test cases

| | Target Position | | | | |
|---------------------|-----------------|--------|--------|-----------|-----------|
| | X (ft) | Y (ft) | Z (ft) | Vx (ft/s) | Vy (ft/s) |
| Target 1 (baseline) | 400000 | 25000 | 0 | 0 | 0 |
| Target 2 | 400000 | -25000 | 0 | 0 | 0 |
| Target 3 | 500000 | 25000 | 0 | 0 | 0 |
| Target 4 | 300000 | 10000 | 0 | 0 | 0 |
| Target 5 | 400000 | 25000 | 0 | 0 | 50 |

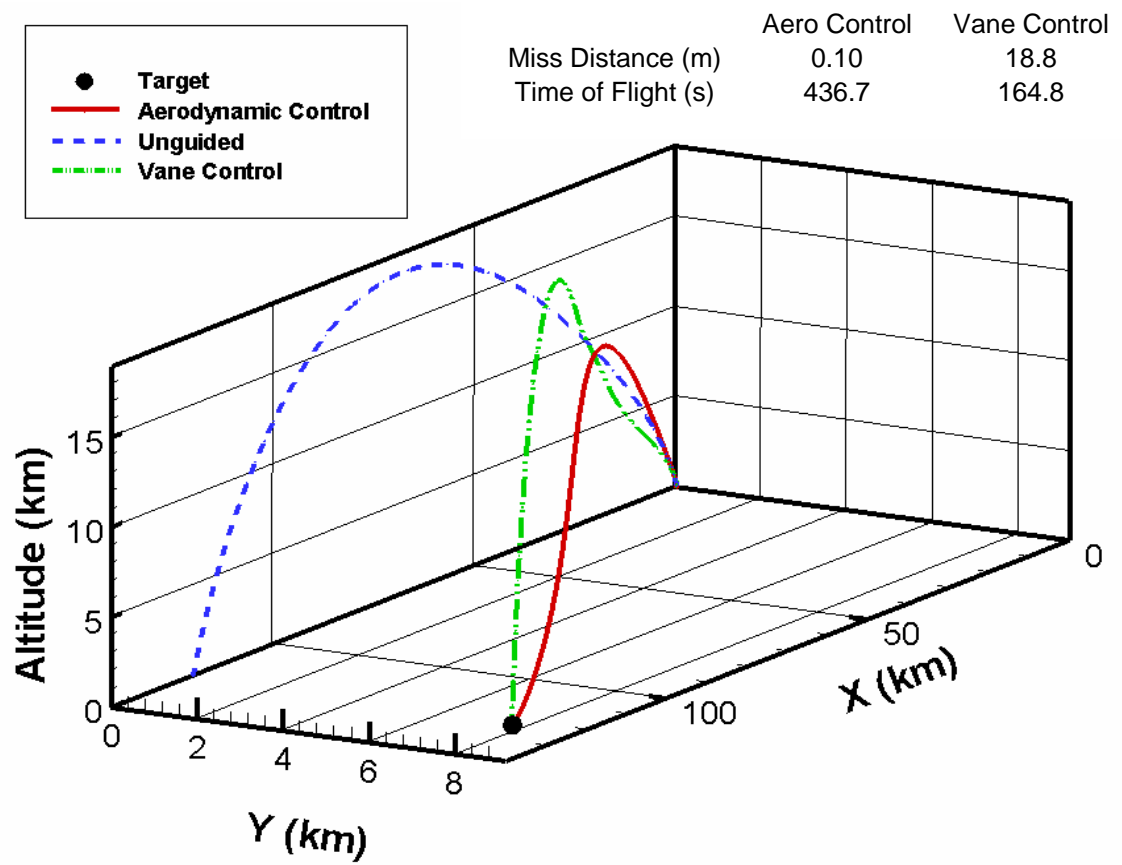


Figure 27: Trajectory plots for target 1

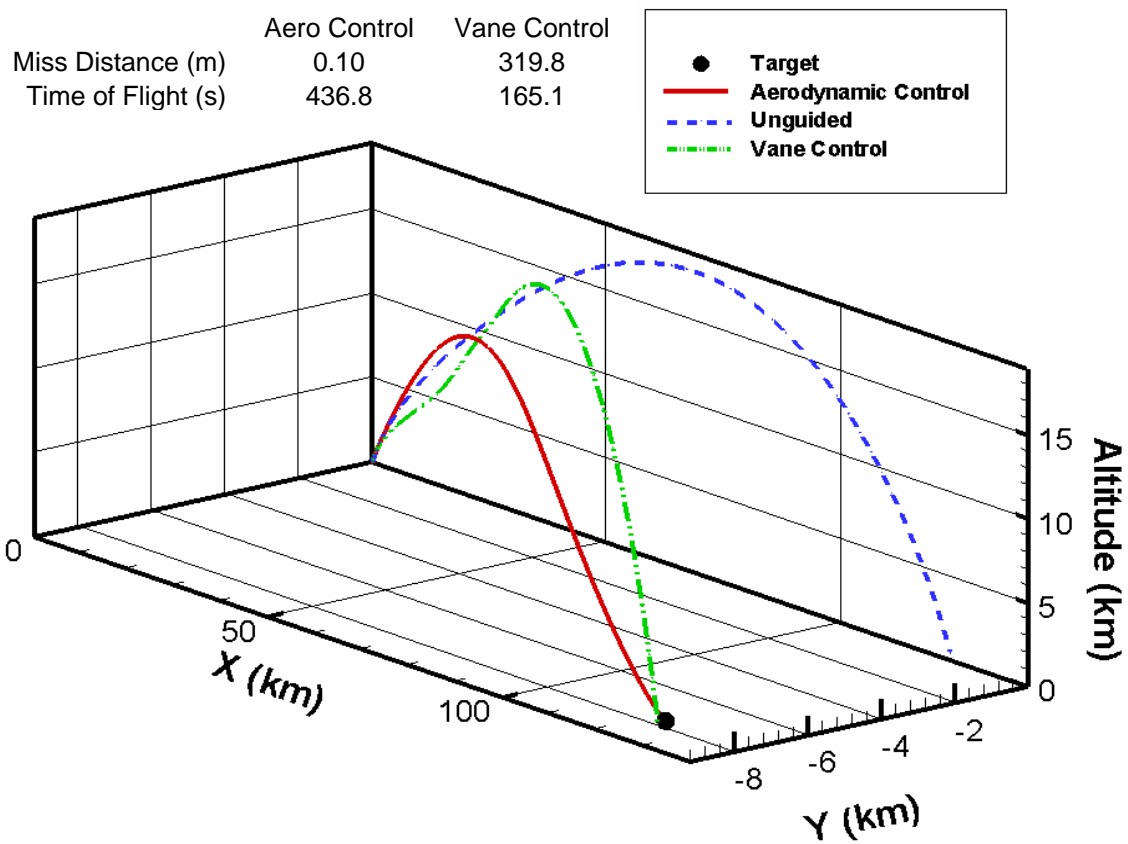


Figure 28: Trajectory plots for target 2

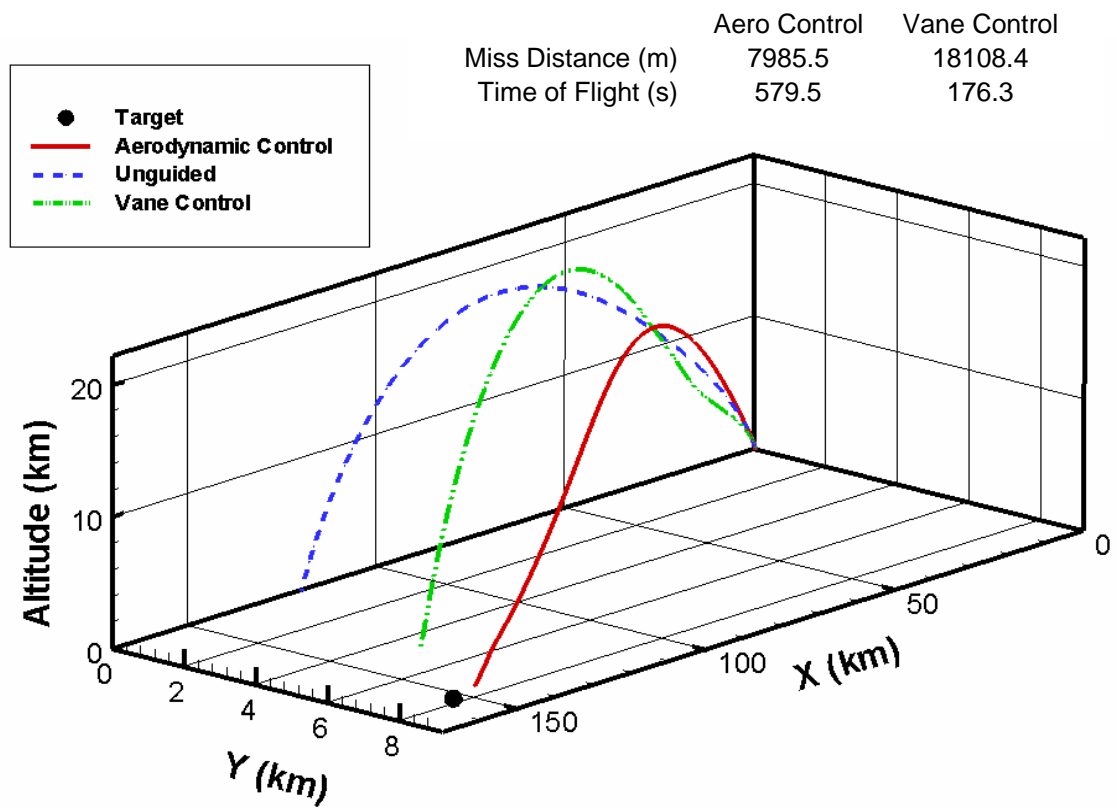


Figure 29: Trajectory plots for target 3

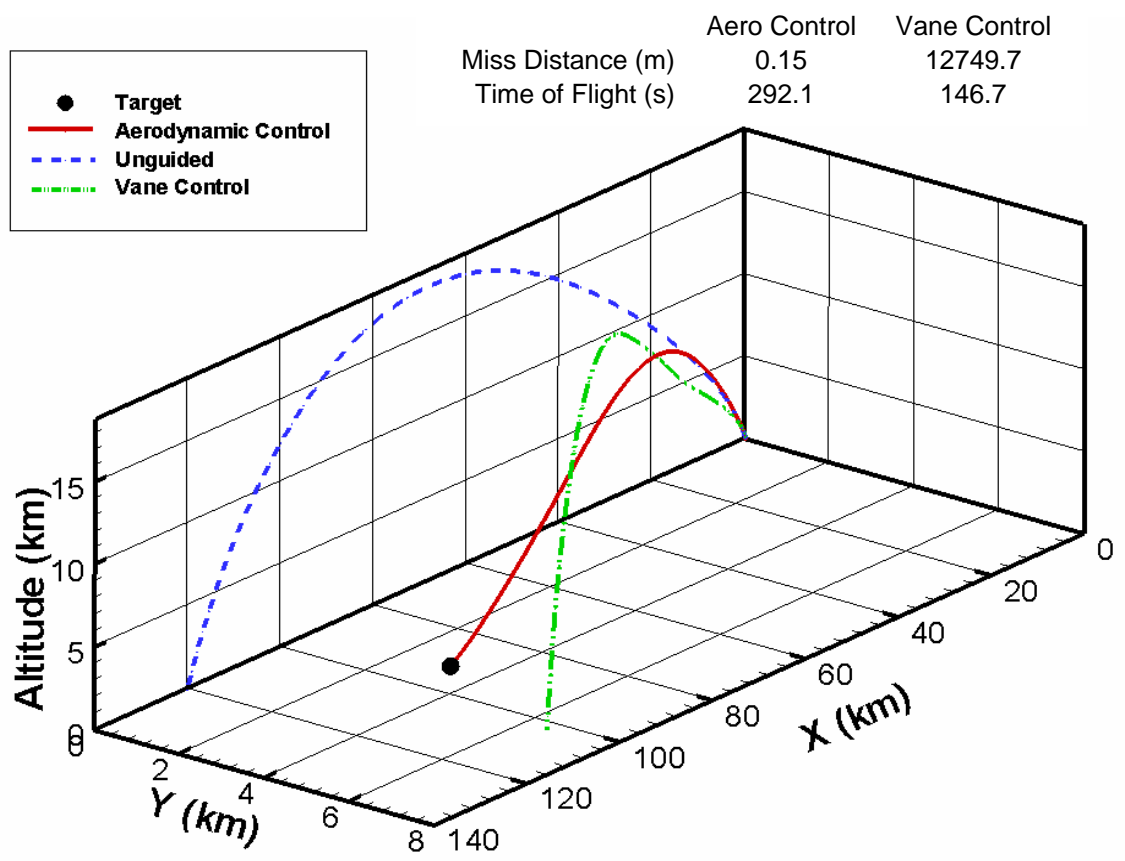


Figure 30: Trajectory plots for target 4

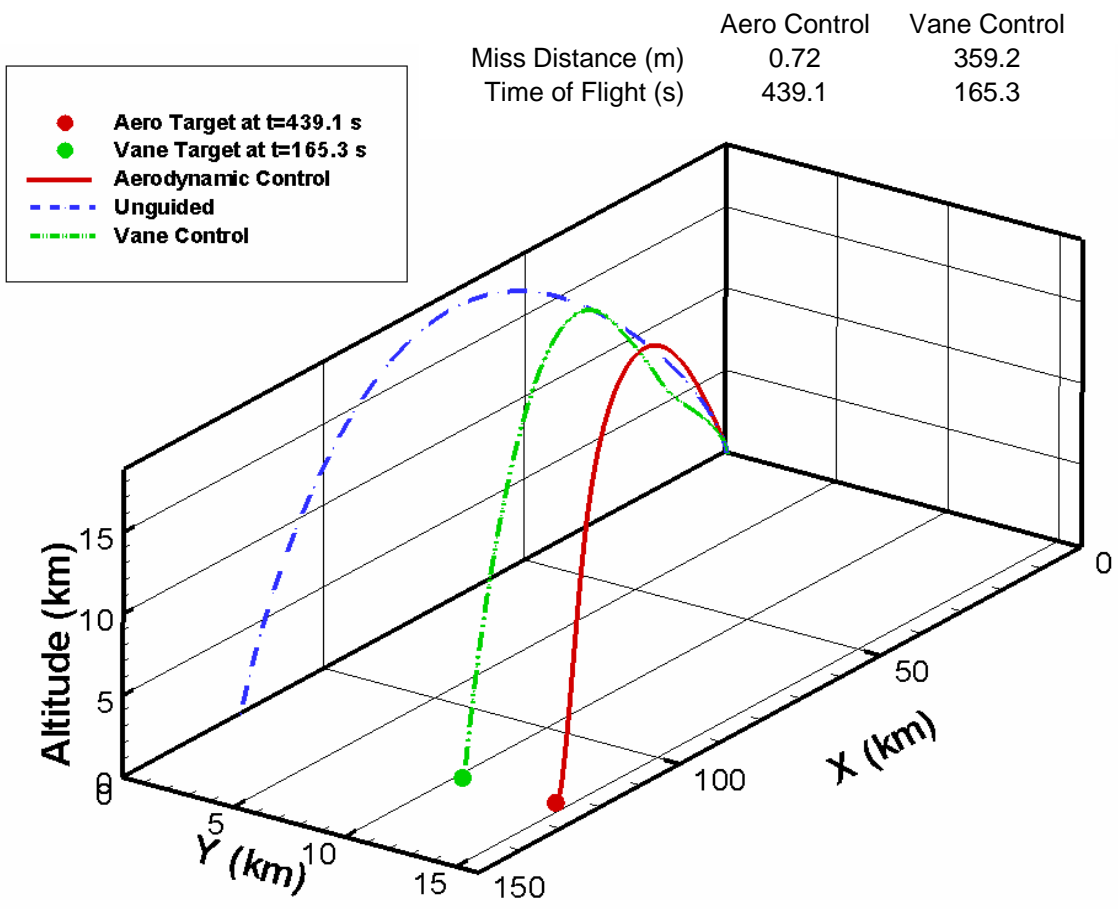


Figure 31: Trajectory plots for target 5

4. CONCLUSIONS AND RECOMMENDATIONS

A program utilizing a genetic algorithm to optimize aerodynamically controlled missile systems has been upgraded and a method of optimizing vane controlled missile systems has been developed. The liquid performance model was validated against a known missile configuration. Two different aerodynamic analysis fast predictor codes were used and their results compared to verify their predictions. A method of determining the specific impulse as a function of equivalence ratio was also developed and used in the optimization program. A jet vane control system model based on Evvard's theory was integrated into the optimization program and validated by comparing the vane force prediction with an estimation from linear supersonic aerodynamic theory. Optimized missiles with no control, aerodynamic control, and vane control were produced and their performance was compared. The suite of performance codes and accompanying GA were shown to be an effective missile optimization tool.

The GA-based optimization code is a powerful tool which allows liquid missile systems to be optimized very quickly with a wide range of inputs and constraints. The optimization of unguided and aerodynamically controlled missiles using Aerodsn has been shown to be very effective but there are several suggestions and improvements that would make the code even more robust. In regards to the variable I_{sp} upgrade, propellant combinations that still have constant values for specific impulse should be updated in the future when the appropriate thermochemical data becomes available.

While the addition of Missile Datcom adds another level of sophistication to the aerodynamic analysis capabilities of the code, it requires more computational time than Aerodsn. For this reason, it is not recommended that it be used as the primary aerodynamic prediction code. In addition, future versions of the program would benefit from a more complete aeroprediction routine. It is suggested that the aeroprediction be extended into the hypersonic range using the modified Newtonian flow model.³⁶ Newtonian theory provides quick and accurate results when the Mach number is large or the flow deflection angle is large. In fact, this model was used in the preliminary design of the Space Shuttle Orbiter.³⁶

For the vane control model, the dimensions of the vanes, which are nondimensionalized by the nozzle exit plane diameter, should be input as GA variables instead of constants. It is recommended that the thrust decrement be validated in some way and that the real gas effects be considered in future revisions. The vane actuators and physical configuration, which were not considered, should be accounted for within the mass properties model and aerodynamic analysis. There is currently no adequate method of optimizing a combined vane and aerodynamically controlled missile as the control systems would have to share one set of guidance and autopilot parameters. Future revisions might be able to avoid this by having separate sets of the control system GA variables for each method of control. Furthermore, as demonstrated by the results, a proportional navigation control algorithm is most likely not the best option for a vane controlled missile. Other control algorithms, such as a line-of-sight model or those unique to a specific class of missile, should be investigated in order to produce more realistic vane control results.

REFERENCES

1. Burkhalter, J.E., Jenkins, R.M., and Hartfield, R.J., "Genetic Algorithms for Missile Analysis," Final Report, Missile and Space Intelligence Center, Redstone Arsenal, AL, February 2003.
2. Hartfield, R.J., Burkhalter, J.E., Jenkins, R.M., and Metts, J., "Genetic Algorithm Upgrade Final Report," submitted to Missile and Space Intelligence Center, Redstone Arsenal, Alabama 35898, 10 June 2005, Reference Contract No. HHM402-04-P-0061.
3. Wollam, J., Kramer, S., and Campbell, S., "Reverse Engineering of Foreign Missiles via Genetic Algorithm", AIAA Paper 2000-0685, 38th Aerospace Sciences Meeting & Exhibit, Reno, NV, January 2000.
4. Metts, J., "Determination of Key Parameters for Reverse Engineering Solid Rocket Power Missiles," MS Thesis, Auburn University, August 3, 2006.
5. Perhinschi, M.G., "A Modified Genetic Algorithm for the Design of Autonomous Helicopter Control System," AIAA-97-3630, Presented at the AIAA Guidance, Navigation, and Control Conference, New Orleans, LA, August 1997.
6. Karr, C.L., Freeman, L.M., and Meredith, D.L., "Genetic Algorithm Based Fuzzy Control of Spacecraft Autonomous Rendezvous," NASA Marshall Space Flight Center, Fifth Conference on Artificial Intelligence for Space Applications, 1990.
7. Mondoloni, S., "A Genetic Algorithm for Determining Optimal Flight Trajectories," AIAA Paper 98-4476, AIAA Guidance, Navigation, and Control Conference and Exhibit, August 1998.
8. Torella, G., Blasi, L., "The Optimization of Gas Turbine Engine Design by Genetic Algorithms," AIAA Paper 2000-3710, 36th AIAA/ASME/SAE/ASEE Joint Propulsion Conference and Exhibit, July 2000.
9. Jang, M., and Lee, J., "Genetic Algorithm Based Design of Transonic Airfoils Using Euler Equations," AIAA Paper 2000-1584, Presented at the 41st AIAA/ASME/ASCE/AHS/ASC Structures, Structural Dynamics, and Materials Conference, April 2000.

10. Jenkins, R.M., Hartfield, R.J., and Burkhalter, J.E., "Optimizing a Solid Rocket Motor Boosted Ramjet Powered Missile Using a Genetic Algorithm," AIAA 2005-3507 presented at the Forty First AIAA/ASME/SAE/ASEE Joint Propulsion Conference, Tucson, AZ, July 10-13, 2005.
11. Anderson, M.B., Burkhalter, J.E., and Jenkins, R.M., "Design of an Air to Air Interceptor Using Genetic Algorithms," AIAA Paper 99-4081, presented at the 1999 AIAA Guidance, Navigation, and Control Conference, Portland, OR, August 1999.
12. Anderson, M.B., "Design of a Missile Interceptor using Genetic Algorithms," PhD Dissertation, Auburn University, December 14, 1998.
13. Perez, R.E., Chung, J., Behdinin, K., "Aircraft Conceptual Design Using Genetic Algorithms," AIAA Paper 2000-4938, Presented at the 8th AIAA/USAF/NASA/ISSMO Symposium on Multidisciplinary Analysis and Optimization, September 2000.
14. Schoonover, P.L., Crossley, W.A., and Heister, S.D., "Application of Genetic Algorithms to the Optimization of Hybrid Rockets," AIAA Paper 98-3349, 34th AIAA/ASME/SAE/ASEE Joint Propulsion Conference and Exhibit, July 1998.
15. Burkhalter, J., Jenkins, R., Hartfield, R., Foster, W., Witt, J., and Heiser, M., "Missile Design Systems Developed With Genetic Algorithms," Final Report for Dynetics, Inc., P.O. Box 5500, Huntsville, AL 35814 and U.S. Army Aviation & Missile Command, Redstone Arsenal, Alabama 35898, October 31, 2001, Prime Contract No. DAAH01-96-C-R194/P39393.
16. Hartfield, R.J., Burkhalter, J.E., Jenkins, R.M., Metts, J.G., Riddle, D.B., and Dyer, J.D., "Genetic Algorithm Developments for Liquid Missile Analysis," submitted to Missile and Space Intelligence Center, Redstone Arsenal, Alabama 35898, 22 September 2006, PAN 50353-05.
17. Bailey, S.L., "Reverse Engineering of a SCUD Missile using a Genetic Algorithm," MS Thesis, Auburn University, May 14, 2004.
18. Billheimer, J.S., "Optimization and Design Simulation in Solid Rocket Design," AIAA Paper 68-488, Presented at the 3rd AIAA Solid Propulsion Conference, June, 1968.
19. Anderson, M.B., Burkhalter, J.E., and Jenkins, R.M., "Multi-Disciplinary Intelligent Systems Approach to Solid Rocket Motor Design, Part I: Single and Dual Goal Optimization," AIAA Paper 2001-3599, presented at the 37th AIAA/ASME/SAE/ASEE Joint Propulsion Conference and Exhibit, Salt Lake City, UT, July 2001.

20. Blake, W.B., "Missile Datcom User's Manual," Volume I, 1998.
21. Sanders, G.A. and Washington, W.D., "Computer Program for Estimating Stability Derivatives of Missile Configurations - Users Manual," U.S. Army Missile Command. 1982.
22. Etkin, B., and Reid, L.D., "Dynamic of Flight: Stability and Control," John Wiley and Sons, Inc. 1996.
23. Reynolds, W.C., "The Element Potential Method for Chemical Equilibrium Analysis Implementation in the Interactive Program STANJAN," Department of Mechanical Engineering, Stanford University, January 1986.
24. Mattingly, J.D., "Elements of Gas Turbine Propulsion," McGraw Hill, Inc., 1996.
25. Sutton, G.P., Biblarz, O., "Rocket Propulsion Elements", John Wiley and Sons, Inc., 2001.
26. Website. <http://en.wikipedia.org/wiki/Scud>, accessed on November 2, 2006.
27. Evvard, J. C., "Distribution of Wave Drag and Lift in the Vicinity of Wing Tips at Supersonic Speeds", NACA Technical Note No. 1382, Flight Propulsion Research Laboratory, Cleveland, Ohio, July 1947.
28. Evvard, J. C., "Theoretical Distribution of Lift on Thin Wings at Supersonic Speeds", NACA Technical Note No. 1585, Flight Propulsion Research Laboratory, Cleveland, Ohio, May 1948.
29. Harmon, S. M. and Jeffrey, I., "Theoretical Lift and Damping in Roll of Thin Wings with Arbitrary Sweep and Taper at Supersonic Speeds," NACA Technical Note No. 2114, Langley Aeronautical Laboratory, Langley Air Force Base, Virginia, May 1950.
30. Mirels, H., "Theoretical Wave Drag and Lift of Thin Supersonic Ring Airfoils," NACA Technical Note No. 1678, Flight Propulsion Laboratory, Cleveland, Ohio, August 1948.
31. Moeckel, W.E. and Evvard, J.C., "Load Distribution due to steady Roll and Pitch for Thin Wings at Supersonic Speeds," NACA Technical Note No. 1689, Flight Propulsion Research Laboratory, Cleveland, Ohio, August 1948.
32. Wilks, B.L., "Aerodynamics of Wrap-Around Fins in Supersonic Flow," MS Thesis, Auburn University, Dec 16, 2005.

33. Giragosian, P.A., "Theoretical and Experimental Aerodynamic Correlation of Jet Vane Control Effectiveness," AIAA-81-1897, AIAA Atmospheric Flight Mechanics Conference, August 1981.
34. Anderson, J.D., "Fundamentals of Aerodynamics," McGraw-Hill Higher Education, 2001.
35. Website. <http://www.janes.com>, accessed on November 15, 2006.
36. Bertin, J.J., "Hypersonic Aerothermodynamics," AIAA Education Series, 1994.

APPENDIX A: GA Input File

```

.false.                                ; micro
.false.                                ; pareto
.false.                                ; steady_state
.false.                                ; maximize
.true.                                  ; elitist
.true.                                  ; creep
.false.                                ; uniform
.true.                                  ; restart
.true.                                  ; remove_dup
.false.                                ; niche
.true.                                  ; phenotype
0.5                                     ; niche diversity percentile goal
61722                                  ; iseed
0.9                                     ; pcross
0.005                                  ; pmutation
0.05                                    ; pcreep
1                                       ; ngoals
1.                                       ; xgls(j)
1.                                       ; domst
2550                                    ; convrg_chk (end of group2)
27                                      ; no_para
'kprop  1' , 4.1 , 4.0 , 0.1 , .false. ;xmax,xmin,resolution,niche_par
'far    2' , 2.0 , 0.5 , .005 , .false. ;xmax,xmin,resolution,niche_par
'po     3' , 2000. , 500. , 5.00 , .true. ;xmax,xmin,resolution,niche_par
'athroat 4' , 60. , 10. , 0.1 , .false. ;xmax,xmin,resolution,niche_par
'eps    5' , 30. , 3. , 0.1 , .false. ;xmax,xmin,resolution,niche_par
'lf     6' , 0.9 , 0.6 , 0.05 , .false. ;xmax,xmin,resolution,niche_par
'tb     7' , 120.0 , 30.0 , 0.1 , .false. ;xmax,xmin,resolution,niche_par
'paymass 8' , 4401. , 4400. , 25.0 , .false. ;xmax,xmin,resolution,niche_par
'dbody  9' , 5.0 , 1.0 , 0.1 , .false. ;xmax,xmin,resolution,niche_par
'lnose  10' , 4.0 , 1.5 , .1 , .false. ;xmax,xmin,resolution,niche_par
'dnose  11' , .20 , .02 , .01 , .false. ;xmax,xmin,resolution,niche_par
'crfin1 12' , 0.002 , .001 , 0.001 , .false. ;xmax,xmin,resolution,niche_par
'trfin1 13' , 0.95 , 0.25 , 0.05 , .false. ;xmax,xmin,resolution,niche_par
'angLE1 14' , 60.0 , 1.00 , 1.00 , .false. ;xmax,xmin,resolution,niche_par
'b2fin1 15' , 2.0 , 0.01 , 0.01 , .false. ;xmax,xmin,resolution,niche_par
'xcrfn1 16' , 0.50 , 0.10 , 0.01 , .false. ;xmax,xmin,resolution,niche_par
'crfin2 17' , 4.00 , 0.50 , 0.20 , .false. ;xmax,xmin,resolution,niche_par
'trfin2 18' , 0.95 , 0.25 , 0.05 , .false. ;xmax,xmin,resolution,niche_par
'angLE2 19' , 60.0 , 1.00 , 1.00 , .false. ;xmax,xmin,resolution,niche_par
'b2fin2 20' , 2.00 , 0.50 , 0.1 , .false. ;xmax,xmin,resolution,niche_par
'xtefn2 21' , 1.00 , 0.90 , 0.1 , .false. ;xmax,xmin,resolution,niche_par
'tdelay 22' , 30.0 , 1.0 , 1.0 , .false. ;xmax,xmin,resolution,niche_par
'tau    23' , 0.80 , 0.10 , 0.01 , .false. ;xmax,xmin,resolution,niche_par
'zeta   24' , 0.99 , 0.50 , 0.01 , .false. ;xmax,xmin,resolution,niche_par
'wcr    25' , 75.0 , 55.0 , 5.00 , .false. ;xmax,xmin,resolution,niche_par
'pronvg 26' , 7.0 , 1.0 , 0.20 , .false. ;xmax,xmin,resolution,niche_par
'theta0 27' , 89.0 , 60.0 , 1.00 , .false. ;xmax,xmin,resolution,niche_par
1                                             ; ifreq
300                                          ; mempops
100                                         ; maxgen

```

APPENDIX B: Global Array Variables

| | | | | | | |
|---------------|-----|------|---|-----------|-----------------------------|----------|
| 3.141592654d0 | ;YY | 1,1 | - | pi | | |
| 2.0926435d7 | ;YY | 1,2 | - | re | radius of the earth | ft |
| 32.174d0 | ;YY | 1,3 | - | gc | acceleration of gravity | ft/sec^2 |
| 57.29577951d0 | ;YY | 1,4 | - | deg/rad | degrees per radian | |
| 0.0d0 | ;YY | 1,5 | - | sref | reference area | ft^2 |
| 0.0d0 | ;YY | 1,6 | - | lref | reference length | ft |
| Densities | | | | | | |
| 0.282d0 | ;YY | 2,1 | - | rhocfair | cyl fairing material | lbm/in3 |
| 0.282d0 | ;YY | 2,2 | - | rhcncone | nose cone fairing matl | lbm/in3 |
| 0.19d0 | ;YY | 2,3 | - | rhon | nozzle material | lbm/in3 |
| 0.08d0 | ;YY | 2,4 | - | rhocarbn | carbon | lbm/in3 |
| 0.289d0 | ;YY | 2,5 | - | rhosteel | steel | lbm/in3 |
| 0.0975d0 | ;YY | 2,6 | - | rhoalum | aluminum | lbm/in3 |
| 0.00d0 | ;YY | 2,7 | - | rhopay1 | payload1 | lbm/in3 |
| 0.00d0 | ;YY | 2,8 | - | rhopay2 | payload2 | lbm/in3 |
| 0.065d0 | ;YY | 2,9 | - | rhoelec1 | electronics1 | lbm/in3 |
| 0.00d0 | ;YY | 2,10 | - | rhoelec2 | electronics2 | lbm/in3 |
| 0.0639d0 | ;YY | 2,11 | - | rhowar1 | warhead1 | lbm/in3 |
| 0.00d0 | ;YY | 2,12 | - | rhowar2 | warhead2 | lbm/in3 |
| 0.00d0 | ;YY | 2,13 | - | rhobox1 | box 1 | lbm/in3 |
| 0.0639d0 | ;YY | 2,14 | - | rhobox2 | box 2 | lbm/in3 |
| 0.00d0 | ;YY | 2,15 | - | rhopump1 | oxygen pump | lbm/in3 |
| 0.00d0 | ;YY | 2,16 | - | rhopump2 | fuel pump | lbm/in3 |
| 0.282d0 | ;YY | 2,17 | - | rhotank1 | tank1 material | lbm/in3 |
| 0.282d0 | ;YY | 2,18 | - | rhotank2 | tank2 material | lbm/in3 |
| 0.282d0 | ;YY | 2,19 | - | rhogast | compressed gas tank | lbm/in3 |
| 0.00d0 | ;YY | 2,20 | - | rhofin1 | average dendency of fin1 | lbm/in3 |
| 0.00d0 | ;YY | 2,21 | - | rhofin2 | average dendency of fin2 | lbm/in3 |
| 0.00d0 | ;YY | 2,22 | - | rhofin3 | average dendency of fin3 | lbm/in3 |
| 0.00d0 | ;YY | 2,23 | - | rhosenr1 | sensor 1 material | lbm/in3 |
| 0.00d0 | ;YY | 2,24 | - | rhosenr2 | sensor 2 material | lbm/in3 |
| 0.00d0 | ;YY | 2,25 | - | rholine1 | insulator 1 material | lbm/in3 |
| 0.00d0 | ;YY | 2,26 | - | rholine2 | insulator 2 material | lbm/in3 |
| 0.00d0 | ;YY | 2,27 | - | rhof | liquid fuel | lbm/in3 |
| 0.00d0 | ;YY | 2,28 | - | rhoox | liquid oxidizer | lbm/in3 |
| 0.00d0 | ;YY | 2,29 | - | rhototal | density of missile | lbm/in3 |
| 0.0105d0 | ;YY | 2,30 | - | rhoeng | engine anf thrust str. | lbm/in3 |
| 0.0061d0 | ;YY | 2,31 | - | rhogimbal | gimbals | lbm/in3 |
| 0.00d0 | ;YY | 2,32 | - | rhogas | compressed gas | lbm/in3 |
| 0.10d0 | ;YY | 2,33 | - | rhoservo | servo actuators | lbm/in3 |
| 0.00d0 | ;YY | 2,34 | - | rhobox3 | box 3 | lbm/in3 |
| 0.00d0 | ;YY | 2,35 | - | rhobox4 | box 4 | lbm/in3 |
| 0.00d0 | ;YY | 2,36 | - | rhobox5 | box 5 | lbm/in3 |
| 0.00d0 | ;YY | 2,37 | - | rhobox6 | box 6 | lbm/in3 |
| masses | | | | | | |
| 2200.0d0 | ;YY | 3,1 | - | warmass | warhead mass | lbm |
| 0.0d0 | ;YY | 3,2 | - | elecma1 | elec 1 mass | lbm |
| 0.00d0 | ;YY | 3,3 | - | elecma2 | elec 2 mass | lbm |
| 0.00d0 | ;YY | 3,4 | - | insulmf1 | fuel tank 1 insulator mass | lbm |
| 0.00d0 | ;YY | 3,5 | - | insulmf2 | fuel tank 2 insulator mass | lbm |
| 0.00d0 | ;YY | 3,6 | - | insulmox1 | ox tank 1 insulator mass | lbm |
| 0.00d0 | ;YY | 3,7 | - | insulmox2 | ox tank 2 insulator mass | lbm |
| 0.00d0 | ;YY | 3,8 | - | compgas1 | com.gas mass, stage 1 | lbm |
| 0.00d0 | ;YY | 3,9 | - | compgas2 | com.gas mass, stage 2 | lbm |
| 0.00d0 | ;YY | 3,10 | - | comptank1 | com.gas tank mass, stage 1 | lbm |
| 0.00d0 | ;YY | 3,11 | - | comptank2 | com.gas tank mass, stage 2 | lbm |
| 0.00d0 | ;YY | 3,12 | - | fuelm1 | fuel mass, stage 1 | lbm |
| 0.00d0 | ;YY | 3,13 | - | fuelm2 | fuel mass, stage 2 | lbm |
| 0.00d0 | ;YY | 3,14 | - | oxm1 | oxidizer mass, stage 1 | lbm |
| 0.00d0 | ;YY | 3,15 | - | oxm2 | oxidizer mass, stage 2 | lbm |
| 0.00d0 | ;YY | 3,16 | - | ftankm1 | fuel tank mass, stage 1 | lbm |
| 0.00d0 | ;YY | 3,17 | - | ftankm2 | fuel tank mass, stage 2 | lbm |
| 0.00d0 | ;YY | 3,18 | - | oxtankm1 | oxidizer tank mass, stage 1 | lbm |
| 0.00d0 | ;YY | 3,19 | - | oxtankm2 | oxidizer tank mass, stage 2 | lbm |
| 0.00d0 | ;YY | 3,20 | - | engmass1 | engine mass, stage 1 | lbm |
| 0.00d0 | ;YY | 3,21 | - | engmass2 | engine mass, stage 2 | lbm |

| | | | | | | |
|-------------------|-----|------|---|------------|----------------------------|-----|
| 0.00d0 | ;YY | 3,22 | - | nosfairm1 | nose fairing mass, stage 1 | lbm |
| 0.00d0 | ;YY | 3,23 | - | nosfairm2 | nose fairing mass, stage 2 | lbm |
| 0.00d0 | ;YY | 3,24 | - | cylfairm1 | cyl fairing mass, stage 1 | lbm |
| 0.00d0 | ;YY | 3,25 | - | cylfairm2 | cyl fairing mass, stage 2 | lbm |
| 0.00d0 | ;YY | 3,26 | - | finm1 | total finset 1 mass | lbm |
| 0.00d0 | ;YY | 3,27 | - | finm2 | total finset 2 mass | lbm |
| 0.00d0 | ;YY | 3,28 | - | finm3 | total finset 3 mass | lbm |
| 0.00d0 | ;YY | 3,29 | - | gimm1 | gimbal mass, stage 1 | lbm |
| 0.00d0 | ;YY | 3,30 | - | gimm2 | gimbal mass, stage 2 | lbm |
| 0.00d0 | ;YY | 3,31 | - | wirem1 | wiring mass, stage 1 | lbm |
| 0.00d0 | ;YY | 3,32 | - | wirem2 | wiring mass, stage 2 | lbm |
| 0.00d0 | ;YY | 3,33 | - | entmas1 | nozzle entrance mass 1 | lbm |
| 0.00d0 | ;YY | 3,34 | - | thrmas1 | nozzle throat mass 1 | lbm |
| 0.00d0 | ;YY | 3,35 | - | bellmas1 | bell nozzle mass 1 | lbm |
| 0.00d0 | ;YY | 3,36 | - | entmas2 | nozzle entrance mass 2 | lbm |
| 0.00d0 | ;YY | 3,37 | - | thrmas2 | nozzle throat mass 2 | lbm |
| 0.00d0 | ;YY | 3,38 | - | bellmas2 | bell nozzle mass 2 | lbm |
| 0.00d0 | ;YY | 3,39 | - | nozmas1 | nozzle mass 1 | lbm |
| 0.00d0 | ;YY | 3,40 | - | nozmas2 | nozzle mass 2 | lbm |
| 0.00d0 | ;YY | 3,41 | - | servomas | servo actuators mass | lbm |
| 0.00d0 | ;YY | 3,42 | - | sensorsmas | sensors mass | lbm |
| 2.00d0 | ;YY | 3,43 | - | boxmas1 | box-1 mass | lbm |
| 00.00d0 | ;YY | 3,44 | - | boxmas2 | box-2 mass | lbm |
| 0.00d0 | ;YY | 3,45 | - | boxmas3 | box-3 mass | lbm |
| 0.00d0 | ;YY | 3,46 | - | boxmas4 | box-4 mass | lbm |
| 0.00d0 | ;YY | 3,47 | - | boxmas5 | box-5 mass | lbm |
| 0.00d0 | ;YY | 3,48 | - | boxmas6 | box-6 mass | lbm |
| 0.00d0 | ;YY | 3,49 | - | totalmas | initial total mass | lbm |
| center of gravity | | | | | | |
| 0.00d0 | ;YY | 4,1 | - | warcg | warhead cg | ft |
| 0.00d0 | ;YY | 4,2 | - | eleccg1 | elec 1 cg | ft |
| 0.00d0 | ;YY | 4,3 | - | eleccg2 | elec 2 cg | ft |
| 0.00d0 | ;YY | 4,4 | - | insulgf1 | fuel tank 1 insulator cg | ft |
| 0.00d0 | ;YY | 4,5 | - | insulgf2 | fuel tank 2 insulator cg | ft |
| 0.00d0 | ;YY | 4,6 | - | insulgox1 | ox tank 1 insulator cg | ft |
| 0.00d0 | ;YY | 4,7 | - | insulgox2 | ox tank 2 insulator cg | ft |
| 0.00d0 | ;YY | 4,8 | - | compgacg1 | com.gas cg, stage 1 | ft |
| 0.00d0 | ;YY | 4,9 | - | compgacg2 | com.gas cg, stage 2 | ft |
| 0.00d0 | ;YY | 4,10 | - | comtancg1 | com.gas tank cg, stage 1 | ft |
| 0.00d0 | ;YY | 4,11 | - | comtancg2 | com.gas tank cg, stage 2 | ft |
| 0.00d0 | ;YY | 4,12 | - | fuelcg1 | fuel cg, stage 1 | ft |
| 0.00d0 | ;YY | 4,13 | - | fuelcg2 | fuel cg, stage 2 | ft |
| 0.00d0 | ;YY | 4,14 | - | oxcg1 | oxidizer cg, stage 1 | ft |
| 0.00d0 | ;YY | 4,15 | - | oxcg2 | oxidizer cg, stage 2 | ft |
| 0.00d0 | ;YY | 4,16 | - | ftankcg1 | fuel tank cg, stage 1 | ft |
| 0.00d0 | ;YY | 4,17 | - | ftankcg2 | fuel tank cg, stage 2 | ft |
| 0.00d0 | ;YY | 4,18 | - | oxtankcg1 | oxidizer tank cg, stage 1 | ft |
| 0.00d0 | ;YY | 4,19 | - | oxtankcg2 | oxidizer tank cg, stage 2 | ft |
| 0.00d0 | ;YY | 4,20 | - | engcg1 | engine cg, stage 1 | ft |
| 0.00d0 | ;YY | 4,21 | - | engcg2 | engine cg, stage 2 | ft |
| 0.00d0 | ;YY | 4,22 | - | nosfairg1 | nose fairing cg, stage 1 | ft |
| 0.00d0 | ;YY | 4,23 | - | nosfairg2 | nose fairing cg, stage 2 | ft |
| 0.00d0 | ;YY | 4,24 | - | cylfairg1 | cyl fairing cg, stage 1 | ft |
| 0.00d0 | ;YY | 4,25 | - | cylfairg2 | cyl fairing cg, stage 2 | ft |
| 0.00d0 | ;YY | 4,26 | - | fincg1 | total finset 1 cg | ft |
| 0.00d0 | ;YY | 4,27 | - | fincg2 | total finset 2 cg | ft |
| 0.00d0 | ;YY | 4,28 | - | fincg3 | total finset 3 cg | ft |
| 0.00d0 | ;YY | 4,29 | - | gimcg1 | gimbal cg, stage 1 | ft |
| 0.00d0 | ;YY | 4,30 | - | gimcg2 | gimbal cg, stage 2 | ft |
| 0.00d0 | ;YY | 4,31 | - | wirecg1 | wiring cg, stage 1 | ft |
| 0.00d0 | ;YY | 4,32 | - | wirecg2 | wiring cg, stage 2 | ft |
| 0.00d0 | ;YY | 4,33 | - | entcg1 | nozzle entrance cg 1 | in |
| 0.00d0 | ;YY | 4,34 | - | thrcg1 | nozzle throat cg 1 | in |
| 0.00d0 | ;YY | 4,35 | - | bellcg1 | bell nozzle cg 1 | in |
| 0.00d0 | ;YY | 4,36 | - | entcg2 | nozzle entrance cg 2 | in |
| 0.00d0 | ;YY | 4,37 | - | thrcg2 | nozzle throat cg 2 | in |
| 0.00d0 | ;YY | 4,38 | - | bellcg2 | bell nozzle cg 2 | in |
| 0.00d0 | ;YY | 4,39 | - | nozcg1 | nozzle cg 1 | in |
| 0.00d0 | ;YY | 4,40 | - | nozcg2 | nozzle cg 2 | in |

| | | | | | | |
|--------------------|-----|------|---|-----------|---------------------------|---------|
| 0.00d0 | ;YY | 4,41 | - | totalcg | initial overall cg | ft |
| 0.00d0 | ;YY | 4,42 | - | servocg | servo actuator cg | ft |
| 0.00d0 | ;YY | 4,43 | - | cgbox1 | box 1 cg | ft |
| 0.00d0 | ;YY | 4,44 | - | cgbox2 | box 2 cg | ft |
| 0.00d0 | ;YY | 4,45 | - | cgbox3 | box 3 cg | ft |
| 0.00d0 | ;YY | 4,46 | - | cgbox4 | box 4 cg | ft |
| 0.00d0 | ;YY | 4,47 | - | cgbox5 | box 5 cg | ft |
| 0.00d0 | ;YY | 4,48 | - | cgbox6 | box 6 cg | ft |
| 0.00d0 | ;YY | 4,49 | - | avioncg | avionics cg | ft |
| moments of inertia | | | | | | |
| 0.00d0 | ;YY | 5,1 | - | warix | warhead ix | lbm-ft2 |
| 0.00d0 | ;YY | 5,2 | - | elecix1 | elec 1 ix | lbm-ft2 |
| 0.00d0 | ;YY | 5,3 | - | elecix2 | elec 2 ix | lbm-ft2 |
| 0.00d0 | ;YY | 5,4 | - | insuixf1 | fuel tank 1 insulator ix | lbm-ft2 |
| 0.00d0 | ;YY | 5,5 | - | insuixf2 | fuel tank 2 insulator ix | lbm-ft2 |
| 0.00d0 | ;YY | 5,6 | - | insuiox1 | ox tank 1 insulator ix | lbm-ft2 |
| 0.00d0 | ;YY | 5,7 | - | insuiox2 | ox tank 2 insulator ix | lbm-ft2 |
| 0.00d0 | ;YY | 5,8 | - | compgaix1 | com.gas ix, stage 1 | lbm-ft2 |
| 0.00d0 | ;YY | 5,9 | - | compgaix2 | com.gas ix, stage 2 | lbm-ft2 |
| 0.00d0 | ;YY | 5,10 | - | comtanix1 | com.gas tank ix, stage 1 | lbm-ft2 |
| 0.00d0 | ;YY | 5,11 | - | comtanix2 | com.gas tank ix, stage 2 | lbm-ft2 |
| 0.00d0 | ;YY | 5,12 | - | fuelix1 | fuel ix, stage 1 | lbm-ft2 |
| 0.00d0 | ;YY | 5,13 | - | fuelix2 | fuel ix, stage 2 | lbm-ft2 |
| 0.00d0 | ;YY | 5,14 | - | oxix1 | oxidizer ix, stage 1 | lbm-ft2 |
| 0.00d0 | ;YY | 5,15 | - | oxix2 | oxidizer ix, stage 2 | lbm-ft2 |
| 0.00d0 | ;YY | 5,16 | - | ftankix1 | fuel tank ix, stage 1 | lbm-ft2 |
| 0.00d0 | ;YY | 5,17 | - | ftankix2 | fuel tank ix, stage 2 | lbm-ft2 |
| 0.00d0 | ;YY | 5,18 | - | oxtankix1 | oxidizer tank ix, stage 1 | lbm-ft2 |
| 0.00d0 | ;YY | 5,19 | - | oxtankix2 | oxidizer tank ix, stage 2 | lbm-ft2 |
| 0.00d0 | ;YY | 5,20 | - | engix1 | engine ix, stage 1 | lbm-ft2 |
| 0.00d0 | ;YY | 5,21 | - | engix2 | engine ix, stage 2 | lbm-ft2 |
| 0.00d0 | ;YY | 5,22 | - | nosfaiix1 | nose fairing ix, stage 1 | lbm-ft2 |
| 0.00d0 | ;YY | 5,23 | - | nosfaiix2 | nose fairing ix, stage 2 | lbm-ft2 |
| 0.00d0 | ;YY | 5,24 | - | cylfaiix1 | cyl fairing ix, stage 1 | lbm-ft2 |
| 0.00d0 | ;YY | 5,25 | - | cylfaiix2 | cyl fairing ix, stage 2 | lbm-ft2 |
| 0.00d0 | ;YY | 5,26 | - | finix1 | total finset 1 ix | lbm-ft2 |
| 0.00d0 | ;YY | 5,27 | - | finix2 | total finset 2 ix | lbm-ft2 |
| 0.00d0 | ;YY | 5,28 | - | finix3 | total finset 3 ix | lbm-ft2 |
| 0.00d0 | ;YY | 5,29 | - | gimix1 | gimbal ix, stage 1 | lbm-ft2 |
| 0.00d0 | ;YY | 5,30 | - | gimix2 | gimbal ix, stage 2 | lbm-ft2 |
| 0.00d0 | ;YY | 5,31 | - | wireix1 | wiring ix, stage 1 | lbm-ft2 |
| 0.00d0 | ;YY | 5,32 | - | wireix2 | wiring ix, stage 2 | lbm-ft2 |
| 0.00d0 | ;YY | 5,33 | - | entix1 | nozzle entrance ix 1 | lbm-ft2 |
| 0.00d0 | ;YY | 5,34 | - | thrix1 | nozzle throat ix 1 | lbm-ft2 |
| 0.00d0 | ;YY | 5,35 | - | bellix1 | bell nozzle ix 1 | lbm-ft2 |
| 0.00d0 | ;YY | 5,36 | - | entix2 | nozzle entrance ix 2 | lbm-ft2 |
| 0.00d0 | ;YY | 5,37 | - | thrix2 | nozzle throat ix 2 | lbm-ft2 |
| 0.00d0 | ;YY | 5,38 | - | bellix2 | bell nozzle ix 2 | lbm-ft2 |
| 0.00d0 | ;YY | 5,39 | - | nozix1 | nozzle ix 1 | lbm-ft2 |
| 0.00d0 | ;YY | 5,40 | - | nozix2 | nozzle ix 2 | lbm-ft2 |
| 0.00d0 | ;YY | 5,41 | - | totalix | initial overall ix | lbm-ft2 |
| 0.00d0 | ;YY | 5,42 | - | wariy | warhead iy | lbm-ft2 |
| 0.00d0 | ;YY | 5,43 | - | eleciy1 | elec 1 iy | lbm-ft2 |
| 0.00d0 | ;YY | 5,44 | - | eleciy2 | elec 2 iy | lbm-ft2 |
| 0.00d0 | ;YY | 5,45 | - | insuiyf1 | fuel tank 1 insulator iy | lbm-ft2 |
| 0.00d0 | ;YY | 5,46 | - | insuiyf2 | fuel tank 2 insulator iy | lbm-ft2 |
| 0.00d0 | ;YY | 5,47 | - | insuiyox1 | ox tank 1 insulator iy | lbm-ft2 |
| 0.00d0 | ;YY | 5,48 | - | insuiyox2 | ox tank 2 insulator iy | lbm-ft2 |
| 0.00d0 | ;YY | 5,49 | - | compgaiy1 | com.gas iy, stage 1 | lbm-ft2 |
| 0.00d0 | ;YY | 5,50 | - | compgaiy2 | com.gas iy, stage 2 | lbm-ft2 |
| 0.00d0 | ;YY | 5,51 | - | comtaniy1 | com.gas tank iy, stage 1 | lbm-ft2 |
| 0.00d0 | ;YY | 5,52 | - | comtaniy2 | com.gas tank iy, stage 2 | lbm-ft2 |
| 0.00d0 | ;YY | 5,53 | - | fueliy1 | fuel iy, stage 1 | lbm-ft2 |
| 0.00d0 | ;YY | 5,54 | - | fueliy2 | fuel iy, stage 2 | lbm-ft2 |
| 0.00d0 | ;YY | 5,55 | - | oxiy1 | oxidizer iy, stage 1 | lbm-ft2 |
| 0.00d0 | ;YY | 5,56 | - | oxiy2 | oxidizer iy, stage 2 | lbm-ft2 |
| 0.00d0 | ;YY | 5,57 | - | ftankiy1 | fuel tank iy, stage 1 | lbm-ft2 |
| 0.00d0 | ;YY | 5,58 | - | ftankiy2 | fuel tank iy, stage 2 | lbm-ft2 |
| 0.00d0 | ;YY | 5,59 | - | oxtankiy1 | oxidizer tank iy, stage 1 | lbm-ft2 |

| | | | | | | |
|-------------|-----|-------|---|-----------|---------------------------|---------|
| 0.00d0 | ;YY | 5,60 | - | oxtankiy2 | oxidizer tank iy, stage 2 | lbm-ft2 |
| 0.00d0 | ;YY | 5,61 | - | engiy1 | engine iy, stage 1 | lbm-ft2 |
| 0.00d0 | ;YY | 5,62 | - | engiy2 | engine iy, stage 2 | lbm-ft2 |
| 0.00d0 | ;YY | 5,63 | - | nosfaiiy1 | nose fairing iy, stage 1 | lbm-ft2 |
| 0.00d0 | ;YY | 5,64 | - | nosfaiiy2 | nose fairing iy, stage 2 | lbm-ft2 |
| 0.00d0 | ;YY | 5,65 | - | cylfaiiy1 | cyl fairing iy, stage 1 | lbm-ft2 |
| 0.00d0 | ;YY | 5,66 | - | cylfaiiy2 | cyl fairing iy, stage 2 | lbm-ft2 |
| 0.00d0 | ;YY | 5,67 | - | finiy1 | total finset 1 iy | lbm-ft2 |
| 0.00d0 | ;YY | 5,68 | - | finiy2 | total finset 2 iy | lbm-ft2 |
| 0.00d0 | ;YY | 5,69 | - | finiy3 | total finset 3 iy | lbm-ft2 |
| 0.00d0 | ;YY | 5,70 | - | gimiy1 | gimbal iy, stage 1 | lbm-ft2 |
| 0.00d0 | ;YY | 5,71 | - | gimiy2 | gimbal iy, stage 2 | lbm-ft2 |
| 0.00d0 | ;YY | 5,72 | - | wireiy1 | wiring iy, stage 1 | lbm-ft2 |
| 0.00d0 | ;YY | 5,73 | - | wireiy2 | wiring iy, stage 2 | lbm-ft2 |
| 0.00d0 | ;YY | 5,74 | - | entiy1 | nozzle entrance iy 1 | lbm-ft2 |
| 0.00d0 | ;YY | 5,75 | - | thriy1 | nozzle throat iy 1 | lbm-ft2 |
| 0.00d0 | ;YY | 5,76 | - | belliy1 | bell nozzle iy 1 | lbm-ft2 |
| 0.00d0 | ;YY | 5,77 | - | entiy2 | nozzle entrance iy 2 | lbm-ft2 |
| 0.00d0 | ;YY | 5,78 | - | thriy2 | nozzle throat iy 2 | lbm-ft2 |
| 0.00d0 | ;YY | 5,79 | - | belliy2 | bell nozzle iy 2 | lbm-ft2 |
| 0.00d0 | ;YY | 5,80 | - | noziy1 | nozzle iy 1 | lbm-ft2 |
| 0.00d0 | ;YY | 5,81 | - | noziy2 | nozzle iy 2 | lbm-ft2 |
| 0.00d0 | ;YY | 5,82 | - | totaliy | initial overall iy | lbm-ft2 |
| 0.00d0 | ;YY | 5,83 | - | wariz | warhead iz | lbm-ft2 |
| 0.00d0 | ;YY | 5,84 | - | eleciz1 | elec 1 iz | lbm-ft2 |
| 0.00d0 | ;YY | 5,85 | - | eleciz2 | elec 2 iz | lbm-ft2 |
| 0.00d0 | ;YY | 5,86 | - | insuizf1 | fuel tank 1 insulator iz | lbm-ft2 |
| 0.00d0 | ;YY | 5,87 | - | insuizf2 | fuel tank 2 insulator iz | lbm-ft2 |
| 0.00d0 | ;YY | 5,88 | - | insuizox1 | ox tank 1 insulator iz | lbm-ft2 |
| 0.00d0 | ;YY | 5,89 | - | insuizox2 | ox tank 2 insulator iz | lbm-ft2 |
| 0.00d0 | ;YY | 5,90 | - | compgaiz1 | com.gas iz, stage 1 | lbm-ft2 |
| 0.00d0 | ;YY | 5,91 | - | compgaiz2 | com.gas iz, stage 2 | lbm-ft2 |
| 0.00d0 | ;YY | 5,92 | - | comtaniz1 | com.gas tank iz, stage 1 | lbm-ft2 |
| 0.00d0 | ;YY | 5,93 | - | comtaniz2 | com.gas tank iz, stage 2 | lbm-ft2 |
| 0.00d0 | ;YY | 5,94 | - | fueliz1 | fuel iz, stage 1 | lbm-ft2 |
| 0.00d0 | ;YY | 5,95 | - | fueliz2 | fuel iz, stage 2 | lbm-ft2 |
| 0.00d0 | ;YY | 5,96 | - | oxiz1 | oxidizer iz, stage 1 | lbm-ft2 |
| 0.00d0 | ;YY | 5,97 | - | oxiz2 | oxidizer iz, stage 2 | lbm-ft2 |
| 0.00d0 | ;YY | 5,98 | - | ftankiz1 | fuel tank iz, stage 1 | lbm-ft2 |
| 0.00d0 | ;YY | 5,99 | - | ftankiz2 | fuel tank iz, stage 2 | lbm-ft2 |
| 0.00d0 | ;YY | 5,100 | - | oxtankiz1 | oxidizer tank iz, stage 1 | lbm-ft2 |
| 0.00d0 | ;YY | 5,101 | - | oxtankiz2 | oxidizer tank iz, stage 2 | lbm-ft2 |
| 0.00d0 | ;YY | 5,102 | - | engiz1 | engine iz, stage 1 | lbm-ft2 |
| 0.00d0 | ;YY | 5,103 | - | engiz2 | engine iz, stage 2 | lbm-ft2 |
| 0.00d0 | ;YY | 5,104 | - | nosfaiiz1 | nose fairing iz, stage 1 | lbm-ft2 |
| 0.00d0 | ;YY | 5,105 | - | nosfaiiz2 | nose fairing iz, stage 2 | lbm-ft2 |
| 0.00d0 | ;YY | 5,106 | - | cylfaiiz1 | cyl fairing iz, stage 1 | lbm-ft2 |
| 0.00d0 | ;YY | 5,107 | - | cylfaiiz2 | cyl fairing iz, stage 2 | lbm-ft2 |
| 0.00d0 | ;YY | 5,108 | - | finiz1 | total finset 1 iz | lbm-ft2 |
| 0.00d0 | ;YY | 5,109 | - | finiz2 | total finset 2 iz | lbm-ft2 |
| 0.00d0 | ;YY | 5,110 | - | finiz3 | total finset 3 iz | lbm-ft2 |
| 0.00d0 | ;YY | 5,111 | - | gimiz1 | gimbal iz, stage 1 | lbm-ft2 |
| 0.00d0 | ;YY | 5,112 | - | gimiz2 | gimbal iz, stage 2 | lbm-ft2 |
| 0.00d0 | ;YY | 5,113 | - | wireiz1 | wiring iz, stage 1 | lbm-ft2 |
| 0.00d0 | ;YY | 5,114 | - | wireiz2 | wiring iz, stage 2 | lbm-ft2 |
| 0.00d0 | ;YY | 5,115 | - | entiz1 | nozzle entrance iz 1 | lbm-ft2 |
| 0.00d0 | ;YY | 5,116 | - | thriz1 | nozzle throat iz 1 | lbm-ft2 |
| 0.00d0 | ;YY | 5,117 | - | belliz1 | bell nozzle iz 1 | lbm-ft2 |
| 0.00d0 | ;YY | 5,118 | - | entiz2 | nozzle entrance iz 2 | lbm-ft2 |
| 0.00d0 | ;YY | 5,119 | - | thriz2 | nozzle throat iz 2 | lbm-ft2 |
| 0.00d0 | ;YY | 5,120 | - | belliz2 | bell nozzle iz 2 | lbm-ft2 |
| 0.00d0 | ;YY | 5,121 | - | noziz1 | nozzle iz 1 | lbm-ft2 |
| 0.00d0 | ;YY | 5,122 | - | noziz2 | nozzle iz 2 | lbm-ft2 |
| 0.00d0 | ;YY | 5,123 | - | totaliz | initial overall iz | lbm-ft2 |
| 0.00d0 | ;YY | 5,124 | - | servoix | servo ix | lbm-ft2 |
| 0.00d0 | ;YY | 5,125 | - | servoiy | servo iy | lbm-ft2 |
| 0.00d0 | ;YY | 5,126 | - | servoiz | servo iz | lbm-ft2 |
| target data | | | | | | |
| 400000.0d0 | ;YY | 6,1 | - | xtarg | x location of target | ft |

| | | | | | |
|--------------------------------------|----------|---|-----------|-------------------------------|---------|
| 25000.0d0 | ;YY 6,2 | - | ytarg | y location of target | ft |
| 0.0d0 | ;YY 6,3 | - | ztarg | z location of target | ft |
| 0.0d0 | ;YY 6,4 | - | vxtarg | x velocity of target | ft/sec |
| -50.0d0 | ;YY 6,5 | - | vytarg | y velocity of target | ft/sec |
| 0.0d0 | ;YY 6,6 | - | vztarg | z velocity of target | ft/sec |
| initiation of launch data | | | | | |
| 30.0d0 | ;YY 7,1 | - | xlamda | initial latitude | deg |
| 86.5d0 | ;YY 7,2 | - | y0 | initial longitude | deg |
| 1.00d0 | ;YY 7,3 | - | z0 | initial altitude | deg |
| 0.00d0 | ;YY 7,4 | - | u0 | initial u-velocity | ft/sec |
| 0.00d0 | ;YY 7,5 | - | v0 | initial v-velocity | ft/sec |
| 0.00d0 | ;YY 7,6 | - | w0 | initial w-velocity | ft/sec |
| -1.0d0 | ;YY 7,7 | - | tht0 | initial Euler angle | deg |
| 00.0d0 | ;YY 7,8 | - | phi0 | initial Euler angle | deg |
| 00.0d0 | ;YY 7,9 | - | psi0 | initial Euler angle | deg |
| 0.00d0 | ;YY 7,10 | - | q0 | initial pitch rate | deg/sec |
| 0.00d0 | ;YY 7,11 | - | p0 | initial roll rate | deg/sec |
| 0.00d0 | ;YY 7,12 | - | r0 | initial yaw rate | deg/sec |
| 0.00d0 | ;YY 7,13 | - | clpct | fin cant multiplier | |
| 0.00d0 | ;YY 7,14 | - | dxcg0 | initial CG-CP offset | ft |
| -1.0d0 | ;YY 7,15 | - | tdelay | auto-pilot on delay time | sec |
| -1.0d0 | ;YY 7,16 | - | tau | autopilot time const | |
| -1.0d0 | ;YY 7,17 | - | zeta | autopilot pitch damping | |
| -1.0d0 | ;YY 7,18 | - | wcr | cross over frequency | Hz |
| -1.0d0 | ;YY 7,19 | - | pronvgn | pronav gain (guidance) | |
| 60.0d0 | ;YY 7,20 | - | rol_wcr | cross over freq (roll) | rad/sec |
| 45.0d0 | ;YY 7,21 | - | des_ph | desired phase mar in roll | deg |
| program lengths,limits and constants | | | | | |
| 40000.0d0 | ;YY 8,1 | - | tmaxd | max flight run time | sec |
| 285000.0d0 | ;YY 8,2 | - | fbd | max bending stress-1 | lb/in2 |
| 135000.0d0 | ;YY 8,3 | - | sigmad | max motor case stress | lb/in2 |
| 9000.0d0 | ;YY 8,4 | - | pcmax 1 | max chamber pressure | lb/in2 |
| 50.0d0 | ;YY 8,5 | - | pcmin 1 | min chamber pressure | lb/in2 |
| 0.0d0 | ;YY 8,6 | - | pcmax 2 | max chamber pressure | lb/in2 |
| 0.0d0 | ;YY 8,7 | - | pcmin 2 | min chamber pressure | lb/in2 |
| 500.0d0 | ;YY 8,8 | - | gmax | max g-limit | |
| 1.50d0 | ;YY 8,9 | - | sfd | motor case safety factor | |
| 0.0d0 | ;YY 8,10 | - | tipchek | dis to TE of fin2 tip | ft |
| 15.0d0 | ;YY 8,11 | - | delmax1 | maximum fin deflection 1 | deg |
| 00.0d0 | ;YY 8,12 | - | delmax2 | maximum fin deflection 2 | deg |
| 00.0d0 | ;YY 8,13 | - | delmax3 | maximum fin deflection 3 | deg |
| 00.0d0 | ;YY 8,14 | - | rodradi1 | actuator1 rod radius | in |
| 00.0d0 | ;YY 8,15 | - | rodradi2 | actuator2 rod radius | in |
| 0.00d0 | ;YY 8,16 | - | warlen | length of warhead | ft |
| 0.00d0 | ;YY 8,17 | - | eleclen1 | length of electronics 1 | ft |
| 0.00d0 | ;YY 8,18 | - | eleclen2 | length of electronics 2 | ft |
| 0.00d0 | ;YY 8,19 | - | comgas1 | length comp gas tank | ft |
| 0.00d0 | ;YY 8,20 | - | tanklen | length comp gas tank | ft |
| 0.00d0 | ;YY 8,21 | - | fueltank1 | length of fuel tank 1 | ft |
| 0.00d0 | ;YY 8,22 | - | fueltank2 | length of fuel tank 2 | ft |
| 0.00d0 | ;YY 8,23 | - | oxtank1 | length of oxidizer tank 1 | ft |
| 0.00d0 | ;YY 8,24 | - | oxtank2 | length of oxidizer tank 2 | ft |
| 0.00d0 | ;YY 8,25 | - | enginell | length of engine 1 | ft |
| 0.00d0 | ;YY 8,26 | - | engine12 | length of engine 2 | ft |
| 0.00d0 | ;YY 8,27 | - | ncone1 | length of nosecone 1 | ft |
| 0.00d0 | ;YY 8,28 | - | ncone2 | length of nosecone 2 | ft |
| 0.00d0 | ;YY 8,29 | - | fair1 | cyl fairing length, stage 1 | ft |
| 0.00d0 | ;YY 8,30 | - | fair2 | cyl fairing length, stage 2 | ft |
| 0.00d0 | ;YY 8,31 | - | giml1 | gimbal length, stage 1 | ft |
| 0.00d0 | ;YY 8,32 | - | giml2 | gimbal length, stage 2 | ft |
| 0.00d0 | ;YY 8,33 | - | wirel1 | wiring length, stage 1 | ft |
| 0.00d0 | ;YY 8,34 | - | wirel2 | wiring length, stage 2 | ft |
| 100.d0 | ;YY 8,35 | - | pprop | propellant press. level | psi |
| 100.d0 | ;YY 8,36 | - | delp | regulator delta p | psi |
| 6000.d0 | ;YY 8,37 | - | pair | pressurization tank press | psi |
| 530.0d0 | ;YY 8,38 | - | tair | pressurization tank temp | deg R |
| 0.00d0 | ;YY 8,39 | - | nozlen | overall nozzle length | ft |
| 0.00d0 | ;YY 8,40 | - | aspect | actual missile fineness ratio | |
| 0.00d0 | ;YY 8,41 | - | boxlen1 | length of box 1 | ft |

| | | | | | | |
|---------------------------------------|-----|-------|---|--------------|---------------------------------|------|
| 0.00d0 | ;YY | 8,42 | - | boxlen2 | length of box 2 | ft |
| 0.00d0 | ;YY | 8,43 | - | boxlen3 | length of box 3 | ft |
| 0.00d0 | ;YY | 8,44 | - | boxlen4 | length of box 4 | ft |
| 0.00d0 | ;YY | 8,45 | - | boxlen5 | length of box 5 | ft |
| 0.00d0 | ;YY | 8,46 | - | boxlen6 | length of box 6 | ft |
| 0.00d0 | ;YY | 8,47 | - | servolen | length of servo actuators | ft |
| 0.00d0 | ;YY | 8,48 | - | areanose | surface area of nose | ft^2 |
| 0.00d0 | ;YY | 8,49 | - | vnose1 | volume of nose section | ft^3 |
| external geometry default variables | | | | | | |
| 0.00d0 | ;YY | 9,1 | - | lcentr1 | cyl. section length 1 | ft |
| -1.0d0 | ;YY | 9,2 | - | dcyl1 | centr sec dia - stage 1 | ft |
| 0.00d0 | ;YY | 9,3 | - | lcentr2 | cyl. section length 2 | ft |
| 0.00d0 | ;YY | 9,4 | - | dcyl2 | centr sec dia - stage 2 | ft |
| 0.00d0 | ;YY | 9,5 | - | dumy | variable | |
| 0.00d0 | ;YY | 9,6 | - | totlen | total body length | ft |
| 0.0d0 | ;YY | 9,7 | - | typfin1 | 0-blades; 1-wrap around 1 | |
| 4.0d0 | ;YY | 9,8 | - | nfin1 | number of fins in fin set 1 | |
| 60.0d0 | ;YY | 9,9 | - | sweple1 | sweep of le in fin set 1 | deg |
| 0.4d0 | ;YY | 9,10 | - | xlefin1 | dis to LE of finset 1 (% body) | |
| 00.0d0 | ;YY | 9,11 | - | xhlfin1 | dis to hinge line-Fin set 1 | in |
| 1.00d0 | ;YY | 9,12 | - | crfin1 | root chord length-Fin set 1 | ft |
| 0.99d0 | ;YY | 9,13 | - | tapfin1 | taper ratio of fin1 | 1 |
| 0.50d0 | ;YY | 9,14 | - | b2fin1 | semi-span-fin set 1 | ft |
| 0.10d0 | ;YY | 9,15 | - | tmaxfin1 | fin1 thickness ratio set 1 | |
| 0.0d0 | ;YY | 9,16 | - | typfin2 | 0-blades; 1-wrap around 2 | |
| 4.0d0 | ;YY | 9,17 | - | nfin2 | number of fins in fin set 2 | |
| -1.0d0 | ;YY | 9,18 | - | sweple2 | sweep of le in fin set 2 | deg |
| 0.0d0 | ;YY | 9,19 | - | xlefin2 | dis to LE of finset 2 (% body) | |
| 0.0d0 | ;YY | 9,20 | - | xhlfin2 | dis to hinge line-Fin set 2 | ft |
| 0.0d0 | ;YY | 9,21 | - | crfin2 | root chord length-Fin set 2 | ft |
| -1.0d0 | ;YY | 9,22 | - | tapfin2 | taper ratio of fin2 2 | |
| 0.0d0 | ;YY | 9,23 | - | b2fin2 | semi-span-Fin set 2 | ft |
| 0.10d0 | ;YY | 9,24 | - | tmaxfin2 | thickness ratio of fin2 2 | |
| 00.0d0 | ;YY | 9,25 | - | typfin3 | 0-blades; 1-wrap around 3 | |
| 00.0d0 | ;YY | 9,26 | - | nfin3 | number of fins in fin set 3 | |
| 00.0d0 | ;YY | 9,27 | - | sweple3 | sweep of le in fin set 3 | deg |
| 00.0d0 | ;YY | 9,28 | - | xlefin3 | dis to LE of Fin set 3 (% body) | |
| 00.0d0 | ;YY | 9,29 | - | xhlfin3 | dis to hinge line-Fin set 3 | ft |
| 0.00d0 | ;YY | 9,30 | - | crfin3 | root chord length-Fin set 3 | ft |
| 0.00d0 | ;YY | 9,31 | - | tapfin3 | taper ratio of finset 3 | |
| 0.00d0 | ;YY | 9,32 | - | b2fin3 | semi-span-Fin set 3 | ft |
| 0.10d0 | ;YY | 9,33 | - | tmaxfin3 | thickness ratio finset 3 | |
| 0.00d0 | ;YY | 9,34 | - | dtail | diameter of body at fin2 | in |
| 0.00d0 | ;YY | 9,35 | - | fin1del | fin1 deflection:1=yes, 0=no | |
| 1.00d0 | ;YY | 9,36 | - | fin2del | fin2 deflection: 1=yes, 0=no | |
| 0.00d0 | ;YY | 9,37 | - | ybarfin1 | spnwise loc of fin1 CP | ft |
| 0.00d0 | ;YY | 9,38 | - | ybarfin2 | spnwise loc of fin2 CP | ft |
| 0.00d0 | ;YY | 9,39 | - | ybarfin3 | spnwise loc of fin22 CP | ft |
| 0.00d0 | ;YY | 9,40 | - | lnose | length of the nose | ft |
| -1.0d0 | ;YY | 9,41 | - | dnose | ratio of (nose dia)/DB | |
| 00.0d0 | ;YY | 9,42 | - | bnose | radius of nose | ft |
| 0.00d0 | ;YY | 9,43 | - | rchamb | radius of combust chamber | in |
| 0.50d0 | ;YY | 9,44 | - | hang | fin2 tip hang over / Dbody | |
| 1.00d0 | ;YY | 9,45 | - | internal noz | 1 - yes; 0 - no | |
| liquid rocket motor default variables | | | | | | |
| -1.0d0 | ;YY | 10,1 | - | prop_typ1 | propellant combo 1 | |
| 0.0d0 | ;YY | 10,2 | - | prop_typ2 | propellant combo 2 | |
| -1.0d0 | ;YY | 10,3 | - | po1 | chamber pressure 1 | psi |
| 0.00d0 | ;YY | 10,4 | - | po2 | chamber pressure 2 | psi |
| -1.0d0 | ;YY | 10,5 | - | athroat1 | area of throat stage 1 | in2 |
| 00.0d0 | ;YY | 10,6 | - | athroat2 | area of throat stage 2 | in2 |
| -1.0d0 | ;YY | 10,7 | - | eps1 | expansion ratio stage 1 | |
| 0.00d0 | ;YY | 10,8 | - | eps2 | expansion ratio stage 2 | |
| 75.0d0 | ;YY | 10,9 | - | thein1 | convergence angle for noz1 | deg |
| 0.00d0 | ;YY | 10,10 | - | thein2 | convergence angle for noz2 | deg |
| 00.0d0 | ;YY | 10,11 | - | angexit1 | noz exit angle stage 1 | deg |
| 00.0d0 | ;YY | 10,12 | - | nozlen1 | nozzle length stage 1 | in |
| 0.382d0 | ;YY | 10,13 | - | sigtht1 | nozzle contour fraction 1 | in |
| 00.0d0 | ;YY | 10,14 | - | nozlen2 | nozzle length stage 2 | in |

| | | | | | | |
|-------------------------------------|-----|-------|---|----------|-------------------------------------|---------|
| 0.382d0 | ;YY | 10,15 | - | sight2 | nozzle contour fraction 2 | in |
| 00.0d0 | ;YY | 10,16 | - | thangle1 | throat angle match 1 | deg |
| 00.0d0 | ;YY | 10,17 | - | thangle2 | throat angle match 2 | deg |
| -1.0d0 | ;YY | 10,18 | - | fn1 | fractional nozzle length 1 | |
| 0.00d0 | ;YY | 10,19 | - | fn2 | fractional nozzle length 2 | |
| 0.98d0 | ;YY | 10,20 | - | etamu1 | nozzle 1 efficiency | |
| 0.98d0 | ;YY | 10,21 | - | etamu2 | nozzle 2 efficiency | |
| 0.00d0 | ;YY | 10,22 | - | thrust1 | engine1 thrust =f(time) | lbs |
| 0.00d0 | ;YY | 10,23 | - | thrust2 | engine2 thrust =f(time) | lbs |
| 0.00d0 | ;YY | 10,24 | - | tvac1 | vacuum thrust, stage 1 | lbs |
| 0.00d0 | ;YY | 10,25 | - | tvac2 | vacuum thrust, stage 2 | lbs |
| -1.0d0 | ;YY | 10,26 | - | tbl | motor burn time, stg 1 | sec |
| 0.00d0 | ;YY | 10,27 | - | tb2 | motor burn time, stg 2 | sec |
| 0.00d0 | ;YY | 10,28 | - | volf1 | fuel tank volume, stg 1 | ft3 |
| 0.00d0 | ;YY | 10,29 | - | volf2 | fuel tank volume, stg 2 | ft3 |
| 0.00d0 | ;YY | 10,30 | - | volox1 | oxidizer tank volume, stg 1 | ft3 |
| 0.00d0 | ;YY | 10,31 | - | volox2 | oxidizer tank volume, stg 2 | ft3 |
| 0.00d0 | ;YY | 10,32 | - | endf1 | fuel tank radius, stg 1 | ft |
| 0.00d0 | ;YY | 10,33 | - | midf1 | fuel tank ctr len, stg 1 | ft |
| 0.00d0 | ;YY | 10,34 | - | endf2 | fuel tank radius, stg 2 | ft |
| 0.00d0 | ;YY | 10,35 | - | midf2 | fuel tank ctr len, stg 2 | ft |
| 0.00d0 | ;YY | 10,36 | - | endox1 | oxidizer tank radius, stg 1 | ft |
| 0.00d0 | ;YY | 10,37 | - | midox1 | oxi tank cntr len, stg 1 | ft |
| 0.00d0 | ;YY | 10,38 | - | endox2 | oxi tank radius, stg 2 | ft |
| 0.00d0 | ;YY | 10,39 | - | midox2 | oxi tank cntr len, stg 2 | ft |
| 0.00d0 | ;YY | 10,40 | - | rmix1 | propellant mix ratio, stg 1 | |
| 0.00d0 | ;YY | 10,41 | - | rmix2 | propellant mix ratio, stg 2 | |
| 0.00d0 | ;YY | 10,42 | - | mdot1 | prop consume rate, stg 1 | lbm/sec |
| 0.00d0 | ;YY | 10,43 | - | mdot2 | prop consume rate, stg 2 | lbm/sec |
| -1.0d0 | ;YY | 10,44 | - | eqr | equivalence ratio | |
| 0.00d0 | ;YY | 10,45 | - | thrust10 | initial motor thrust 1 | lbs |
| 0.00d0 | ;YY | 10,46 | - | thrust20 | initial motor thrust 2 | lbs |
| 200.0d0 | ;YY | 10,47 | - | xrecord | max. no. table record points | |
| 1.0d0 | ;YY | 10,48 | - | typgas | compres gas type:he-1,air-2 | |
| nozzle contour variables | | | | | | |
| 00.0d0 | ;YY | 11,1 | - | thet11 | arc-circle upstream angle | deg |
| 00.0d0 | ;YY | 11,2 | - | aone1 | parabolic arc constant | |
| 00.0d0 | ;YY | 11,3 | - | bone1 | parabolic arc constant | |
| 00.0d0 | ;YY | 11,4 | - | rzero1 | parabolic arc constant | |
| 00.0d0 | ;YY | 11,5 | - | entlen1 | length of entrance section | in |
| 00.0d0 | ;YY | 11,6 | - | xstar1 | axial loc of the throat 1 | in |
| 00.0d0 | ;YY | 11,7 | - | xp | x loc of circ¶b | in |
| 00.0d0 | ;YY | 11,8 | - | yp | y loc of circ¶b | in |
| 00.0d0 | ;YY | 11,9 | - | aone2 | parabolic arc constant | |
| 00.0d0 | ;YY | 11,10 | - | bone2 | parabolic arc constant | |
| 00.0d0 | ;YY | 11,11 | - | rzero2 | parabolic arc constant | |
| 00.0d0 | ;YY | 11,12 | - | entlen2 | length of entrance section | in |
| 00.0d0 | ;YY | 11,13 | - | xstar2 | axial loc of the throat 2 | in |
| 00.0d0 | ;YY | 11,14 | - | xnozzle2 | x location nozzle 2 | in |
| 0.1d0 | ;YY | 11,15 | - | tnoz1 | nozzle thickness, stage 1 | in |
| 00.0d0 | ;YY | 11,16 | - | tnoz2 | nozzle thickness, stage 2 | in |
| atmospheric data and aero constants | | | | | | |
| 00.0d0 | ;YY | 12,1 | - | pinf | atmospheric pressure | psf |
| 00.0d0 | ;YY | 12,2 | - | tinf | atmospheric temperature | deg R |
| 12.0d0 | ;YY | 12,3 | - | nalp | number of alpha's in aero tables | |
| 37.0d0 | ;YY | 12,4 | - | nphi | number of roll angls in aero tables | |
| 14.0d0 | ;YY | 12,5 | - | nmach | number of Mach #'s in aero tables | |
| 0.0d0 | ;YY | 12,6 | - | member | member number in the generation | |
| 0.0d0 | ;YY | 12,7 | - | igen | generation number | |
| 27.0d0 | ;YY | 12,8 | - | novar | No. of variables in 'gannl.dat' | |
| 22.0d0 | ;YY | 12,9 | - | nparts | No of main parts in the missile | |
| 1.0d0 | ;YY | 12,10 | - | ispeed | 0- subsonic; 1 supersonic | |
| aerodynamic constants data | | | | | | |
| 00.0d0 | ;yy | 13,1 | - | tma(1) | table mach number (1) | |
| 00.0d0 | ;yy | 13,2 | - | tma(2) | table mach number (2) | |
| 00.0d0 | ;yy | 13,3 | - | tma(3) | table mach number (3) | |
| 0.0d0 | ;yy | 13,4 | - | tma(4) | table mach number (4) | |
| 0.0d0 | ;yy | 13,5 | - | tma(5) | table mach number (5) | |
| 0.0d0 | ;yy | 13,6 | - | tma(6) | table mach number (6) | |

| | | | | | | | |
|-------------------------------------|-----|-------|---|-----------|--------------------------------|------|-----|
| 0.0d0 | ;yy | 13,7 | - | tma(7) | table mach number | (7) | |
| 0.0d0 | ;yy | 13,8 | - | tma(8) | table mach number | (8) | |
| 00.0d0 | ;yy | 13,9 | - | tma(9) | table mach number | (9) | |
| 00.0d0 | ;yy | 13,10 | - | tma(10) | table mach number | (10) | |
| 00.0d0 | ;yy | 13,11 | - | tma(11) | table mach number | (11) | |
| 00.0d0 | ;yy | 13,12 | - | tma(12) | table mach number | (12) | |
| 00.0d0 | ;yy | 13,13 | - | tma(13) | table mach number | (13) | |
| 00.0d0 | ;yy | 13,14 | - | tma(14) | table mach number | (14) | |
| 0.0d0 | ;yy | 13,15 | - | talp(1) | table alpha | (1) | deg |
| 0.0d0 | ;yy | 13,16 | - | talp(2) | table alpha | (2) | deg |
| 0.0d0 | ;yy | 13,17 | - | talp(3) | table alpha | (3) | deg |
| 0.0d0 | ;yy | 13,18 | - | talp(4) | table alpha | (4) | deg |
| 00.0d0 | ;yy | 13,19 | - | talp(5) | table alpha | (5) | deg |
| 00.0d0 | ;yy | 13,20 | - | talp(6) | table alpha | (6) | deg |
| 00.0d0 | ;yy | 13,21 | - | talp(7) | table alpha | (7) | deg |
| 00.0d0 | ;yy | 13,22 | - | talp(8) | table alpha | (8) | deg |
| 00.0d0 | ;yy | 13,23 | - | talp(9) | table alpha | (9) | deg |
| 00.0d0 | ;yy | 13,24 | - | talp(10) | table alpha | (10) | deg |
| 00.0d0 | ;yy | 13,25 | - | talp(11) | table alpha | (11) | deg |
| 00.0d0 | ;yy | 13,26 | - | talp(12) | table alpha | (12) | deg |
| GA variable data | | | | | | | |
| 00.0d0 | ;yy | 14,1 | - | xray(1) | propellant type | | |
| 00.0d0 | ;yy | 14,2 | - | xray(2) | equivalence ratio | | |
| 00.0d0 | ;yy | 14,3 | - | xray(3) | chamber pressure | | psi |
| 00.0d0 | ;yy | 14,4 | - | xray(4) | nozzle throat area | | in2 |
| 00.0d0 | ;yy | 14,5 | - | xray(5) | nozzle expansion ratio | | |
| 00.0d0 | ;yy | 14,6 | - | xray(6) | fractional nozzle length | | |
| 00.0d0 | ;yy | 14,7 | - | xray(7) | burn time | | sec |
| 00.0d0 | ;yy | 14,8 | - | xray(8) | payload mass | | lbm |
| 00.0d0 | ;yy | 14,9 | - | xray(9) | missile body diameter | | ft |
| 00.0d0 | ;yy | 14,10 | - | xray(10) | length of nose/dbody | | |
| 00.0d0 | ;yy | 14,11 | - | xray(11) | dia of nose/dbody | | |
| 00.0d0 | ;yy | 14,12 | - | xray(12) | fin1 root chord/dbody | | |
| 00.0d0 | ;yy | 14,13 | - | xray(13) | fin1 taper ratio | | |
| 00.0d0 | ;yy | 14,14 | - | xray(14) | fin1 le angle | | deg |
| 00.0d0 | ;yy | 14,15 | - | xray(15) | fin1 b/2 ratio = b2fin1/dbody | | |
| 00.0d0 | ;yy | 14,16 | - | xray(16) | x loc of fin 1 % body length | | |
| 00.0d0 | ;yy | 14,17 | - | xray(17) | fin2 root chord/dbody | | |
| 00.0d0 | ;yy | 14,18 | - | xray(18) | fin2 taper ratio | | |
| 00.0d0 | ;yy | 14,19 | - | xray(19) | fin2 le angle | | deg |
| 00.0d0 | ;yy | 14,20 | - | xray(20) | fin2 b/2 ratio = b2fin2/dbody | | |
| 00.0d0 | ;yy | 14,21 | - | xray(21) | xTE loc of fin 2 % body length | | |
| 00.0d0 | ;yy | 14,22 | - | xray(22) | autopilot time delay | | sec |
| 00.0d0 | ;yy | 14,23 | - | xray(23) | autopilot time constant | | |
| 00.0d0 | ;yy | 14,24 | - | xray(24) | autopilot damping | | |
| 00.0d0 | ;yy | 14,25 | - | xray(25) | cross over frequency | | hz |
| 00.0d0 | ;yy | 14,26 | - | xray(26) | pronav gain | | |
| 00.0d0 | ;yy | 14,27 | - | xray(27) | initial launch angle | | deg |
| reverse engineering/trajectory data | | | | | | | |
| 62.0d0 | ;YY | 15,1 | - | taltburn | motor burnout time | | sec |
| 24.5d0 | ;YY | 15,2 | - | altburn | motor burnout altitude | | km |
| 266.64d0 | ;YY | 15,3 | - | tflight | total flight time | | sec |
| 92.00d0 | ;YY | 15,4 | - | altmax | apogee | | km |
| 901.68d0 | ;YY | 15,5 | - | maxrange | maximum range | | km |
| 1.0d0 | ;YY | 15,6 | - | numgoals | number of GA traj match goals | | |
| 12.55d0 | ;YY | 15,7 | - | fineness | desired missile fineness ratio | | |
| 900000.d0 | ;YY | 15,8 | - | maxThrust | maximum limit on thrust | | lbs |